PLASTIC OBJECT DETECTION WITH AN INFRARED HYPERSPECTRAL IMAGE

A THESIS SUBMITTED TO
THE GRADUATE SCHOOL OF NATURAL AND APPLIED SCIENCES
OF
MIDDLE EAST TECHNICAL UNIVERSITY

BY

MEHMET FATIH DIRI

IN PARTIAL FULFILLMENT OF THE REQUIREMENTS
FOR
THE DEGREE OF MASTER OF SCIENCE
IN
GEODETIC AND GEOGRAPHIC INFORMATION TECHNOLOGIES

JUNE 2019

Approval of the thesis:

PLASTIC OBJECT DETECTION WITH AN INFRARED HYPERSPECTRAL IMAGE

submitted by **MEHMET FATİH DİRİ** in partial fulfillment of the requirements for the degree of **Master of Science in Geodetic and Geographic Information Technologies Department, Middle East Technical University** by,

Prof. Dr. Halil Kalıpçılar
Dean, Graduate School of **Natural and Applied Sciences** _____

Prof. Dr. Zuhal Akyürek
Head of Department, **Geod. and Geog. Inf. Tech.** _____

Prof. Dr. Mehmet Lütfi Süzen
Supervisor, **Geod. and Geog. Inf. Tech., METU** _____

Assoc. Prof. Dr. Koray K. Yılmaz
Co-Supervisor, **Geological Engineering, METU** _____

Examining Committee Members:

Prof. Dr. A. Aydın Alatan
Electrical and Electronics Engineering, METU _____

Prof. Dr. Mehmet Lütfi Süzen
Geod. and Geog. Inf. Tech., METU _____

Assoc. Prof. Dr. Koray K. Yılmaz
Geological Engineering, METU _____

Assoc. Prof. Dr. Bekir Taner San
Geological Engineering, Akdeniz University _____

Assoc. Prof. Dr. Deniz Gerçek Kurt
City and Regional Planning, Kocaeli University _____

Date: 18.06.2019

I hereby declare that all information in this document has been obtained and presented in accordance with academic rules and ethical conduct. I also declare that, as required by these rules and conduct, I have fully cited and referenced all material and results that are not original to this work.

Name, Surname: Mehmet Fatih Diri

Signature:

ABSTRACT

PLASTIC OBJECT DETECTION WITH AN INFRARED HYPERSPECTRAL IMAGE

Diri, Mehmet Fatih
Master of Science, Geodetic and Geographic Information Technologies
Supervisor: Prof. Dr. Mehmet Lütfi Süzen
Co-Supervisor: Assoc. Prof. Dr. Koray K. Yılmaz

June 2019, 94 pages

Undoubtedly, a world without plastic, which is the most important production material in almost every area, seems inconceivable today. The production and consumption chain, by which induced this versatile use, has caused plastic pollution that has devastating effects on the environment and natural ecosystems.

In this thesis, which written with the motivation of contributing to the fight against plastic pollution and to be useful developing effective and sustainable policies, plastic pollution and pollutant types have been investigated; plastic objects have been examined in terms of physical, chemical and spectral aspects; and have been detected on land with an unsupervised manner through shortwave infrared hyperspectral image.

15.5-meter resolution 224 band hyperspectral image which was acquired by AVIRIS is used. In this study, 15 different study field, each of which include significant plastic object samples like a greenhouse, an artificial turf football pitch, a solar panel, and a tent, is determined within the image scene.

The positive value of spectral absorption around 1.72 μm, which is associated with the presence of plastic, has been mathematically expressed using two neighboring shoulders. This algorithm, which has the capability of detecting plastic objects on land quickly and precisely without needing any reference data and using only 3 shortwave

infrared bands, has been named as Plastic Existence Index (PEI). The positive values generated as a result of the algorithm has been called Post Index Positive Value (PIPV).

Since it was not possible to collect any data from the ground, the reference data has been produced by visual inspection method on the true color composite AVIRIS image. After implementation results have been compared with reference data, it is seen that highly-satisfactory outcomes have been obtained which mean value of UA is 90.51%, PA is 89.04% and OA is 97.37.

Keywords: plastic pollution, hyperspectral, shortwave infrared, unsupervised classification, feature detection

ÖZ

KIZILÖTESİ HİPERSPEKTRAL GÖRÜNTÜYLE PLASTİK NESNE TESPİTİ

Diri, Mehmet Fatih
Yüksek Lisans, Jeodezi ve Coğrafi Bilgi Teknolojileri
Tez Danışmanı: Prof. Dr. Mehmet Lütfi Süzen
Ortak Tez Danışmanı: Doç. Dr. Koray K. Yılmaz

Haziran 2019, 94 sayfa

Kuşkusuz, hemen hemen her alanda en önemli üretim malzemesi olan plastiğin olmadığı bir dünya bugün düşünülemez gözükmektedir. Bu çok yönlü kullanımın neden olduğu üretim ve tüketim zinciri, çevre ve doğal ekosistemler üzerinde yıkıcı etkileri olan plastik kirliliğine sebep olmaktadır.

Plastik kirliliği ile mücadeleye katkıda bulunmak ve etkili ve sürdürülebilir politikalar geliştirmek konusunda faydalı olma motivasyonuyla yazılmış bu tez çalışmasında, plastik kirliliği ve kirletici türleri araştırılmış; plastik objeler fiziksel, kimyasal ve spektral yönleri açısından incelenmiş; ve kısa dalga kızılötesi hiperspektral görüntü ile denetimsiz bir şekilde karada tespit edilmiştir.

Çalışmada 15.5-metre çözünürlüğünde 224 hiperspektral banda sahip AVIRIS görüntüsü kullanılmıştır. Bu görüntüde sera, suni çim futbol sahası, güneş paneli ve çadır gibi önemli plastik nesne örnekleri içeren 15 farklı çalışma alanı belirlenmiştir.

1.72 µm civarında oluşan spektral absorbsiyon plastiğin varlığıyla ilişkilendirilmiş ve iki komşu omuz noktası kullanılarak matematiksel olarak ifade edilmiştir. Herhangi bir referans veriye ihtiyaç duymadan ve sadece 3 kısa dalga kızılötesi bant kullanarak karadaki plastik nesneleri hızlı ve hassas bir şekilde tespit edebilme yeteneğine sahip olan bu algoritmaya Plastik Varlık İndeksi (PEI) adı verilmiştir. Algoritma sonucunda

üretilen pozitif değerler ise Endeks Sonrası Pozitif Değer (PIPV) olarak adlandırılmıştır.

Zeminden veri toplamak mümkün olmadığından, referans veri, gerçek renk kompoziti olarak oluşturulan AVIRIS görüntüsü üzerinde görsel inceleme yöntemiyle manuel olarak üretilmiştir. Uygulama sonuçları referans verilerle karşılaştırıldığında oldukça tatmin edici sonuçlar alındığı ve ortalama kullanıcı doğruluğunun %90.51, ortalama üretici doğruluğunun %89.04, ortalama genel doğruluğun ise %97.37 olduğu görülmüştür.

Anahtar Kelimeler: plastik kirliliği, hiperspektral, kısa dalga kızılötesi, denetimsiz sınıflandırma, özellik çıkarımı

to my beloved family, Kübra and Ceren...

ACKNOWLEDGEMENTS

First and foremost, I am grateful to Allah, the Almighty, gave me the strength to complete this master thesis successfully.

I would like to express my deepest appreciation to my advisor Prof. Dr. Mehmet Lütfi Süzen for his guiding and enlightening attitude, valuable criticism and constructive attitude. I sincerely thank this distinguished scientist, whom I wish my relationship to continue for many long years, for the vision he gave me.

I would like to thank valuable scientist, Assoc. Prof. Dr. Koray K. Yılmaz for her sincere and guiding attitudes.

I am thankful to my dear wife, for her endless love, motivation, understanding, encouragement, and patience throughout my study.

I sincerely thank my precious father, who has a devoted and wise character, showing me the right path in every moment of my life. I would like to thank my dear mother, the source of my life, for the great encouragement and pure love she has given me. I would like to thank my dear sister, who honors me with her presence, for the unique bond between us.

On this occasion, I would like to commemorate my dear elder-brother, who I lost early...

I am also thankful to Mr. Caner Demirpolat for his valuable assistance.

In essence, I sincerely wish that this study, which I have done for the wellfare of my beautiful country, can serve its purpose.

TABLE OF CONTENTS

LIST OF TABLES

TABLES

LIST OF FIGURES

FIGURES

LIST OF ABBREVIATIONS

AVIRIS	: Airborne Visible/Infrared Imaging Spectrometer
BPA	: Bisphenol A
ETFE	: Ethylene Tetrafluoroethylene
GSD	: Ground Sample Distance
HC	: Hydrocarbon
HDPE	: High-density polyethylene
HI	: Hydrocarbon Index
HSI	: Hyperspectral Imagery
IRS	: Infrared Reflectance Spectroscopy
JPL	: Jet Propulsion Laboratory
LDPE	: Low-Density Polyethylene
ML	: Maximum Likelihood
MSI	: Multispectral imagery
NDVI	: Normalized Difference Vegetation Index
NIR	: Near-Infrared
NOAA	: National Oceanic and Atmospheric Administration
OA	: Overall Accuracy
PA	: Producer Accuracy
PEI	: Plastic Existence Index
PET /PETE	: Polyethylene Terephthalate
PIPV	: Post Index Positive Value
POD	: Plastic object detection
PP	: Polypropylene
PS	: Polystyrene
PTFE	: Polytetrafluoroethylene
PVC	: Poly Vinyl Chloride
RF	: Random Forest

SAR	: Synthetic Aperture Radar
SF	: Study Field
SMF	: Spectral Math Function
SPI	: The Society of the Plastic Industry
SVM	: Support Vector Machine
SWIR	: Shortwave-Infrared
UA	: User Accuracy
UAV	: Unmanned Aerial Vehicle
USGS	: United States Geological Survey
VNIR	: Near Infrared
WV-3	: WorldView-3

CHAPTER 1

INTRODUCTION

Undoubtedly, a world without plastic, which is the most important production material in almost every area, seems inconceivable today. It is used in a wide range of products from plastic household appliances to medical products, from car parts to electronic products. This versatile use increases plastic production and the raising production triggers consumption. This chain of production and consumption, which can be considered industrially successful, has caused plastic pollution problem that has devastating effects on the environment and natural ecosystems.

Researches show that more than half of the plastic products are produced as packaging and disposable products and that they enter the world ecosystem as garbage in the year of production. A plastic waste, which takes up to 1000 years to dissolve in nature, pollutes the oceans, poisons the soil, kills plants and animals. Plastics and chemicals in it are also seriously threatening human health. When these destructive effects are examined, it may be considered that the use of plastic should be prohibited. However, it is not possible and not even logical. Instead, introducing some limitations on use, production and consumption can be an effective solution.

Academics and environmentalists pay highly attention to the impact of plastic pollution on the seas and the oceans. However, plastic pollution on land, which not only poses a threat to soil and plants and living beings on it but also affects the marine ecosystems extremely negatively, has not been adequately investigated.

In this thesis, plastic and plastic pollution has been discussed in many respects and plastic presence has been detected on the land by using some special remote sensing techniques and technologies in order to make a positive contribution to the solution of plastic pollution and protection of the natural environment.

1.1. Hydrocarbon, Polymer and Plastic

In order to understand the plastic in detail, it is significantly necessary to first understand the hydrocarbon and then the polymer.

Hydrocarbon, one of the most important classes of organic compounds, is mixed of carbon and hydrogen (Olah & Molnár, 2003). Carbon atoms cluster as groups to compose the structure of hydrocarbon, and hydrogen atoms are linked to them in various combinations.

Although hydrocarbons are composed of only two types of atoms, they are highly diverse. This diversity is caused by the lengths and variations of the interatomic bonds and the combinations that may occur depending on them like illustrated in Figure 1.1.

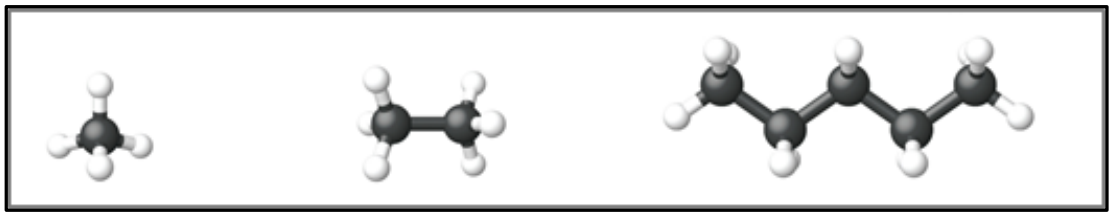

Figure 1.1. Ball and Stick Model for molecules of methane (CH_4), ethane (C_2H_6), and propane (C_3H_8) (Hydrocarbons, 2012).

Hydrocarbons can be found in plants, animals and even in the human body. They are the main constituent of a great number of materials, primarily as petroleum products and polymers and plastics.

Polymers are atomic mass compounds built by the process of reacting monomer molecules jointly in a chemical reaction called polymerization. There are three forms of polymers: elastomers, fibers, and plastics (Ouellette & Rawn, 2015).

Elastomers are known for their flexible structure. After distortion, they recover their original form. Every sole string in elastomers can be extended by stretching but after pressure pass, atomic structure comes back to original conformation. Basically, hybridized carbon atoms provide its elasticity. Rubber is the most known elastomer.

Fibers occur when polymer strings are aligned the same direction. It is classified in two classes: short fiber and long or continuous fiber. Synthetic turf/grass, which is one of the plastic objects to be aimed to detected in this study, is also a fiber sample.

Plastic, made from polymer, is a universal term used to define a multitude of synthetic (manmade) or semi-synthetic materials (Woodford, 2018). Plastic material is made up of polymers, which can be soft or rigid in many colors and in transparent form.

The name of plastic comes from plastikos that means can be shaped in Greek (Liddell & Scott, 1897). Plastic is made by conversion of natural substances or through synthesis from main chemical compounds derived from coal, oil and natural gas. Refinement of unprocessed oil is the beginning phase of plastic material production. This process separates the highly-viscous oil into lighter units called fractions which are basically a compound of hydrocarbon chains. Naphtha, one of the fractions, is significant for plastic production.

Because of their versatility, durability, low cost, and easy manufacturing process, plastics are used in a many products in different scales. Plastic is a lightweight material that substitutes its heavier metallic predecessors like iron or alloys. From healthcare and agriculture to construction energy, plastic is used in everywhere.

The majority of plastics have good corrosion resistance to chemicals like acid or alkali. For example, polytetrafluoroethylene (PTFE) has excellent chemical stability and even better than gold. Majority of plastics are poor electrical conductors. For this reason, plastic is used in many applications in the electronics and machinery industry. Additionally, it has good isolation and used for thermal isolation. Plastics can be hard as steel and stone or soft as cotton and chewing gum and even a knife can be made using different variations. There are many types of plastics and each has its own properties, though they can be divided into two major families: thermoplastics and thermosets.

The Society of the Plastic Industry (SPI) created a system to facilitate the recycling process in 1988 to classify different type of plastic which are polyethylene

terephthalate (PET or PETE), high-density polyethylene (HDPE), vinyl (Polyvinyl Chloride or PVC), low-density polyethylene (LDPE), and polypropylene (PP) or polystyrene (PS) can be seen in Figure 1.2.

Figure 1.2. SPI Plastic Resin Identification Coding System *(Merrington, 2017).*

Poly (ethylene terephthalate) - PET or PETE is the plastic used to bottle the vast of drinks. Approximately one-fourth of plastic bottles are PET. PET bottles can be clear; they are tough and conserve carbon dioxide well (Carraher, 2008).

High-density polyethylene - HDPE is a specific variation of PE. HDPE constitutes approximately 50% of the plastic bottle market. Milk, juices, margarine and lots of food packages on the market are HDPE. It is robust and can be shaped easily.

Poly (vinyl chloride) - PVC or V is used as pure or a mix for generating a variety of products like pipes, package films, solid detergents, and containers.

Low-density polyethylene - LDPE is more elastic than and not as durable as HDPE. Its shapeless form makes it more poriferous than HDPE, but it blocks moisture better. It is a significant material for bread and trash bags.

Polypropylene - PP has a strong resistance to chemicals. PP constitutes nearly 50% of the plastic bottle market and used for juices, milk, margarine, etc. packages.

Polystyrene - PS is used to make a variety of pots, styropor plates, dishes, cups, etc.

1.2. Plastic Pollution Problem

Plastic pollution is the chemical debris which has an enormous negative impact on the environment and wildlife habitat. Natural polymers like rubber and silk abound in nature, but they do not play a role in plastic pollution, due to the fact that they do not persist in nature. However, the industrial type of plastic which produced primarily from petroleum is developed particularly to beat natural deterioration and can persist in nature for centuries.

While their broad-scale production and usage only date back to ~1950, 348 million metric tons of plastics produced in 2017. To comprehend the magnitude of plastic pollution in lands and oceans, plastic pollution must be understood in numbers. Approximately 8.3 billion tons of plastics, of which 8.4% were predicted to be recycled and 9.6% burned, was produced around the world up till now (Geyer, et al., 2017).

Around 4.9 billion tons, ~59% of produced plastics were discarded and inevitably entered the environment illustrated in Figure 1.4 (Geyer, et al., 2017).

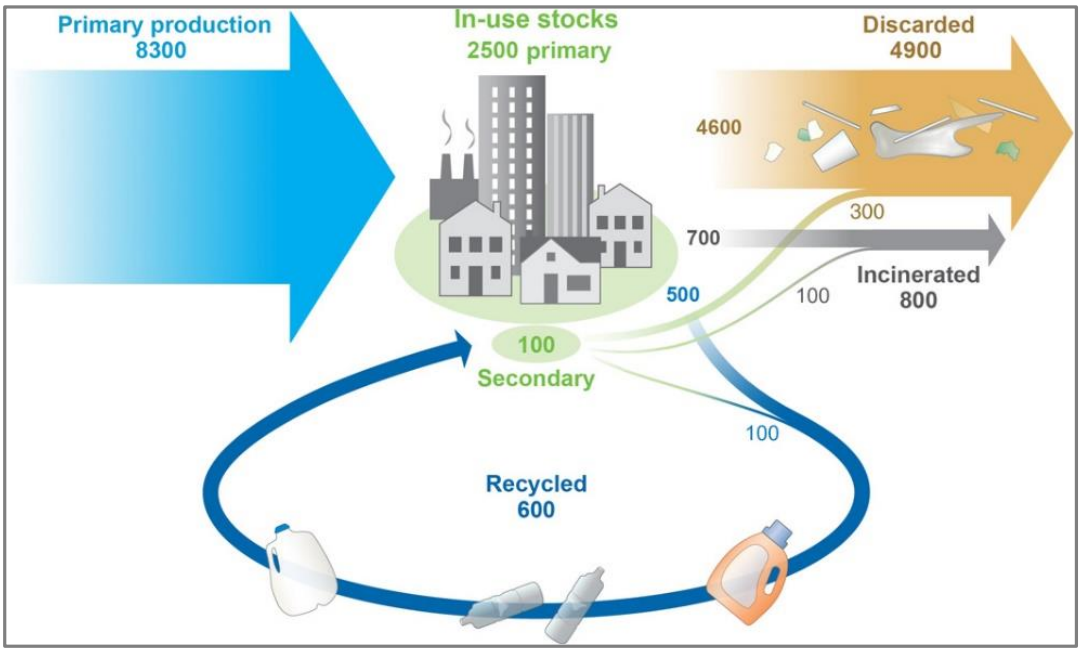

Figure 1.3. Production, use, and cycle of plastics *(Geyer, et al., 2017)*

1.3. Plastic Pollutant Types

Plastic pollutants can be classified into four main classes which given in Table 1.1.

Table 1.1. Plastic Pollutant Classes (Andrady, 2017)

Class	*Seen with*	*Size*
Macroplastics	Naked eye	> 25 mm.
Mesoplastics	Naked eye or optical microscope	25 mm. – 5 mm.
Microplastics	Optical microscope	5 mm. - 1 μm
Nanoplastics	Electron microscope	< 1 μm

Macroplastics exist in bag, packaging, and landfills which derived from industrial components (Barnes, et al., 2009). Macroplastics, which partially cause the formation of microplastics, play an active role in plastic pollution.

Macroplastic pollution is a worldwide issue and is seen as a standout amongst the most serious types of contamination in shorelines, freshwater bodies and marine environment. They are commonly characterized as having a size > 25 mm. (Romeo, et al., 2015), Some of them smell like food and ingested by different marine species like fish and seabirds, the effect is presented in Figure 1.5 (Derraik, 2002).

Figure 1.4. Albatross that poisoned by the macroplastics *(Jordan, 2009)*

The issue of macroplastic pollution has been revealed in the 1990s and is currently secured by a few universal guidelines.

Microplastics are tiny parts of plastic and one of the most significant factors of water sources pollution. They have usually accumulated in urban and municipal centers and water sources. Microplastic dimensions are less than 5 mm according to U.S. National Oceanic and Atmospheric Administration (NOAA).

Plastic debris is also classified as either primary or secondary. In this context, there are two types of microplastics. First one is any plastic particles which were produced smaller than 5 mm. on purpose. Microfibers or fabric pieces are known samples of these types of primary microplastics. Secondary microplastics are plastic particle which dimensions are more than 5 mm. like bottles or bags but turn into very small pieces within a period of degradation and distortion (Hammer, et al., 2012). These kind of microplastics can even turn into nanoplastics.

Due to the fact that it contaminates water and land easily and quickly, microplastics and nanoplastics are extremely destructive for the environment.

1.4. Effects of Plastic Pollution

192 countries which have coasts to Atlantic, Pacific and Indian oceans, or the Mediterranean and the Black Sea, generated approximately 275 million tons of plastic debris in 2010 (Jambeck, et al., 2015). It is estimated that 4,8 to 12,7 million tons of plastic debris which is equivalent to 1,7% to 4,6% of total waste entered the ocean in the same year (Jambeck, et al., 2015). This garbage entering the oceans is toxic to marine life. Planktonic organisms, fish species, birds, marine mammals, sea turtles and eventually the human race are exposed to these highly noxious chemicals by means of the food chain. One being in anywhere in this food chain may come to face with cancer, immune faults, and birth defects (Fernandez, et al., 1999).

Due to some factors like wind and ocean flows, coastal and urban geography, and trade roads, the spread of plastic debris in nature is changeable. People also play a

critical role in this issue. Plastics may cause a distribution of organisms to remote locations, and may also be carriers for certain chemicals, such as organic pollutants and heavy metals. As a result of the release of harmful plastics chemicals to the soil, the groundwater and other water sources are polluted and damage the ecosystem. It also harms the species that drink this contaminated water. Tap waters are also under the threat. Level of tap waters, which include the pollutants of plastics is %83 (Mason, et al., 2018).

Plastic debris effects on land are not limited to water and ecosystem. Due to the fact that degradation of many different types of plastics in landfills through nylon-eating bacteria, methane gas arise which has a significant effect on global warming. Additionally, the release of dangerous chemicals on land causes breeding areas for diseases and reducing beneficial natural cycle.

Plastic pollution has serious effects not only on nature and animals but also on humans. Because almost everything includes plastics, the great majority of the human population are exposed to the chemicals. Plastics, because of the use of chemicals during production, can cause an endocrine defect and have cancerogenic effects on human (Barnes, et al., 2009). These chemical additives used in plastic production can cause dermatitis in case of direct contact with skin. As mentioned before chemicals derived from plastics contaminated tap water. In the US, 95% of adults have an appreciable rating of Bisphenol A (BPA) in their urine. BPA exposure has been associated with some health problems like thyroid hormone-disruptions, infertility defects, reproductive health and maturation of sex (North & Halden, 2013).

To summarize, the plastic and the chemicals in it have destructive effects in many respects on the environment and all species living in it.

1.5. Problem Statement

Scientific studies have mostly focused on plastic pollution in seas and oceans, and there is not considerable amount of study on the plastic pollution based on land. However, the plastic pollution in marine environment is mostly caused by pollution formed mainly on land and coasts. For instance, any size of plastic on the land undergoes a series of dissolution, transforms into microplastics and enters the soil and water, and then enters the seas and oceans under the influence of rivers and wind.

For this reason, plastic pollution on land, which not only poses a threat to soil and plants and living beings on it but also affects the marine ecosystems extremely negatively, should be investigated and then the results should be analyzed.

While plastic detection on land is a challenging issue, it is possible via remotely sensed images using a number of specific techniques. As a result of this determination, for example, synthetic polymers used for agricultural purposes, in other words plasticulture can be detected. Thus, it is possible to decide on the level of the use of plastic in agriculture and whether it requires restriction. By means of this detection, future planning can also be done by determining the rate of increase or decrease of plastic usage at past years on land.

1.6. Thesis Contribution

This thesis consisted of investigations and practices to define plastics in a broad perspective, to present brief information about types and effects of plastic pollution and to emphasize the abilities of short wave infrared bands with a high amount of spectral information to detect plastic objects.

It has been observed that there are academic studies using multispectral and hyperspectral data for plastic detection. However, a practice to detect plastic objects used for different purposes in different locations with one single algorithm has not been seen. In addition, academic studies have mostly focused on plastic pollution in marine environment. Studies about plastic pollution on land are insufficient.

The thesis aims to further develop algorithms that use spectral information and having capabilities of quickly and precisely detecting different types of plastic objects used for different purposes in different locations on land with using only 3 shortwave infrared (SWIR) bands and without reference data.

Although there is valuable information in almost every region of the SWIR spectrum, the PEI algorithm has been developed to use only 3 bands of the SWIR spectrum. The reason for this approach is that the payload, which is planned to work in harmony with the PEI algorithm, is intended to be developed in a simple, low-cost and uncomplicated way.

CHAPTER 2

BACKGROUND INFORMATION AND LITERATURE SURVEY

Plastic object detection (POD) can be carried out in many different ways and in a variety of different environments. Detection method can be classified by the source and type of data or by technique used. This section, the common methods used and adopted are mentioned, can also be considered as a literature review.

2.1. Data Types Used for Plastic Object Detection

It is possible to categorize data to three classes on account of POD. These are multispectral, hyperspectral and synthetic aperture radar (SAR) images.

Multispectral imagery (MSI) and hyperspectral imagery (HSI) can be used in analysis using spectral signatures. Simply, the main distinction between MSI and HSI is the count and the interval size of the bands. MSI is generally under 10 bands and HSI gathers more than 100 narrower bands. These amazing imageries provide significant information that cannot gather with visible or single band images. MSI and HSI can be used to extract target data like distinguishing proof of a compound (Gundlach, 2012).

SAR lights up an objective and after that measure and process the reflectance of signal like other radars. Moreover, SAR utilizes the forward movement of the UA-mounted radar to deliver the impact of a long radio wire without having a physically long reception apparatus (Gundlach, 2012). These systems are generally more complicated than conventional optical systems because of convoluted architecture of antenna and prerequisites of processing procedures. Despite the fact that SAR images can partially look like electro optical images, radar images can offer unique and valuable information.

Data types used for POD can be classified into three main categories; ground, aerial and satellite based in terms of source and acquisition.

Ground based imageries are relatively more successful in POD due to the fact that it is not exposed to the atmosphere and its effects. El-Magd, et al. (2014) used ASD spectrometer to examine spectral properties of water and contaminants. In some studies, multiple data sources are used together for better results. Scafutto, et al. (2017) used both ground based and aerial based spectrometers for simultaneous measument of materials.

In a ground-based implementation, the study area can be considered as a laboratory environment. These high-tech systems utilize many regions of the electromagnetic spectrum, but get benefit more from reflection and absorption values in the near infrared and shortwave infrared region for special purposes. These electro-optical systems have a technical ability to easily extract plastic and even determine the type of the plastic. An example of such applications can be seen in the Figure 2.1.

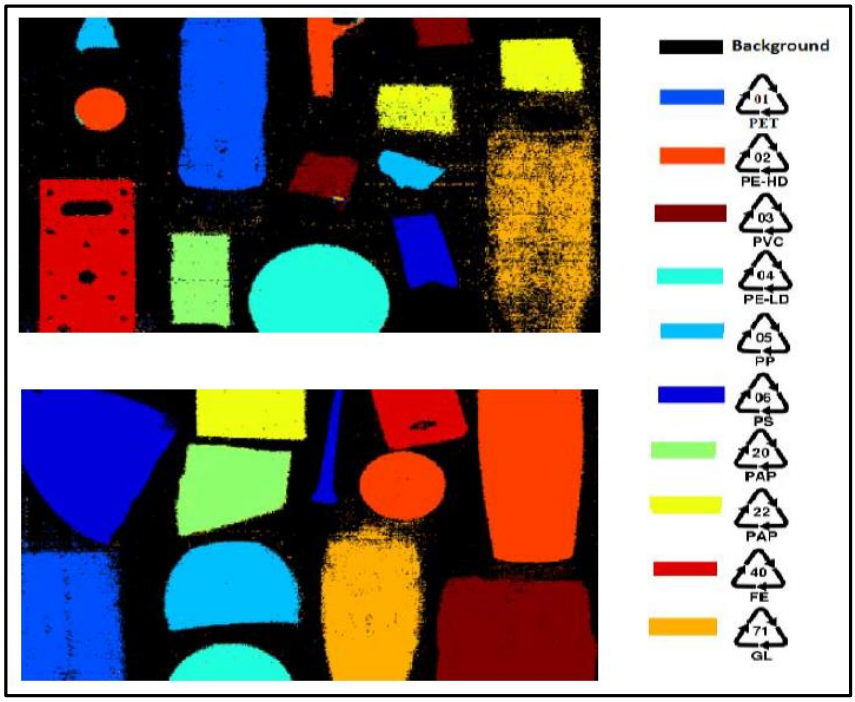

Figure 2.1. SVM classification map for plastic waste sorting using SWIR *(Karaca, et al., 2013)*

Determination of the type of plastic provides more efficient recycling process. Ground based image which is generally used for industrial purposes, is not suitable for environmental studies.

Aerial imageries are important sources for POD. Aerial images are obtained with the help of special cameras, which can be mounted on aircraft or unmanned aerial vehicles (UAV) and customized according to the needs. An aerial image has some advantages like being able to cover larger areas than ground-based imageries and to offer high spatial resolution than satellite imageries. Another important advantage of the aerial imageries is that the platforms, where they are produced, are can quickly and easily be taken action and modified. Sensors used in such platforms may also contain more than two hundred bands to record the radiation values in each region of the electromagnetic spectrum more effectively given in Table 2.1.

Table 2.1. Some Airborne Hyperspectral Sensors *(Thenkabail & Lyon, 2016)*

Sensor	*Number of Bands*	*Spectral Range*(μm)
AISA Eagle	Up to 488	0.40 – 0.97
AISA Eaglet	Up to 410	0.40 – 1.00
AISA Hawk	254	0.97 – 2.50
AISA Dual	Up to 500	0.40 – 2.50
AISA Owl	Up to 84	8.00 – 12.00
AVIRIS	**224**	**0.40 – 2.50**
CASI-550	288	0.40 – 1.00
CASI-1500	288	0.38 – 1.05
SASI-600	100	0.95 – 2.45
MASI-600	64	3.00 – 5.00
TASI-600	32	8.00 – 11.50
DAIS 7915	79	0.43 – 12.30
DAIS 21115	211	0.40 – 12.00
EPS-H	150	0.43 – 12.50
HYDICE	210	0.40 – 2.50
HyMap	128	0.45 – 2.48
Hyspex	704	0.40 – 2.50
PROBE-1	128	0.40 – 2.50

Satellites imageries are indispensable data source for remote sensing applications. Satellite imageries have low spatial resolution compared to aerial photographs but used frequently in environmental research as it can cover larger areas. Platforms producing satellite images record radiation values from many regions of the electromagnetic spectrum, such as platforms that producing air imageries, but may be relatively low in terms of the number of bands they contain.

Although satellite imageries types differ according to the technique used and the purpose; for POD, satellite image which contain near infrared and short wave infrared bands can be more practical. Asadzadeh and de Souza Filho (2016) simulated the WorldView-3 SWIR bands using libraries spectra and some datasets to examine the hyrdocarbon detection performance of WorldView-3.

It is beneficial to look at the comparison of some satellites which produce shortwave infrared imageries which given in table 2.2 due to the fact that they can be an alternative to the data which is a shortwave infrared airborne image that used in this study.

Table 2.2. Satellites with Shortwave Infrared Bands

Satellite	*Spatial Resolution (SWIR)*	*Spectral Range (SWIR)*	*Number of Bands (SWIR)*
WorldView-3	**3.7 m.**	**1.19 µm - 2.36 µm**	**8**
Aster	30 m.	1.60 µm - 2.43 µm	6
EO-1 Hyperion	30 m.	0.85 µm - 2.57 µm	172
Landsat-7	30 m.	1.55 µm - 1.75 µm, 2.09 µm - 2.35 µm	2
Landsat-8	30 m.	1.56 µm - 1.65 µm, 2.11 µm - 2.30 µm	2
Sentinel-2	20 m. – 60 m.	1.37 µm, 1.61 µm, 2.20 µm (center)	3

2.2. Techniques Used for Plastic Object Detection

POD through remote sensing components and technologies is a significant and intriguing but also compelling issue. As mentioned in sections 2.1.1 and 2.1.2 POD can be carried out in a variety of data source and type. Depending on the characteristic of the data, the technique used also varies.

If a MSI is used as the data type for POD, conventional supervised classification techniques are commonly used. Support Vector Machine (SVM), Maximum Likelihood (ML) and Random Forest (RF) are the supervised techniques used widely for the POD.

ML is used more than other supervised classification techniques. The ground of the ML classification is probability density function which supposes that the stats distribution is normal for each class and computes the probability that a pixel member of a class. Agüera, et al. (2008) used ML classifier, hough transform and loop elimination to detect and describe greenhouses.

RF and SVM algorithms, which comparatively new classification techniques, are nonparametric. The RF is a committee-based learning method which uses decision-tree, whereas SVM is a classifier built on statistical learning concept (Koç San, 2013). Chen, et al. (2016) proposed a new technique uses textural and spectral features together for POD, interpreted performance of SVM and then compared it with ML.

Spectral analysis or Infrared Reflectance Spectroscopy is another significant technique used for POD using NIR and SWIR imageries. All material has a specific spectral signature which can be considered as a function of reflectance or emissivity of the wavelength (Gundlach, 2012). Spectral reflectance can change dependent on physical structure, compound attributes, temperature elements, illumination and atmospheric circumstances of the material. The spectral signatures can be found in libraries to help analysis.

A spectral analysis to be used for POD is generally can be called Infrared Reflectance Spectroscopy (IRS). Masoumi, et al. (2012) developed a “two-filter” identification system based on NIR reflectance spectroscopy which, consist of two different optical systems to separate two specific wavelengths, that examining some parameters like contamination of surface, thickness and label of sample to classify plastic waste.

There are many different indices in the literature to identify different materials using spectral information, such as the most well-known Normalized Difference Vegetation Index (NDVI). These indices are created with image processing techniques with the help of a number of software or more easily using band ratios. Antonio and Tarantino (2015) used three different indices in addition to NDVI which are plastic surface index, rescaled brightness temperature and normalized difference sandy index for POD.

SAR imageries are also surprisingly used for POD. It is possible to detect plastic object by applying RF and SVM algorithms to the backscattering intensity obtained from the C-Band Full Polarization SAR image, which has been subjected to a number of processes and made more suitable to the POD (Chen & Li, 2017).

In addition to main methods, basic techniques of image processing also used for enhancement of POD. El-Magd, et al. (2014) used streching and convolution filters for disciriminate oil spills.

2.3. Optical Properties of Plastic Objects

The optical properties of plastic objects vary depending on many parameters. For example, if the plastic floats over the water, the reflected spectrum changes due to different refractive indices.

Pure plastics such as PE are homogeneous and cause less scattering because they are brighter (Kutz, 2011). The use of heterogeneous substances in the homogenous object causes scattering of light (Hong & Pine, 2005). Depending on the purpose, when an object is more opaque it absorbs more light. Covering the plastic with a coat may reduce scattering and increase reflection.

Two cases are remarkable for the optical properties of a plastic object:

i. Small plastic particles scatter light more than larger plastics.

ii. Reducing the refractive index contrast between the plastic particle and its surrounding environment reduces the amount of light scattered by the plastic particle (Law, et al., 2014).

For these reasons, the amount of light scattered by the plastic particles in the water is relatively high (1.333), while the amount of light scattered by the plastic in the air is tolerable due to the fact that the refractive index of the air is close to 1 under normal conditions (1.003).

Another mentionable parameter is the structure of the surface. On a flat and smooth surface, the reflected light and the incoming light make the same angle as the normal and no scattering occurs. On the rough surface, light is scattered in several directions (Albregtsen, 2008).

In brief, various parameters such as chemical properties, color, texture, opacity, surface roughness, reflection and scattering properties of plastic object affect the optical properties of light reflected from plastic.

2.4. Spectral Properties of Plastic Object

The spectral reflection of a substance may vary depending on the ambient conditions, the production method and the equipment used. Plastic spectra, in addition to these factors, depends on various parameters like plastic type, homogeneity, size and color. In this section, the spectra of different types of plastics acquired in different environments by using different equipment and techniques has been examined. Although the spectra generated from the satellite image are not the same with spectra generated in laboratory environment due to the atmosphere and effects of it even if the material is the same, it is still significantly similar. This proposal can be seen in clearly in Figure 2.2 which shows spectra comparison of alunite acquired from four different sensors.

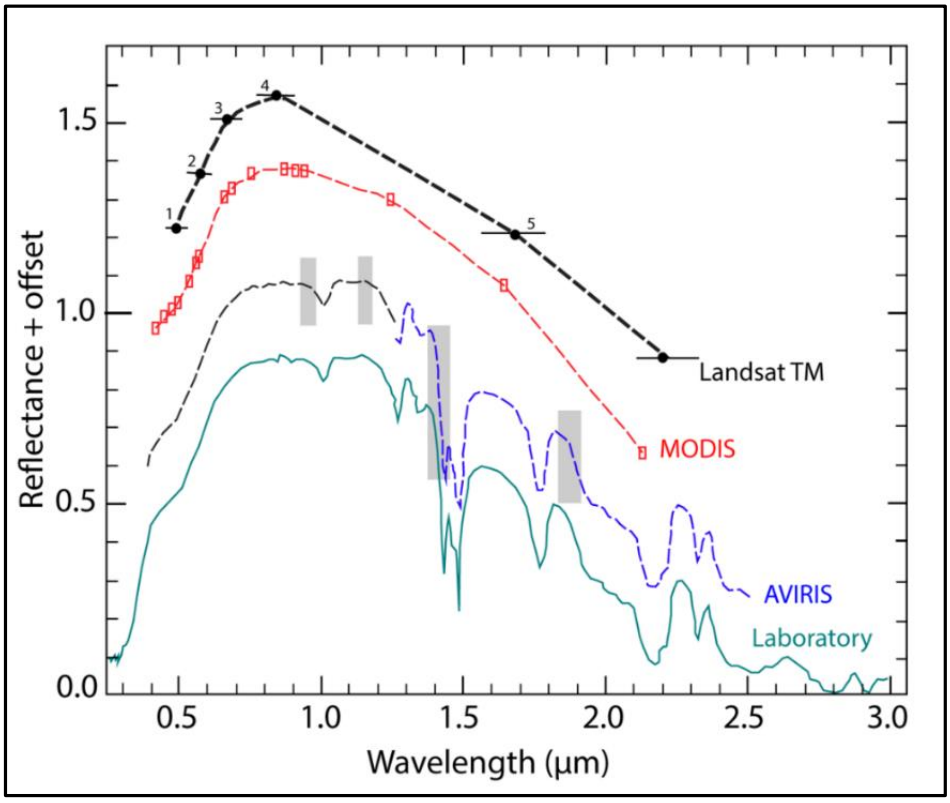

Figure 2.2. Spectra comparison of alunite from four hyperspectral sensors *(Smith, et al., 2016)*

In this context it is more meaningful to look at the spectra which purified as much as possible from atmospheric effects and external parameters in the reliable libraries.

Jet Propulsion Laboratory (JPL) spectral library which another name is ECOSTRESS suitable for this examination. More than 3400 man-made and natural material spectra can be found in ECOSTRESS (Ecostress Spectral Library, n.d.). Three samples, respectively white fiberglass unspecified rubber, white rubberized coating and black unspecified rubber obtained from the laboratory are given below.

White fiberglass unspecified rubber (Sample No.: 0834UUURBR), which particle size is solid, classified as a manmade roofing material. The plot shows that an absorption, which neighbor to two shoulders, exists around 1.72 µm which is important point in terms of the prediction of plastic existence. Plot can be seen in Figure 2.4.

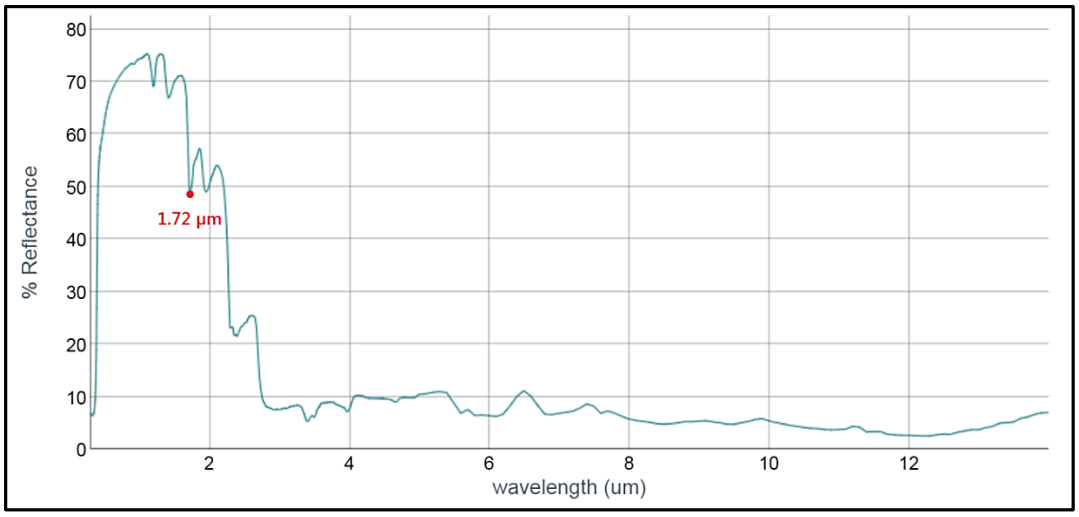

Figure 2.3. Spectra of white fiberglass unspecified rubber *(Ecostress Spectral Library, n.d.)*

White rubberized coating (Sample No.: 0795UUURBR), which particle size is solid, manmade roofing material, sub classified as rubber. The plot is similar to the white fiberglass unspecified rubber plot and shows that an absorption, which neighbor to two shoulders, exists around 1.72 µm. can be seen in Figure 2.6.

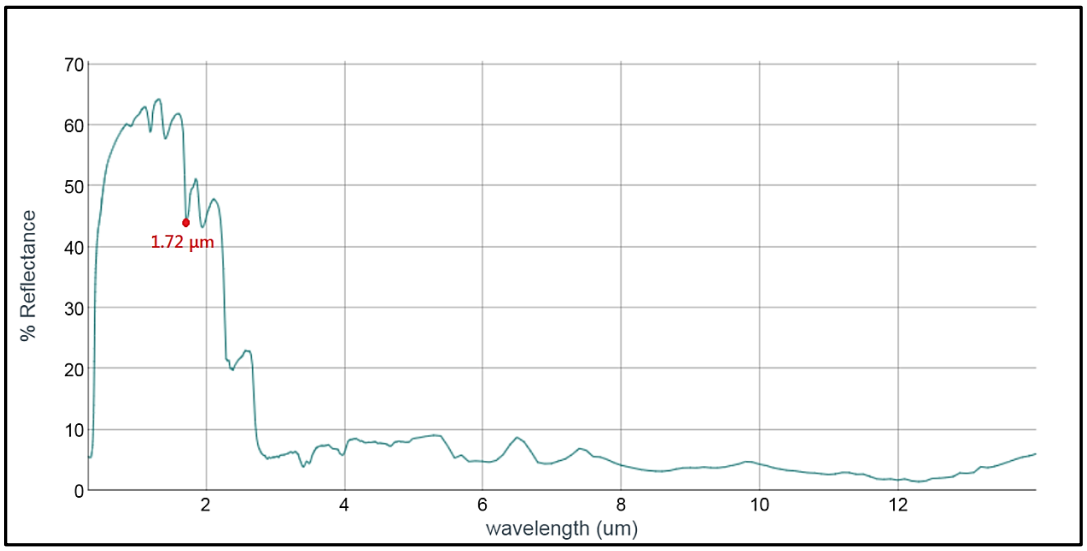

Figure 2.4. Spectra of white rubberized coating *(Ecostress Spectral Library, n.d.)*

Black unspecified rubber (Sample No.: 0833UUURBR), which particle size is solid and classified as a manmade roofing material, sub classified as rubber. As the material is black, it is clearly seen that the light is absorbed greatly. It is difficult to make a prediction if this material is plastic or not by looking only at its spectral plot can be seen in Figure 2.6.

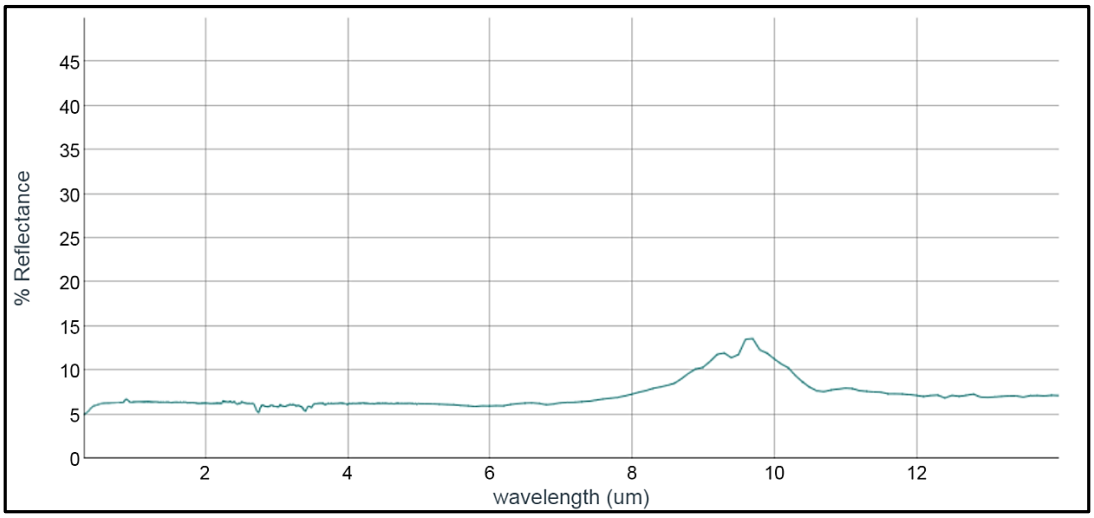

Figure 2.5. Spectra of black unspecified rubber *(Ecostress Spectral Library, n.d.)*

United States Geological Survey (USGS) Spectroscopy Library is another valuable source that can be utilized. USGS Lab focuses on identifying materials via remote sensing technologies on the earth and solar system. Five samples, respectively HDPE, LDPE, PETE, PVC and Vinyl, obtained from the laboratory given below.

Spectral behavior of HDPE plastic (Sample ID.: GDS351), which classified as a manmade material can be seen in Figure 2.7 (Kokaly, et al., 2017). There is an absorption, which neighbor to two shoulders, exists around 1.72 μm.

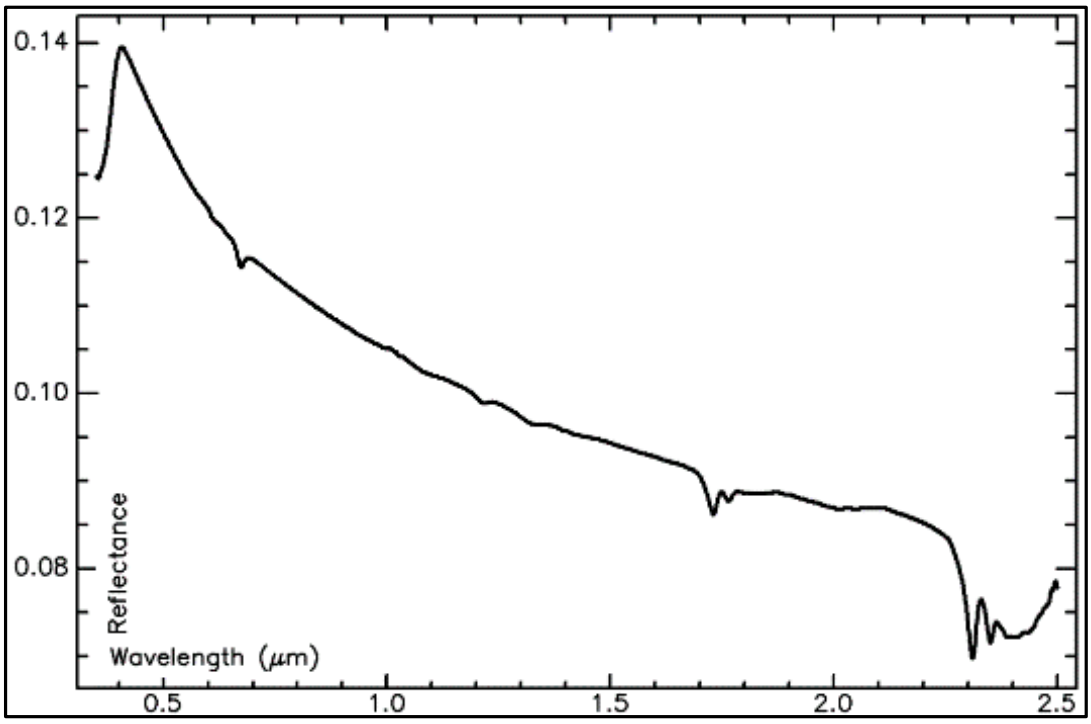

Figure 2.6. Spectra of HDPE plastic *(Kokaly, et al., 2017)*

LDPE plastic (Sample ID.: GDS402) spectra, which classified as a manmade material can be seen in Figure 2.8. Sample is a piece of plastic bag (Kokaly, et al., 2017). There is an apparent absorption, which neighbor to two shoulders, exists around 1.72 μm.

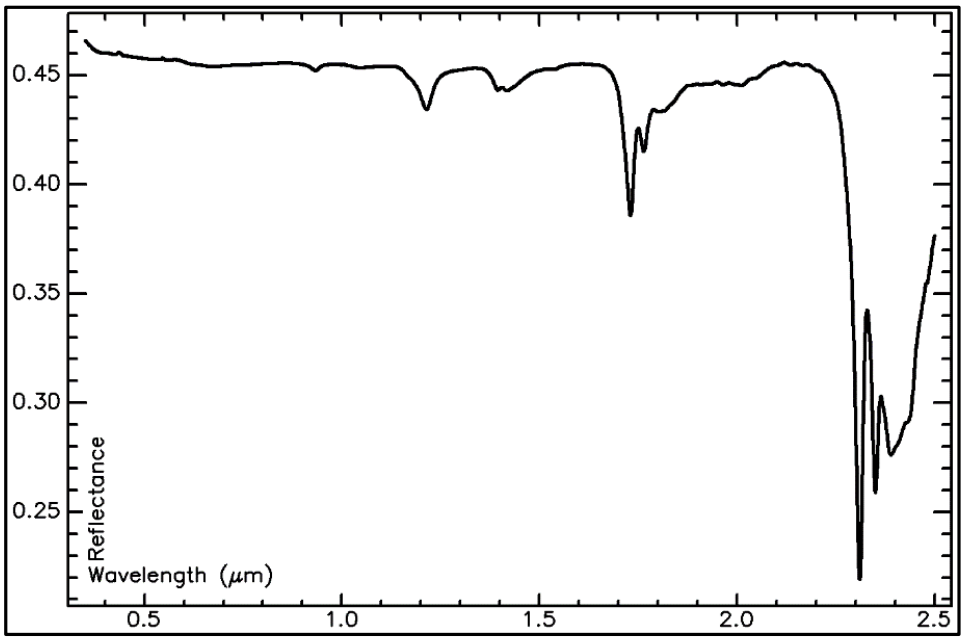

Figure 2.7. Spectra of LDPE plastic *(Kokaly, et al., 2017)*

PETE plastic (Sample ID.: GDS383) spectra is acquired from piece of a blue food container (Kokaly, et al., 2017) can be seen in Figure 2.9. There is also an apparent absorption, which neighbor to two shoulders, exists around 1.72 μm.

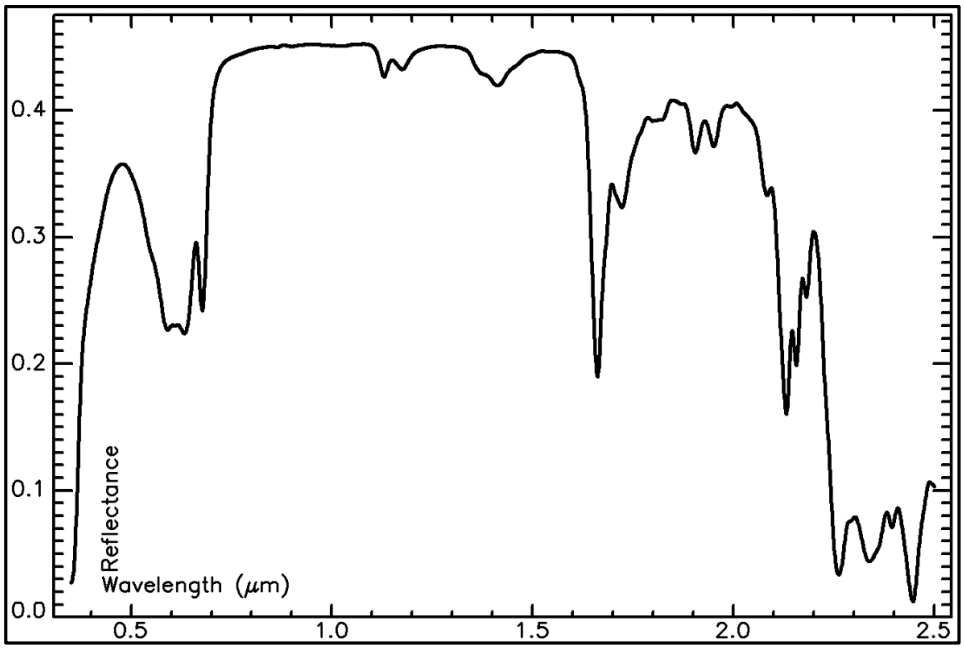

Figure 2.8. Spectra of PETE plastic *(Kokaly, et al., 2017)*

PVC plastic (Sample ID.: GDS338) spectra, which classified as a manmade material can be seen in Figure 2.10. Sample is a piece of white PVC pipe (Kokaly, et al., 2017). An absorption can be seen around 1.72 μm which neighbor to two shoulders.

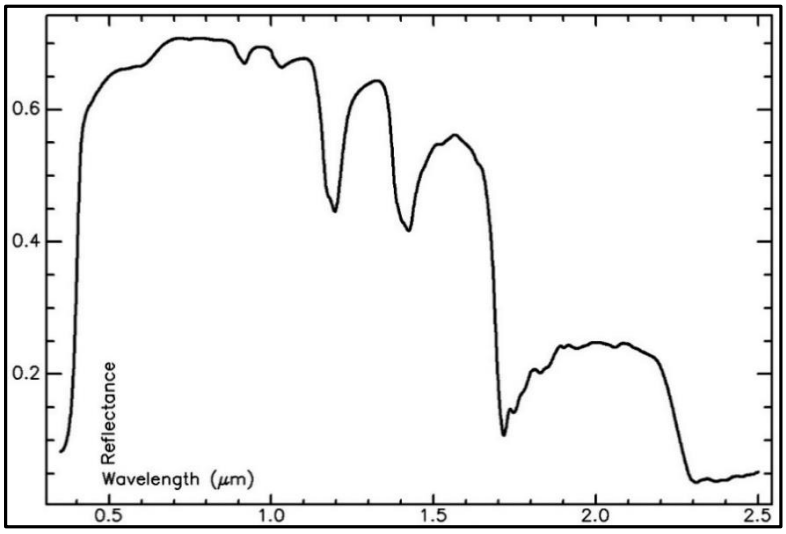

Figure 2.9. Spectra of PVC plastic *(Kokaly, et al., 2017)*

Vinyl plastic (Sample ID.: GDS372) spectra can be seen in Figure 2.11. Sample is a piece of white plastic vinyl sheet (Kokaly, et al., 2017). An absorption can be seen around 1.72 μm which neighbor to two shoulders.

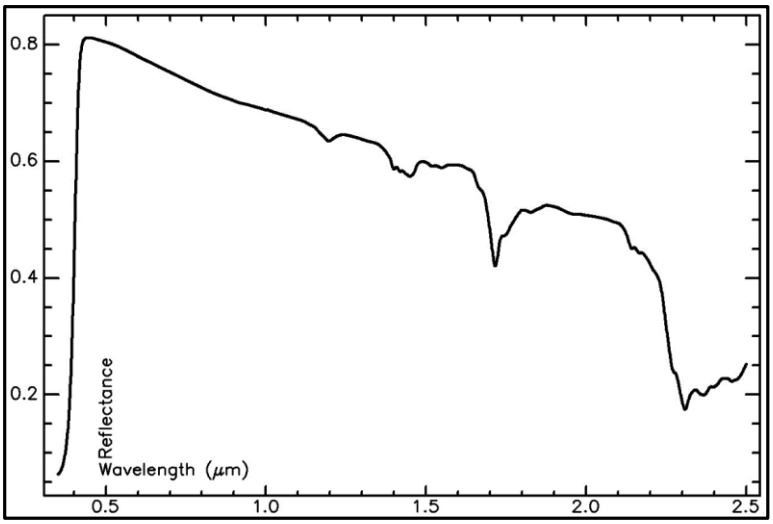

Figure 2.10. Spectra of vinyl plastic *(Kokaly, et al., 2017)*

CHAPTER 3

DATASET, TARGETS AND METHODOLOGY

3.1. Data and Parameters

Airborne Visible/Infrared Imaging Spectrometer (AVIRIS) is an Earth Remote Sensing tool which has 224 spectral bands, distributed between 380 and 2500 nanometers. Each of 224 different detectors has nearly 10-nanometer wavelength sensitive range that provides to cover the entire range between 380 nm and 2500 nm.

In this thesis, HSI, which is calibrated, orthocorrected and atmospherically uncorrected radiance data, is used that acquired by AVIRIS f170612t01p00r10 number flight, under the direction of the researcher Robert Green (AVIRIS Data Portal, 2019). Quicklook of image can be seen in Figure 3.1.

Figure 3.1. Quicklook Image *(AVIRIS Data Portal, 2019)*

The flight was held to cover an area of 446 kilometers in the northwest-southeast direction and 27 kilometers wide in the northeast-southwest direction in Los Angeles basin on 12.06.2017. Some technical specifications of the flight are given in table 3.1.

Table 3.1. Technical Specifications of the Flight f170612t01 *(AVIRIS Data Portal, 2019)*

Site Name	Solar Elevation	Solar Azimuth	Rotation
Southern California	70.5	241.64	66

The image, acquired by flight f170612t01, projection is UTM Zone 11 North and datum is WGS-84. Flight is rated as 85% clean and ground sample distance (GSD) is 15.5 meter. The starting and ending coordinates of image are given in table 3.2 (AVIRIS Flight: f170612t01, 2019).

Table 3.2. Starting and Ending Coordinates *(AVIRIS Flight: f170612t01, 2019)*

NASA Log#	Run ID	Start Lat.	Start Long.	Stop Lat.	Stop Long.
14203	p00_r10	34.471216	-119.0403167	33.0481311	-114.996019

3.2. Major Study Area and Study Fields

The whole image, which has been consciously chosen due to the fact that it contains various significant samples of plastic objects, is determined major study area which can be seen in Figure 3.2.

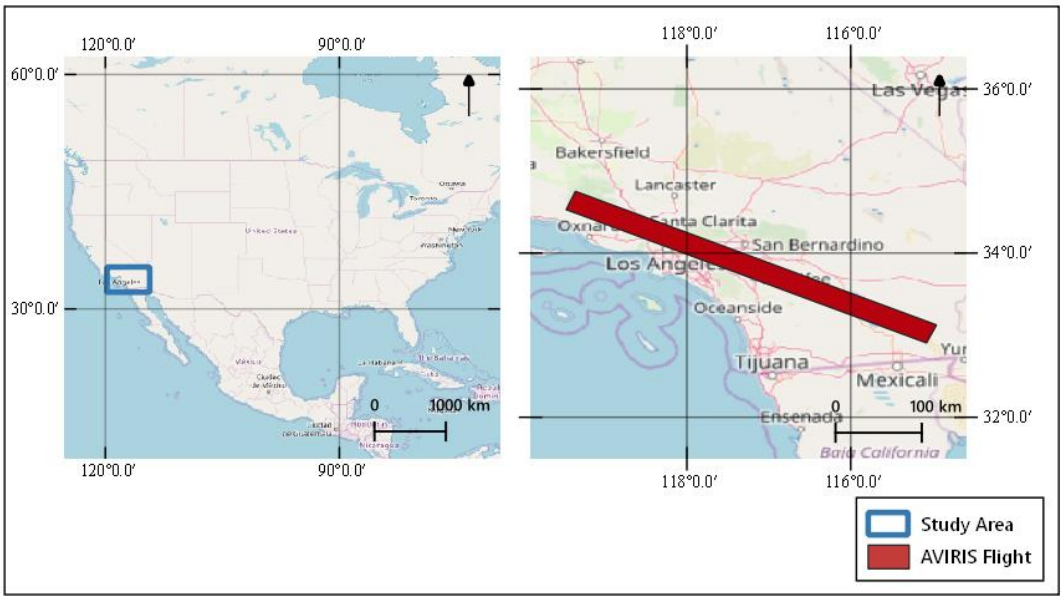

Figure 3.2. Study Area

In addition to study area, 15 divergent study field (SF) has been determined in this 446-kilometer-long large area shown in Figure 3.3.

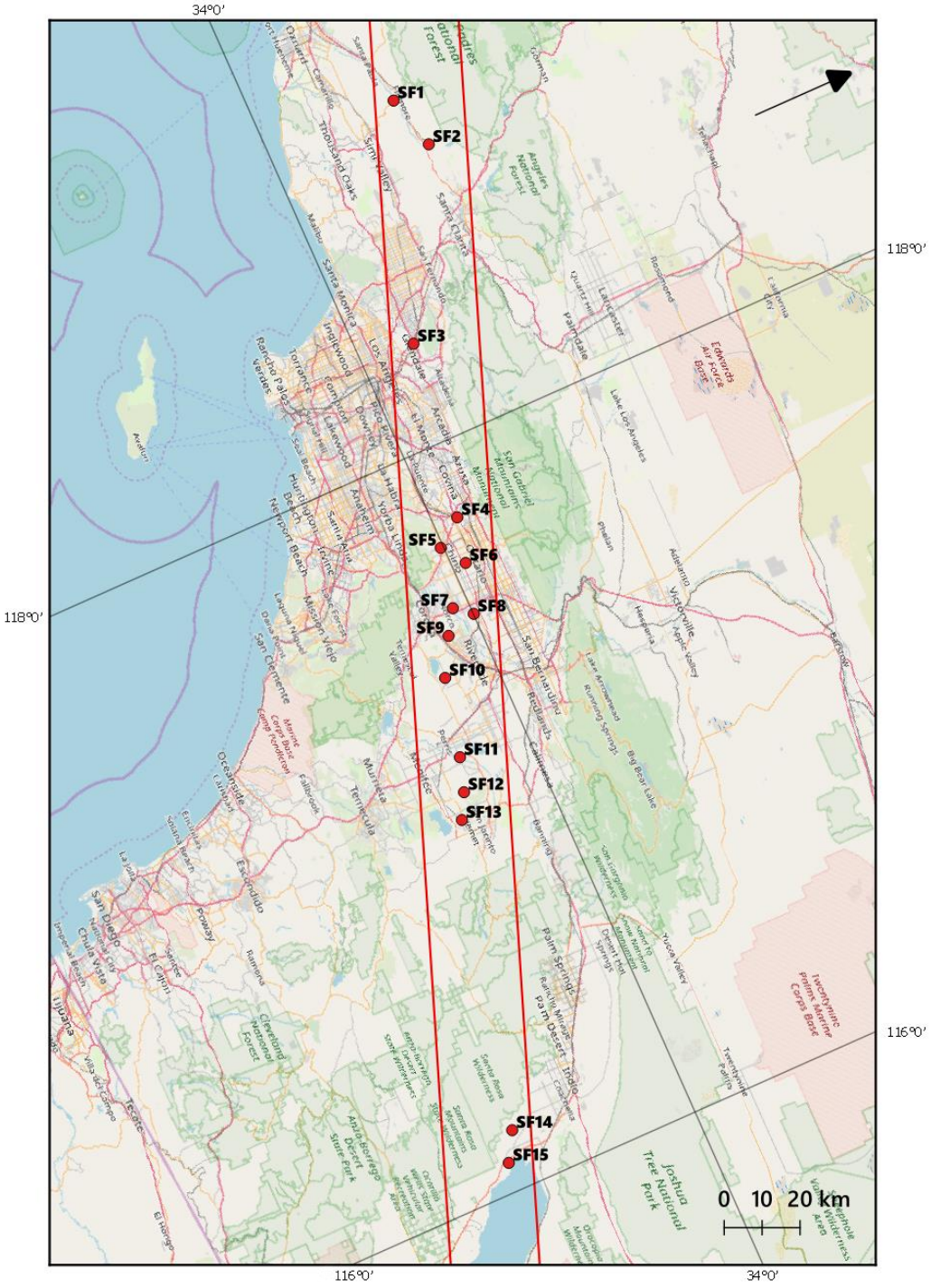

Figure 3.3. Study Fields

As a result of investigation these 15 SF, 4 different usage type of plastic objects, which discussed in section 3.3 and 3.4, have been detected with different size and spectra can be seen in Table 3.3.

Table 3.3. Study Fields Specifications

SF No	Latitude	Longitude	Area	Usage
SF1	34.38056	118.92764	4.71 km^2	Greenhouse
SF2	34.42079	118.77579	4.44 km	Greenhouse
SF3	34.15469	118.28343	0.45 km	Artificial Football Pitch
SF4	34.06912	117.78984	1.30 km	Artificial Football Pitch and Solar Panel
SF5	33.99201	117.73056	1.15 km	Artificial Football Pitch and Solar Panel
SF6	34.03849	117.66385	1.74 km	Artificial Football Pitch and Solar Panel
SF7	33.95424	117.56258	3.05 km	Artificial Football Pitch and Tent
SF8	34.00124	117.52425	1.19 km	Artificial Football Pitch and Solar Panel
SF9	33.91193	117.49670	0.40 km	Artificial Football Pitch
SF10	33.85522	117.39299	1.62 km	Greenhouse
SF11	33.80288	117.17344	15.55 km	Greenhouse
SF12	33.77350	117.07937	0.65 km	Tent-like Structure
SF13	33.73639	117.01055	4.49 km	Solar Panel
SF14	33.51189	116.16044	7.98 km	Greenhouse
SF15	33.46610	116.08084	45.55 km	Greenhouse, Solar Panel and Tent-like Structure

3.3. Target Objects Specifications

Due to the low resolution of the image used in this study, it is aimed to detect large sized plastics such as greenhouses. It is considered that if the techniques used to allow possible to detect large size plastics in the low-resolution image, it will be possible to detect small size plastics in the high-resolution image using the same techniques

There are many plastic objects of different sizes in the study area. Obviously study fields are chosen according to the existence and density of plastic as mentioned in section 3.2. A brief look at the targeted plastic objects, which aimed to be detected in this thesis, such as greenhouses and plastic mulched farmlands, artificial football pitches, solar panels and tent-like structures may be useful.

Greenhouses have provided a positive contribution to agricultural production and brought the plasticulture term to literature. On the other hand, they also have played a significant role in soil pollution. Previously, glass was usually used to cover greenhouses, but for the last few decades' plastic has been used more. The use of plastics in agriculture is not only in the form of conventional greenhouses but also as plastic mulched farmland can be seen in Figure 3.4. The main plastic types used for covering greenhouses and plastic mulched farmlands are polycarbonate, polyethylene, fiberglass, acrylic and PVC (vinyl).

Figure 3.4. Plastic greenhouses and plastic mulched farmlands *(Chen & Li, 2017)*

Another plastic object that is larger than the greenhouses is artificial football pitches. The usual football pitches are natural grass, but some special types of them are covered with synthetic/artificial turf/grass. Synthetic turf/grass is another form of plastic which can be seen in Figure 3.5. It is mostly formed by fibers which derived from polypropylene or nylon.

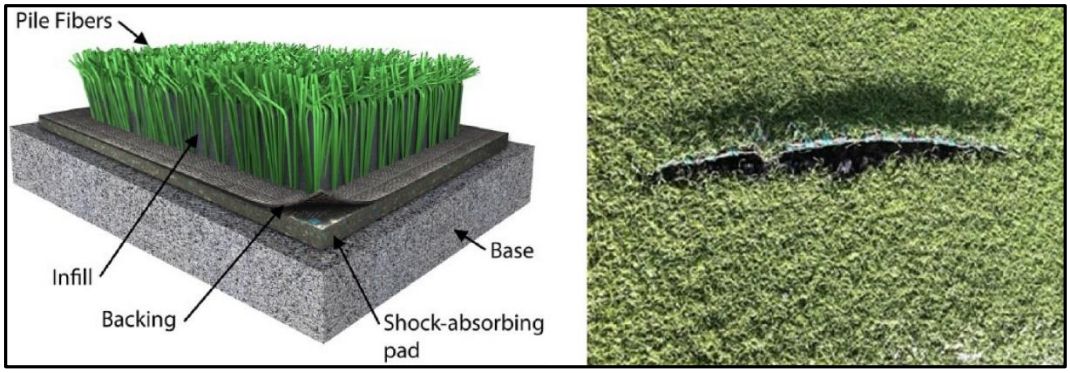

Figure 3.5. Components of synthetic turf/grass and seam damage on it. *(Jastifer, et al., 2019)*

Solar panels are not made up by plastic material, but generally, have a specific protective covering which usually consists of glass. This protective covering material can also have made up of plastic. Ethylene tetrafluoroethylene (ETFE) or Polyethylene terephthalate (PET) are commonly used as covering material of solar panel illustrated in Figure 3.6 (Svarc, 2018).

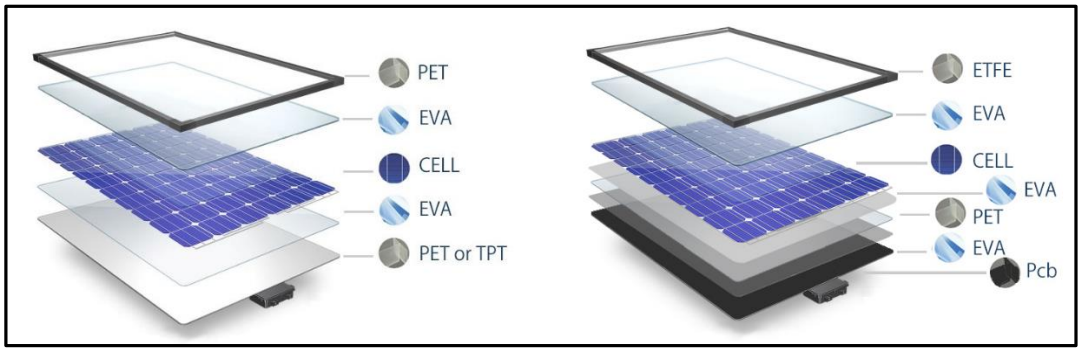

Figure 3.6. Plastic protective covering material and other layers of solar panel *(Svarc, 2018)*

The last plastic object aimed to be detected is tent or tent-like structure. The tent can be of many different sizes and types for its intended use. PVC (vinyl) is usually used in the production of plastic tents can be seen in Figure 3.7.

Figure 3.7. Vinyl personnel tents and vinyl tent strips *(Lloyd, et al., 2013)*

3.4. Spectra Samples of Target and Non-Target Objects

In this section, the spectral behaviors of the target plastic objects in the study fields are investigated. Spectra samples from four main objects which mention in section 3.3 has been gathered from AVIRIS image.

Figure 3.8 shows that greenhouse spectra have absorption around 1.72 µm which indicate that potential of plastic existence. Typical shoulder-feature-shoulder norm is also formed.

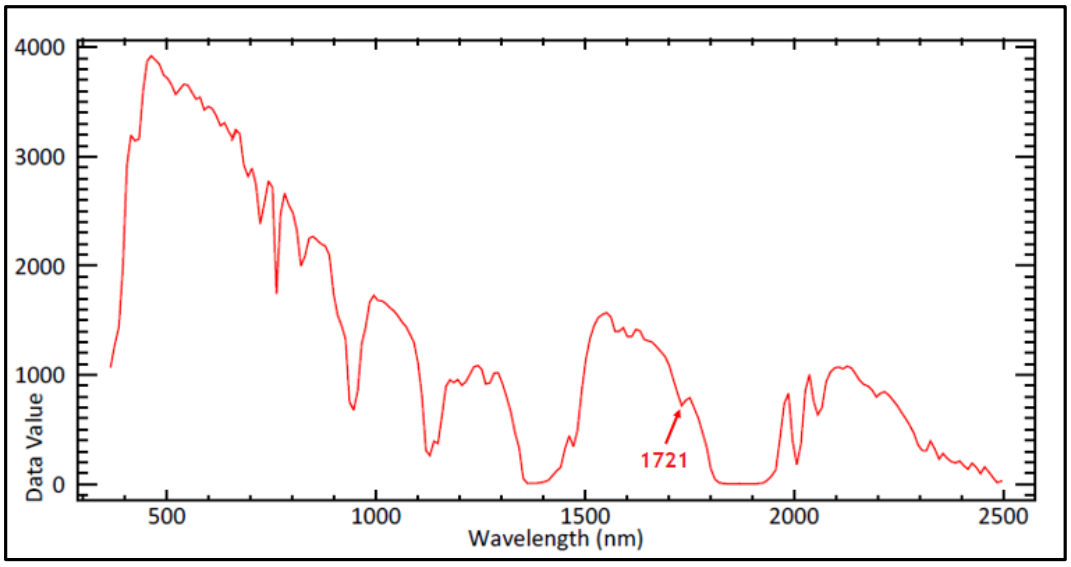

Figure 3.8. Spectra of greenhouse in SF1

Figure 3.9 shows that, solar panel have absorption around 1.72 µm which indicate that potential of plastic existence. Right shoulder can be interpreted as weak.

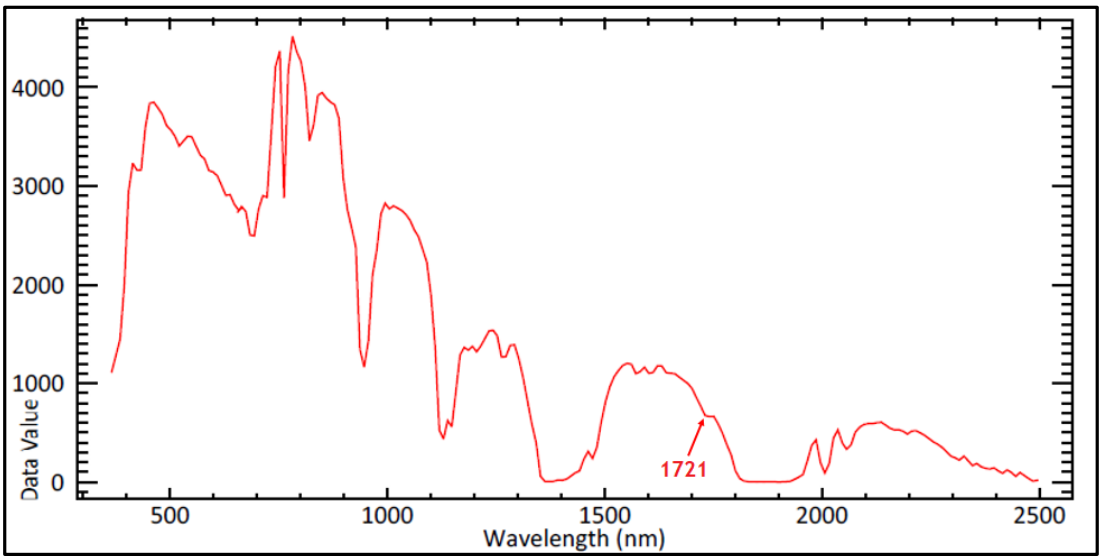

Figure 3.9. Spectra of solar panel in SF6

Figure 3.10 shows that, solar panel have absorption around 1.72 µm which indicate that potential of plastic existence The rate of absorption in the solar panels may vary on material used.

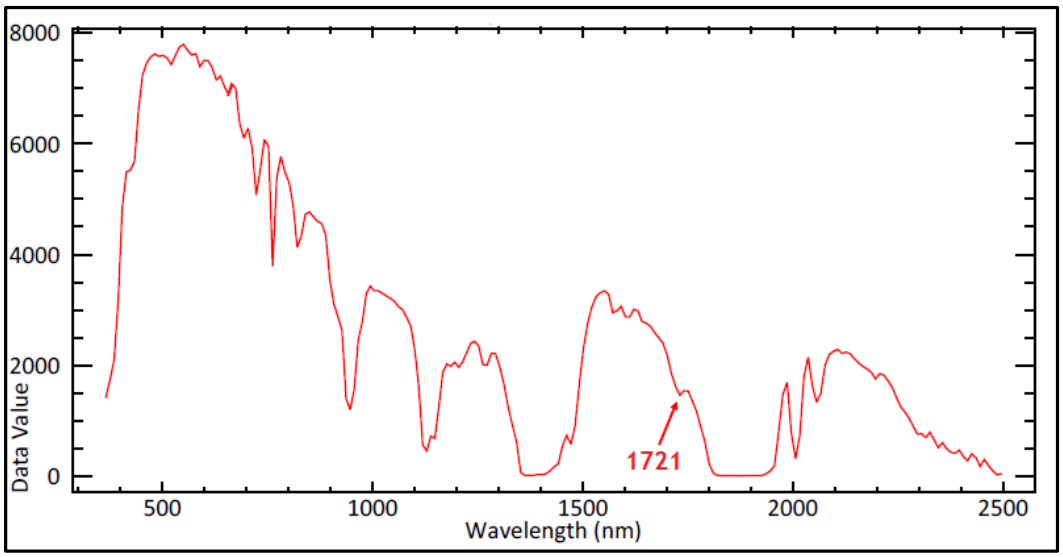

Figure 3.10. Spectra of solar panel in SF5

Figure 3.11 shows that, artificial football pitch spectra have absorption around 1.72 µm which indicate that potential of plastic existence. Plot clearly shows that the right shoulder is much stronger than in the greenhouse and solar panel.

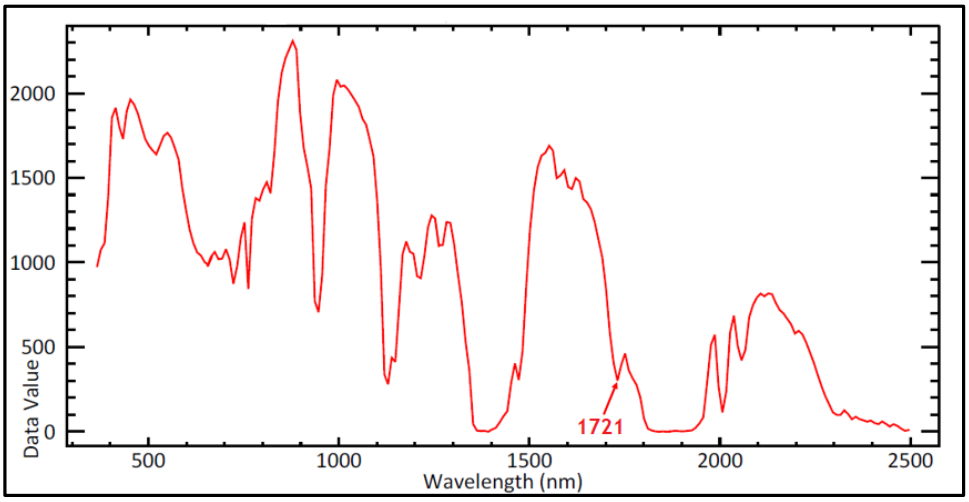

Figure 3.11. Spectra of synthetic turf/grass in SF3

Figure 3.11 shows that, tent-like structure spectra have absorption around 1.72 µm which indicate that potential of plastic existence. Typical shoulder-feature-shoulder norm also formed.

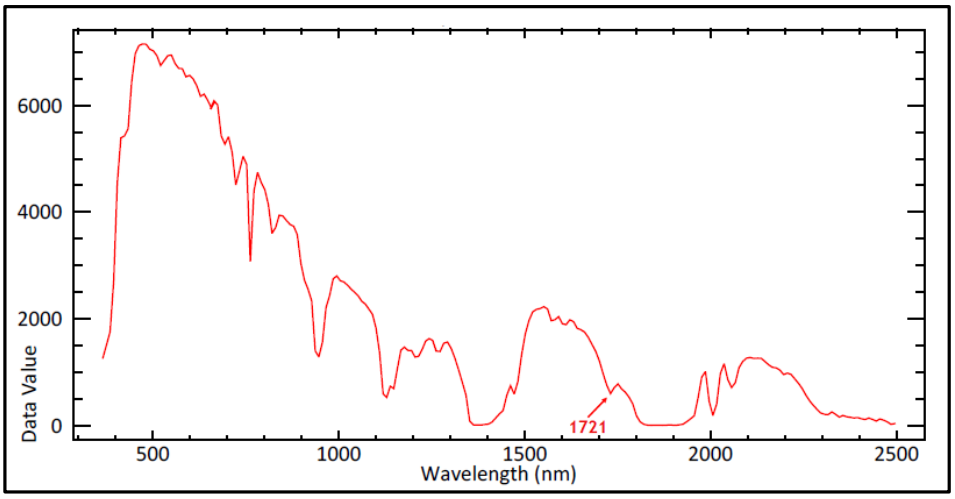

Figure 3.12. Spectra of tent in SF15

A glance at the spectra of other materials and substances around 1.72 µm in the same image allows comparison with the plastic spectra.

When the soil spectra are examined, it is seen that almost straight line is formed around 1.72 µm can be seen in Figure 3.13. This linear behavior indicates the absence of plastic.

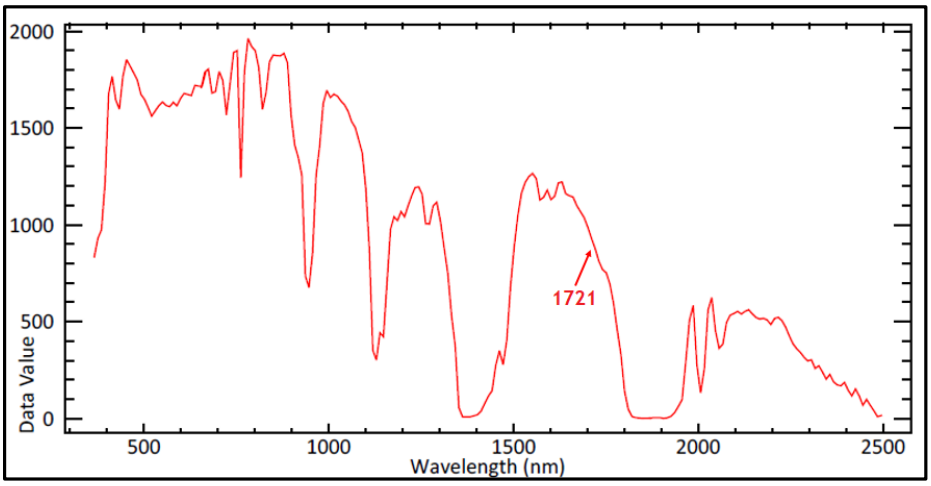

Figure 3.13. Spectra of soil

While exhibiting a different character, the asphalt's spectra also turns into an almost straight line around 1.72 µm, such as the soil's spectra, which again indicates the absence of plastic can be seen in Figure 3.14.

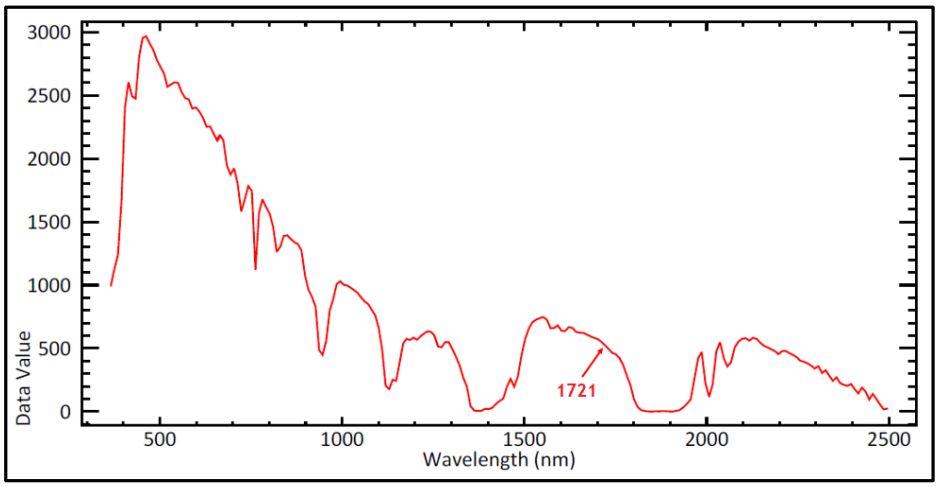

Figure 3.14. Spectra of asphalt

3.5. Outline of the Plastic Existence Index Algorithm

It is beneficial to investigate Hydrocarbon Index (HI) before defining Plastic Existence Index (PEI).

HI is a mathematical algorithm which developed by Kühn, et al. (2004) for the direct detection of HC. HI basically evaluates the geometry around 1.73 µm. and runs a perpendicular line (BB') as a HC existence indicator illustrated in Figure 3.15.

According to HI algorithm, plot geometry forms two cases:

i. If A, B and C constitute a triangle, then HI>0, then HC exist.

ii. If A, B, and C constitute nearly a straight line, then HI=0, then HC is absent.

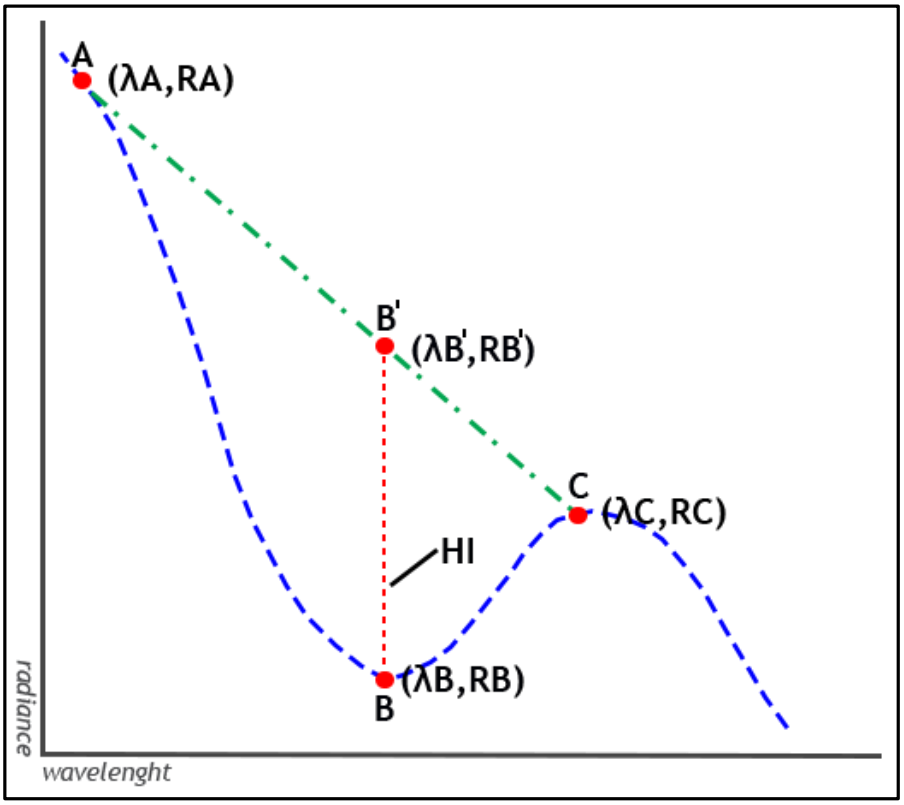

Figure 3.15. Enlarged view of spectra around 1.73 µm *(Kühn, et al., 2004)*

HI can be calculated with using Equation 3.1 (Kühn, et al., 2004).

$$HI = (\lambda B - \lambda A)\frac{RC - RA}{\lambda C - \lambda A} + RA - RB \quad (3.1)$$

The formula can also be expressed as shown in Equation 3.2 (Kühn, et al., 2004).

$$HI = \frac{(\lambda B - \lambda A)}{(\lambda C - \lambda A)} \times (RC - RA) + RA - RB \quad (3.2)$$

where $R_{A;}$ λ_A, $R_{B;}$ λ_B, $R_{C;}$ λ_C *are* radiance/wavelength pairs (Kühn, et al., 2004).

Kühn, et al., (2004) stated that 1.73 μm is the key point for HC detection in their HyMAP data. However, when the spectra of different plastic materials in AVIRIS data are examined, it is seen that point 1.72 μm is more meaningful for POD which given in Figure 3.8, Figure 3.9, Figure 3.10, Figure 3.11, and Figure 3.12.

Moreover, plastic spectra samples in reliable libraries support this suggestion which given in Figure 2.5, Figure 2.6, Figure 2.8, Figure 2.9, Figure 2.10, Figure 2.11, and Figure 2.12.

In addition to the values observed from AVIRIS data, since the spectral values examined from reliable libraries are taken as a reference, 1721.231 nm has been determined as the feature point, which symbolized with the B.

When spectra plots are analyzed, it has been observed that left shoulder is longer that right shoulder. Correspondingly, the A is selected as a distant point, 1681.383 nm as left shoulder in order to obtain a greater curve and thus make the HI line more prominent.

1731.92, which is very close to B and known to be used in the detection of HC, has been consciously left inside the geometry. Since a downward movement is generally seen after the point 1741.153 nm which is the closest point after 1731.92, this point has been chosen as right shoulder to maintain geometrical form.

As a result of the algorithm implemented with selected bands (A:1681.383 nm, B:1741.153 nm, C: 1721.231), it is observed that plastic objects take positive data values and extracted from non-plastic objects. When the spectral profiles of plastic objects are examined, it is observed that the data values are mostly intensified between 50 and 150 can be seen in Figure 3.16 and Figure3.17.

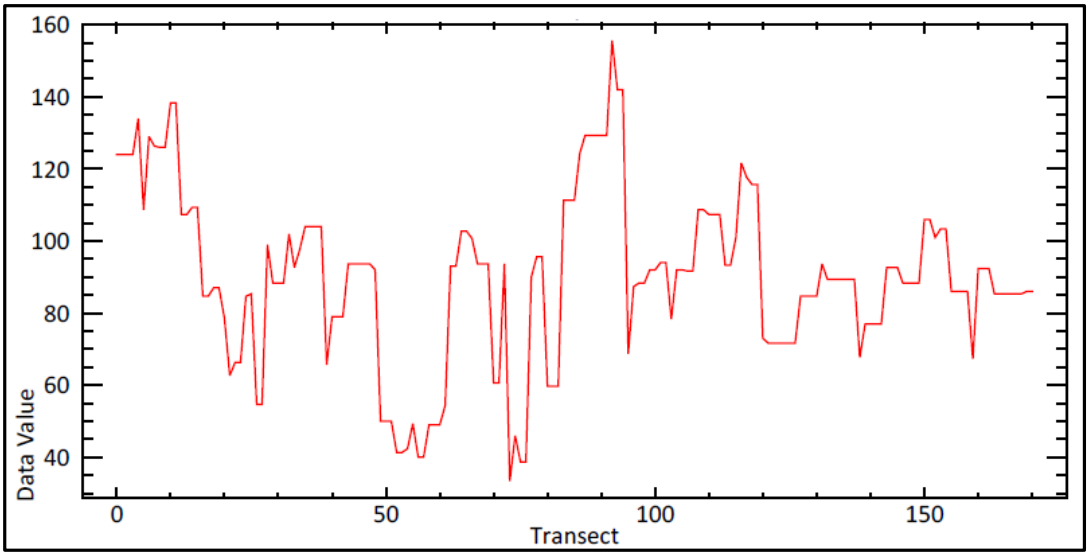

Figure 3.16. Spectral profile of a greenhouse in SF15

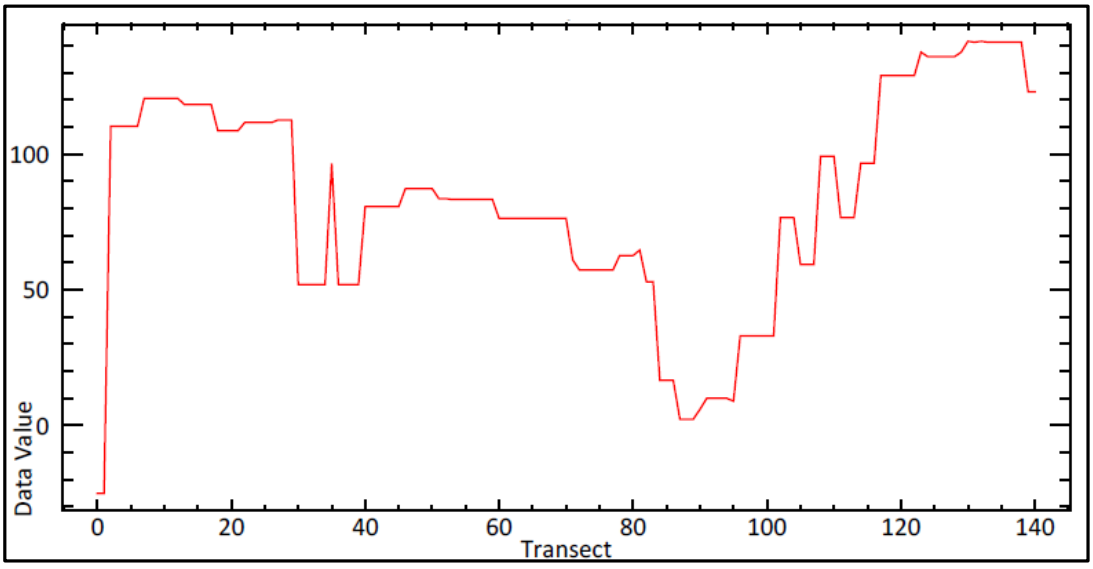

Figure 3.17. Spectral profile of a greenhouse in SF11

It is observed that non-plastic objects such as soil and water take negative values extensively but can also take a very small proportion of positive value can be seen in Figure 3.18 and Figure 3.19.

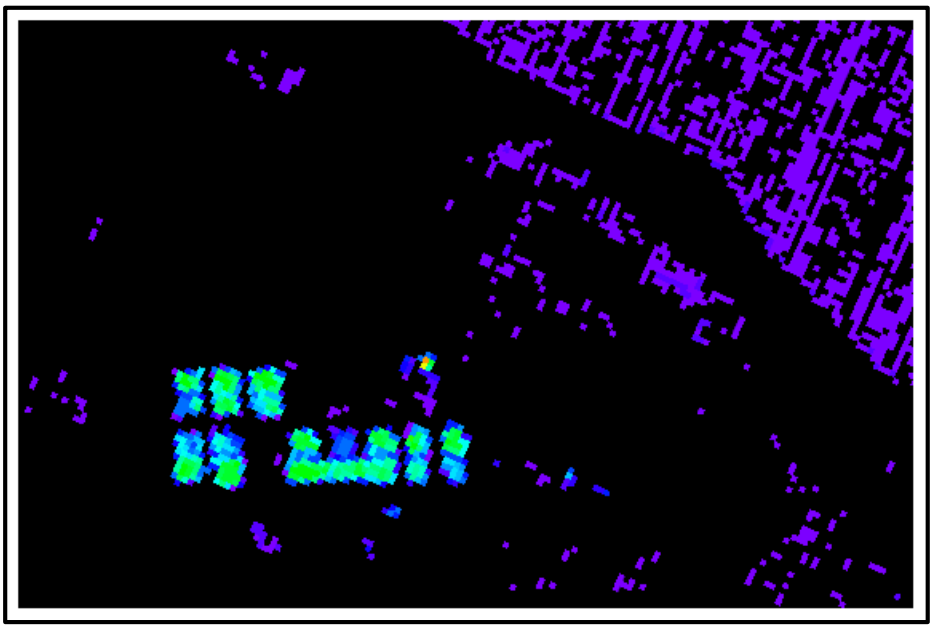

Figure 3.18. Undesirable noise-like pixel around greenhouses in the west of the Salton Sea (SF15)

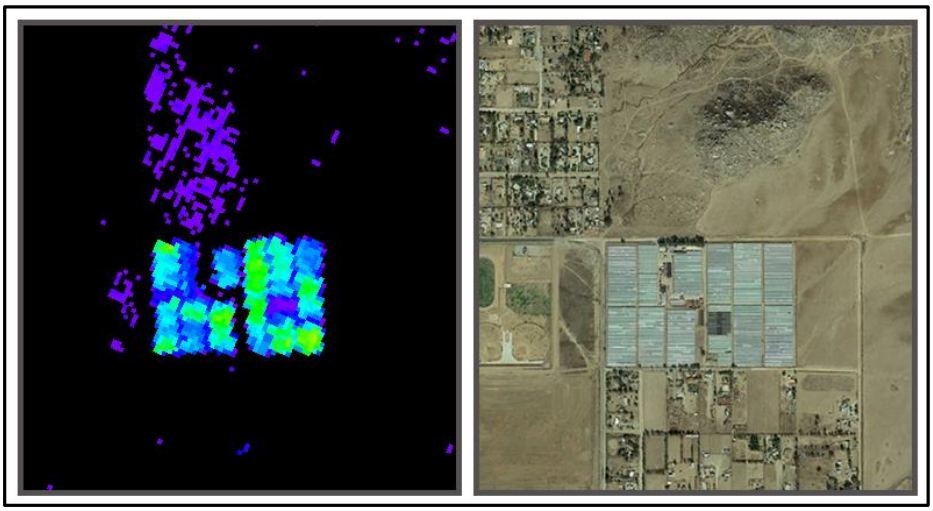

Figure 3.19. Undesirable noise-like pixels around greenhouses and corresponding 22.10.2016 dates high-resolution satellite image (SF11)

The reasons for this unexpected situation, which is thought to be caused by multiple issues, have been explained by examining the situation in two different study field.

Lenz, et al. (2015) stated that atmospheric water has an absorption feature around 1730 Nm. Some plastic objects in the study area are very close to the water masses can be seen in Figure 3.18. Due to the fact that the concentration of water vapor in the air is intense near water masses, data values of a non-plastic object near these areas may include positive values.

Additionally, in areas like soil and rocks, which sample of it can be seen in Figure 3.19, where there is no plastic existence, oil or its derivative hydrocarbon seepage or another chemical substance effect also may cause positive data values.

Another important factor is the resolution of the image. A plastic whose size is below the image resolution can blend with a non-plastic object and form mixed pixel issue and this probably results in positive data values.

When the spectral profiles of these non-plastic objects and areas are examined, it is observed that positive data values are generally intensified in the range 0 through 10 given in Figure 3.20 and 3.21.

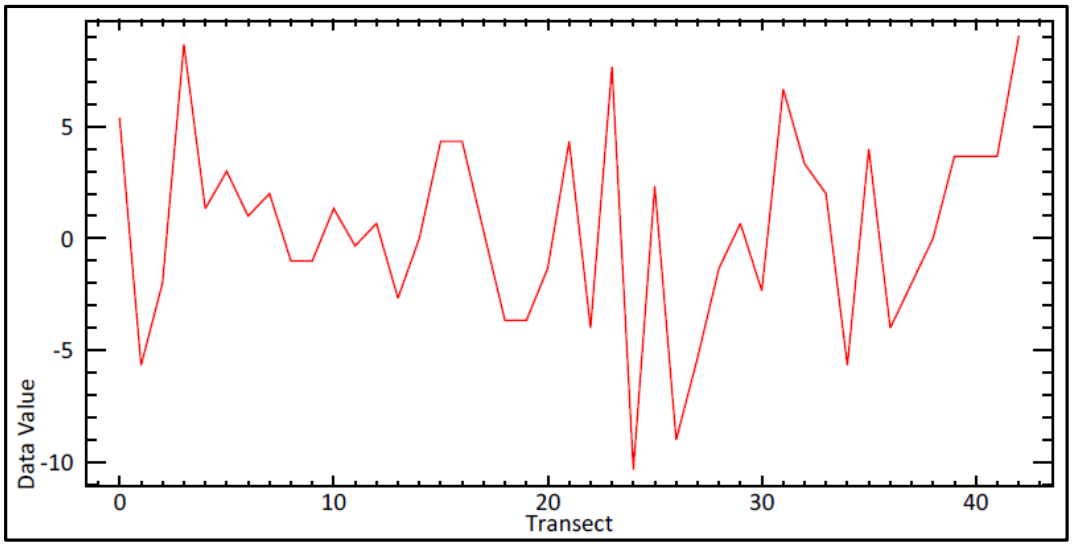

Figure 3.20. Spectral profile of noise-like pixel around greenhouses in the west of the Salton Sea in SF15

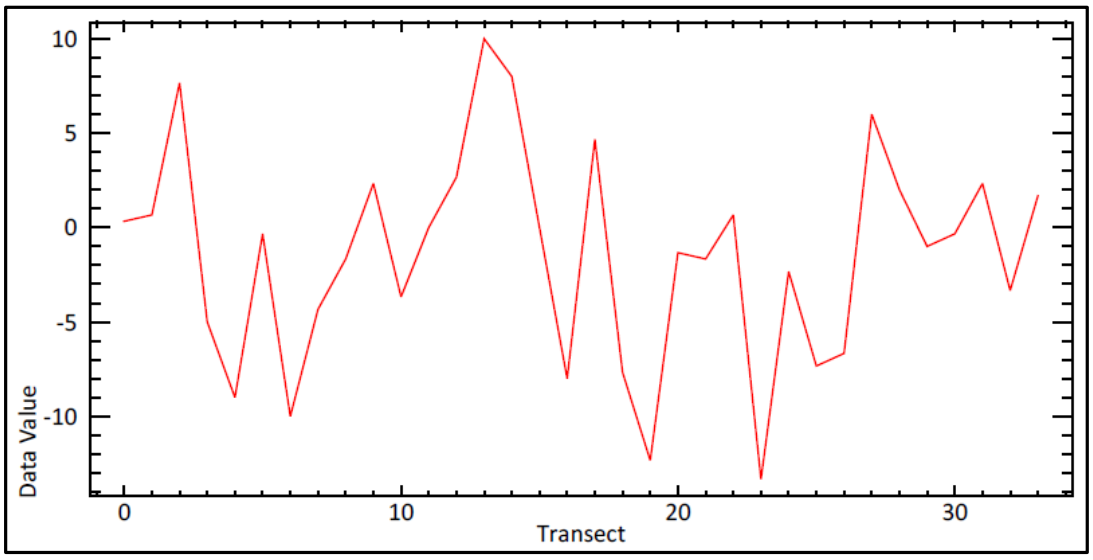

Figure 3.21. Spectral profile of the noise-like pixels in the north of the greenhouse in SF11

With taking account of spectral profiles of the non-plastics objects that take positive values, reducing the amount of the output value of the algorithm amount as N, substantially eliminate this situation which can be defined as hyperspectral algorithm-noise.

It is true that some pixels will be lost as a result of this process. But note that main purpose is the detection of a certain size of the plastic, which is directly related to the resolution of the image, and this loss has been considered as negligible.

The constant N value, which is a tool that acquires sharper results and to get rid of the noise-like pixels, has been determined as 10.

The comparative image before and after the reducing process can be seen in Figure 3.22. and Figure 3.23.

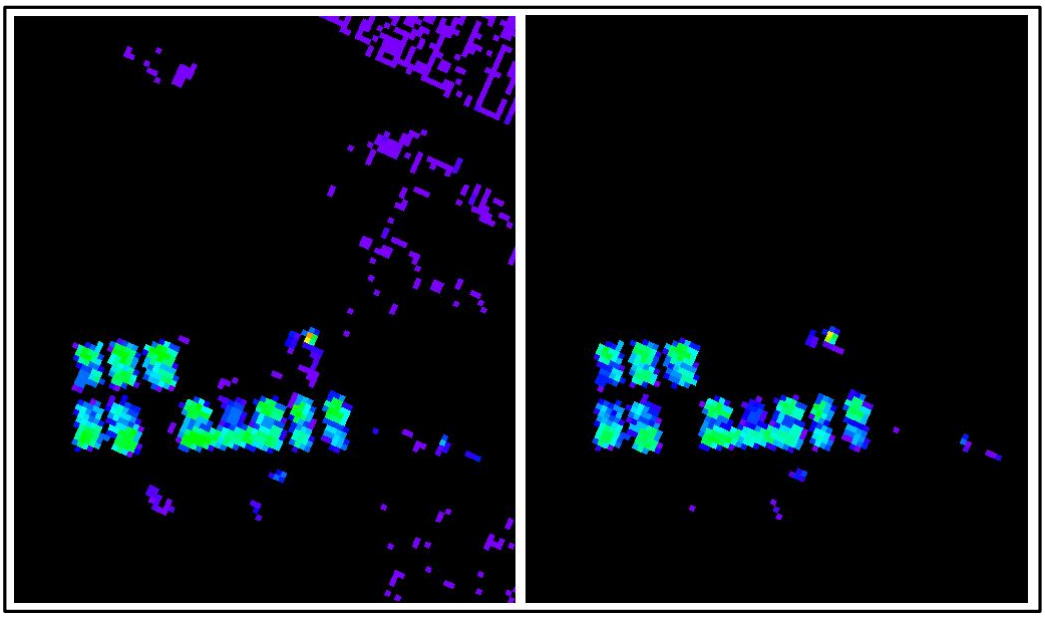

Figure 3.22. Noisy-like pixels before and after the reducing process in SF15

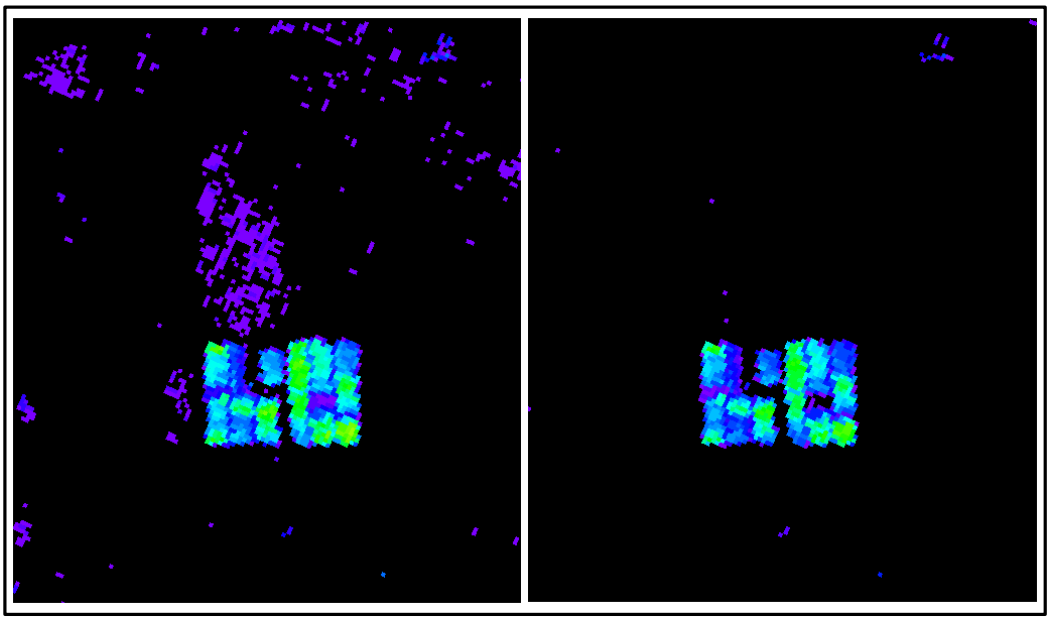

Figure 3.23. Noisy-like pixels before and after the reducing process in SF11

After corrections and changes mentioned above, the algorithm has been referred to as the plastic existence index (PEI) henceforth.

Considering this modification, it is useful to examine how the formula is composed. The formula has been developed based on the similarity theorem as shown in Figure 3.24.

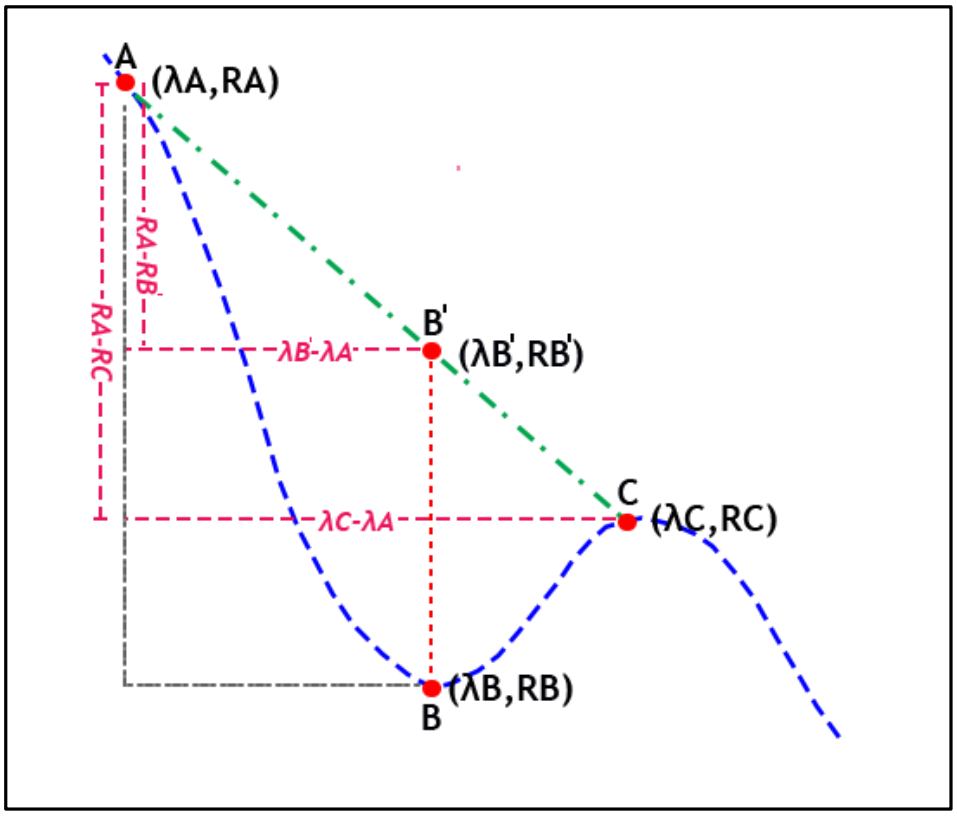

Figure 3.24. Geometrical expression of the algorithm

Equation 3.3 and Equation 3.4 are obtained as a result of similarity theorem using index point difference values.

$$\frac{(RA - RB')}{(\lambda B - \lambda A)} = \frac{(RA - RC)}{(\lambda C - \lambda A)} \tag{3.3}$$

$$(RB' - RA) = \frac{(\lambda B - \lambda A)}{(\lambda C - \lambda A)} \times (RC - RA) \tag{3.4}$$

If equivalent of the *(RB'-RA)* expression in Equation 3.4 is inserted to Equation 3.1, Equation 3.5 is obtained.

$$HI = RB' - RA + RA - RB \tag{3.5}$$

Consequently, if RB' = RB there is no positive value BB' line which means there is no plastic. The magnitude of BB', which is directly related to the radiance value, gives a clue to the level of purity and homogeneity of the plastic object.

For a clear understanding of the algorithm steps, the flowchart of the algorithm is shown in Figure 3.25.

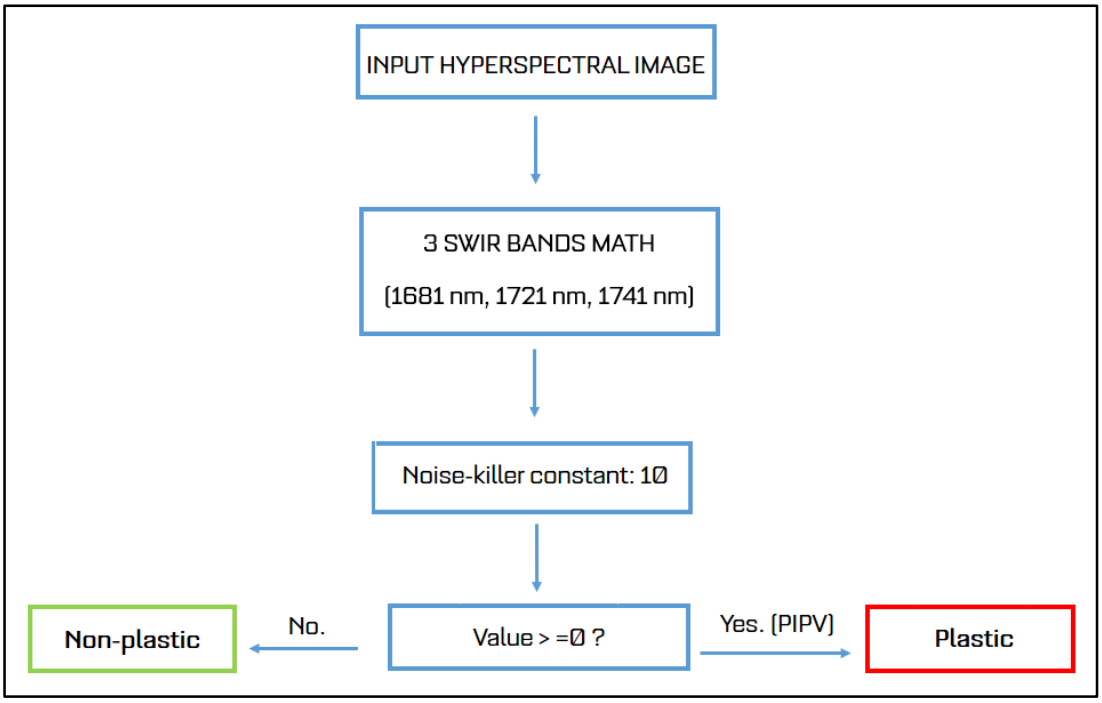

Figure 3.25. Flowchart of PEI Algorithm

CHAPTER 4

IMPLEMENTATION OF THE METHODOLOGY

4.1. Data Preprocessing

Data size is 23.91 GB. In order to process this great size image more efficiently, 15 different subset images have been generated from it based on the SF borders. Corrections have not applied to data, only the format is converted to TIFF in order to eliminate problems that may occur during the implementation of the algorithm and related processes in QGIS, ENVI and MATLAB programs.

After the image has been resized, the reference data which can be called ground truth has been determined for the purpose of assessing the accuracy of the results. The ground truth has been produced manually based on the true color composite AVIRIS data can be seen in Figure 4.1.

Due to the fact that GSD of the image is rather low (15.5 meter) it is possible to have some errors in the ground truth. In order to minimize these errors as much as possible, the ground truth has been tried to produce as precisely as possible.

It is considered that the detection process using the same image will contain very similar errors resulting from the GSD and that the errors in the same direction will eliminate each other and that a slight improvement in the error tolerances will occur.

Ground truth data, which produced in vector format and .shp extension, has been converted to raster image format and tiff extension in order to compare with PEI Algorithm results.

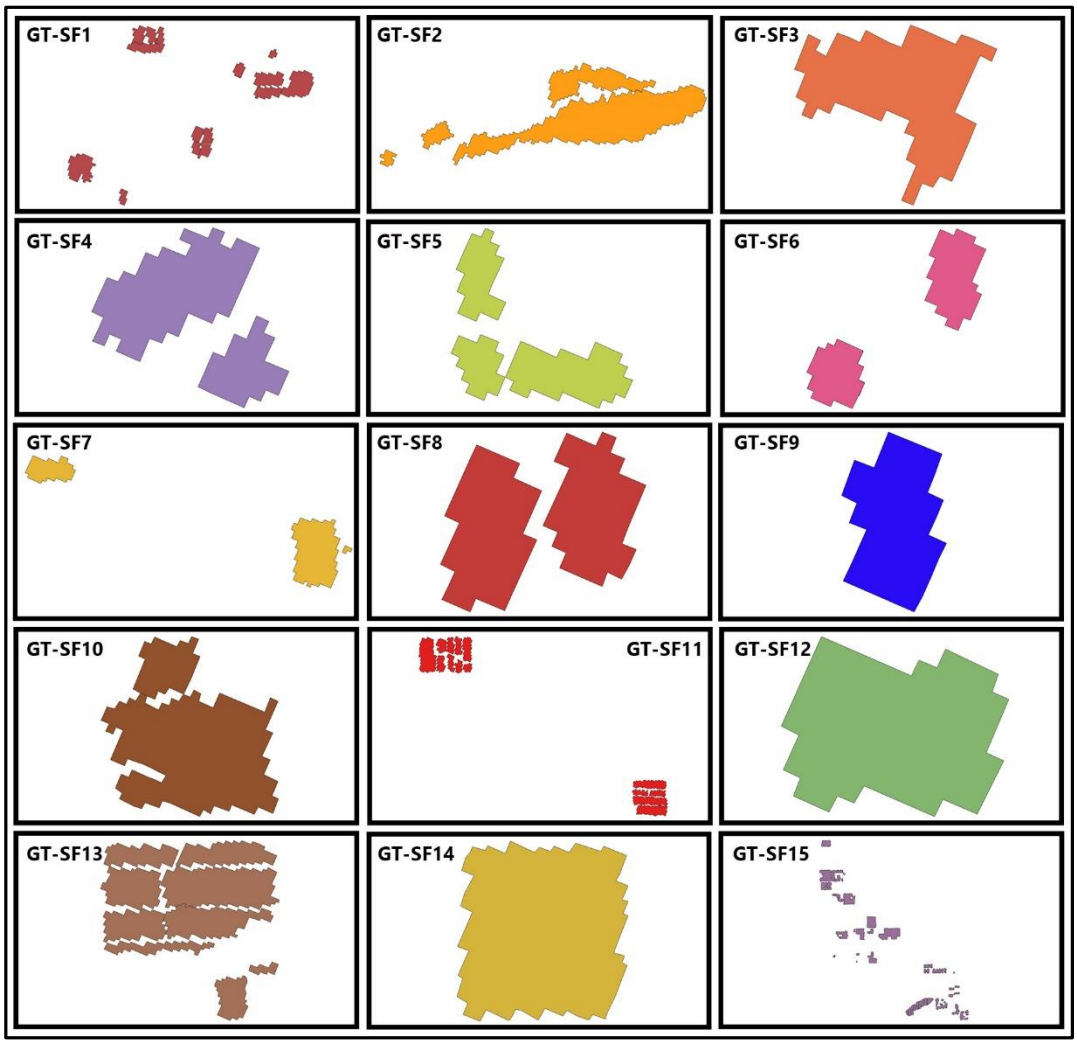

Figure 4.1. Manually produced ground truth data

4.2. Plastic Existence Index Algorithm Results

Based on the equations mentioned in section 3.5, PEI can be computed as shown in Equation 4.1.

$$PEI = (\frac{(1721\ nm - 1681\ nm)}{(1741\ nm\ - 1681\ nm)} \times (R1741 - R1681) + R1681 - R1721) - 10 \quad (4.1)$$

And it can be expressed that shown in Equation 4.2.

$$PEI = (0.67 \times (R1741 - R1701) + R1701 - R1731) - 10 \quad (4.2)$$

where *10* is noise killer constant value.

Resultant can be written in ENVI Band Math as follows as given in Equation 4.3.

$$PEI = (0.67 \times ((float(B146) - float(B140)) + float(B140) - float(B144) - 10 \quad (4.3)$$

The presence of the plastic has been successfully detected as a result of implementing the function given in Equation 4.3. Results have been visualized with the figures given below.

PEI Algorithm results in both positive and negative values. Since the presence of a plastic object is associated with positive values, it is thought that using a new term which named Post Index Positive Value (PIPV) for positive output values is conceptually useful.

The interval between the maximum and minimum PIPV, except outliners, has been divided into 30 equal and converted to a color scale from blue to red for a better visual experience.

The lightest tone of blue represents the smallest positive value resulting from the algorithm, in other words, the plastic object with the lowest spectral reflection.

The darkest tone of red represents the highest positive value resulting from the algorithm, in other words, the plastic object with the highest spectral reflection. Histogram of correctly classified plastic pixels is given in figures between 5.1 and 5.15, in section 5.1.

The following figures present comparative images of each study field Same concept is in every figure for ease of examination. The image generated after PEI Algorithm is shown with A, 12.06.2017 dated true color composite (R:647.97 nm, G:550.30 nm, B:453.07 nm) AVIRIS image is shown with B, and high-resolution satellite image that can be found closest to 12.06.2017 and corresponding to SFs is shown in C. In order to give some details, D has been formed in some figures.

Figure 4.2 presents the comparative images of the SF1. The greenhouses, which marked with red rectangles in 4.2.C., have been successfully detected by the algorithm. PIPV is between 1.33 and 105.66.

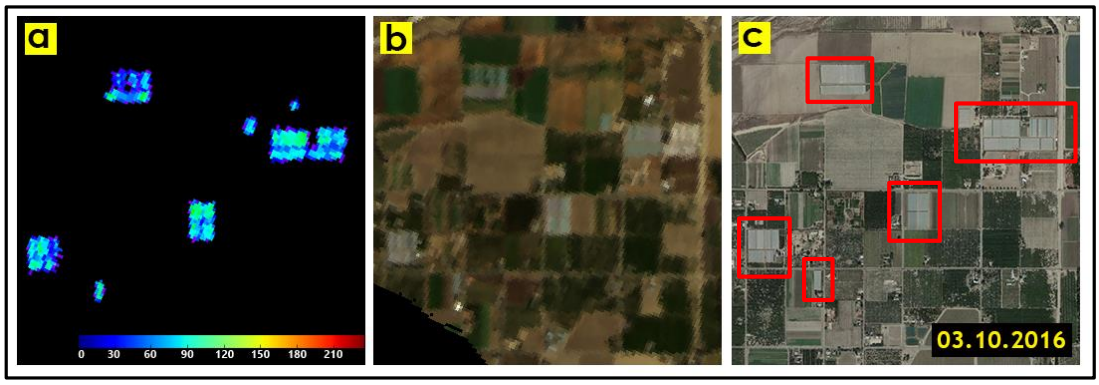

Figure 4.2. PEI Algorithm results and comparative images of SF1

Figure 4.3 presents the comparative images of the SF2. The greenhouses have been successfully detected by the algorithm. PIPV is between 2.66 and 101.66.

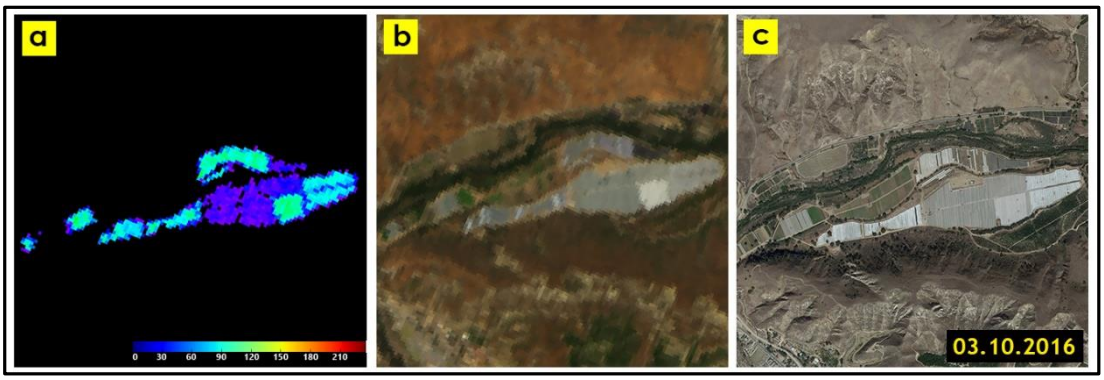

Figure 4.3. PEI Algorithm results and comparative images of SF2

Figure 4.4 presents the comparative images of the SF3. Four artificial football pitches have been successfully detected by the algorithm. PIPV is between 0.66 and 233.00. Next to the artificial football pitches, there are three more football fields, which are relatively larger and covered with natural grass. The PIPV of these fields is below zero.

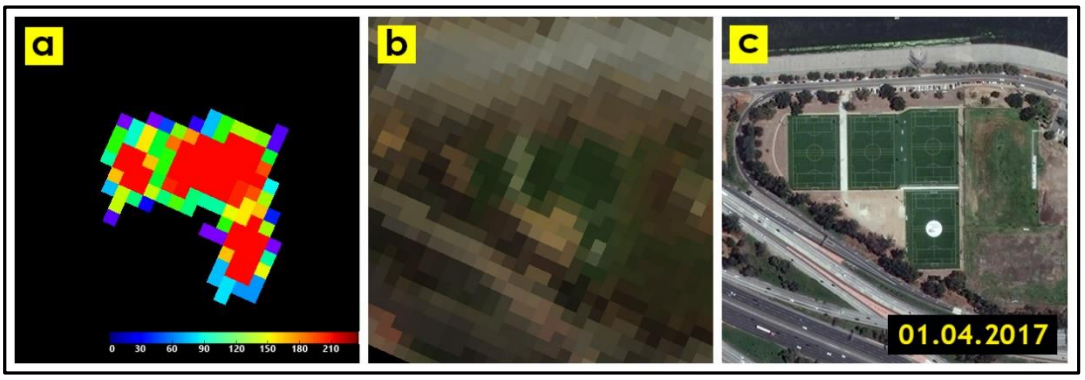

Figure 4.4. PEI Algorithm results and comparative images of SF3

Figure 4.5 presents the comparative images of the SF4. An artificial football pitch and solar panel have been successfully detected by the algorithm. PIPV is between 0.66 and 130.00.

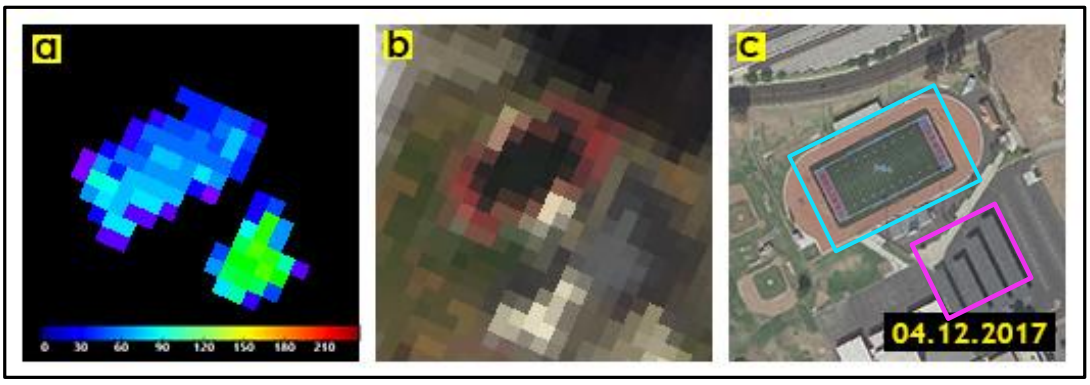

Figure 4.5. PEI Algorithm results and comparative images of SF4

Figure 4.6 presents the comparative images of the SF5. An artificial football pitch and solar panels have been successfully detected by the algorithm. PIPV is between 1.00 and 233.33. An artificial football pitch is marked with a cyan rectangle and solar panels are marked with a magenta rectangle in 4.6.C. PIPV of nearby green areas is below zero.

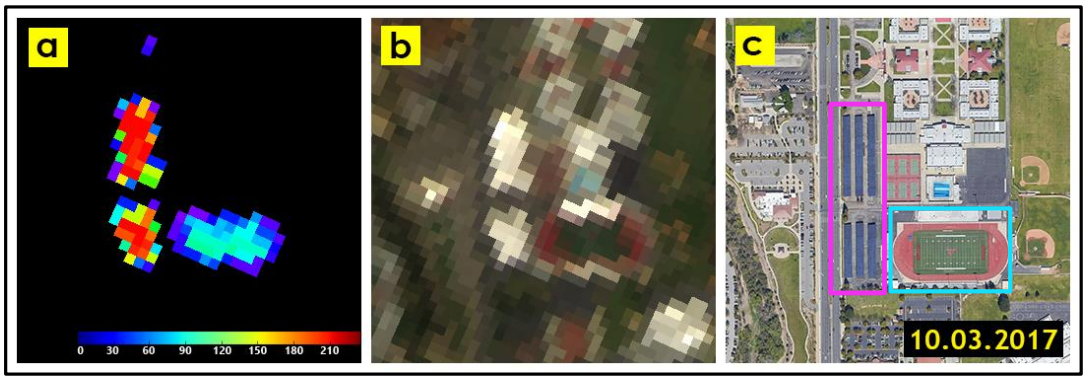

Figure 4.6. PEI Algorithm results and comparative images of SF5

Figure 4.7 presents the comparative images of the SF6. An artificial football pitch and solar panels have been successfully detected by the algorithm. An artificial football pitch is marked with a cyan rectangle and solar panels are marked with a magenta rectangle in 4.7.C. The algorithm has also identified 4 buildings as plastic. The unusual situation here has also been addressed in the Chapter 5. PIPV is between 1.11 and 87.66.

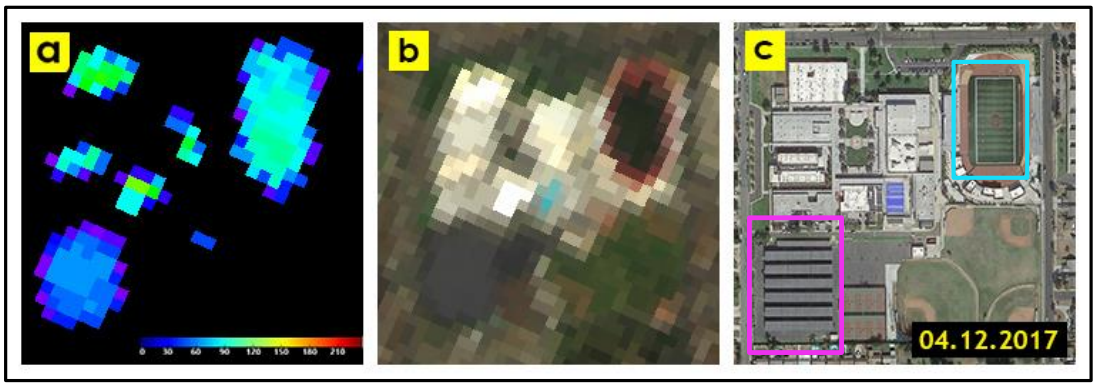

Figure 4.7. PEI Algorithm results and comparative images of SF6

Figure 4.8 presents the comparative images of the SF7. Four adjacent and one discrete artificial football pitches and a tent have been successfully detected by the algorithm. An artificial football pitches are marked with a cyan rectangle in 4.8.C. Tent can be seen in detail in 4.8.D. PIPV is between 1.66 and 183.33.

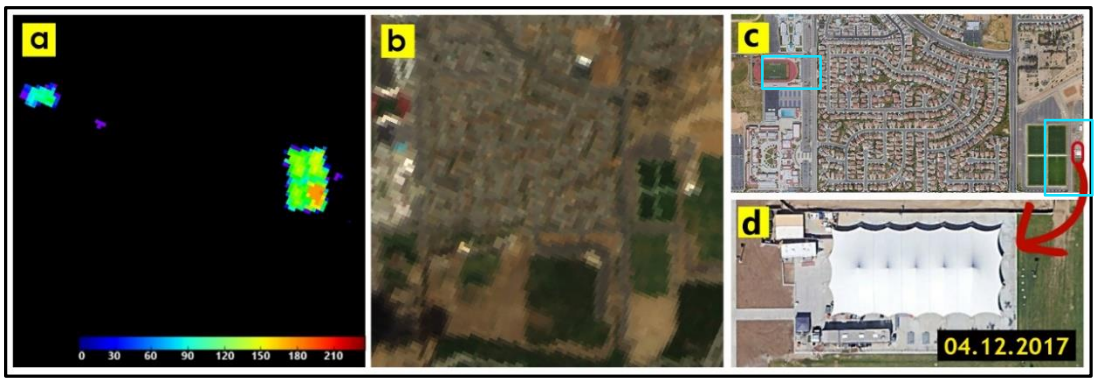

Figure 4.8. PEI Algorithm results and comparative images of SF7

Figure 4.9 presents the comparative images of the SF8. An artificial football pitch and solar panels have been successfully detected by the algorithm. An artificial football pitch is marked with a cyan rectangle and solar panels are marked with a magenta rectangle in 4.9.C. PIPV is between 1.00 and 108.33.

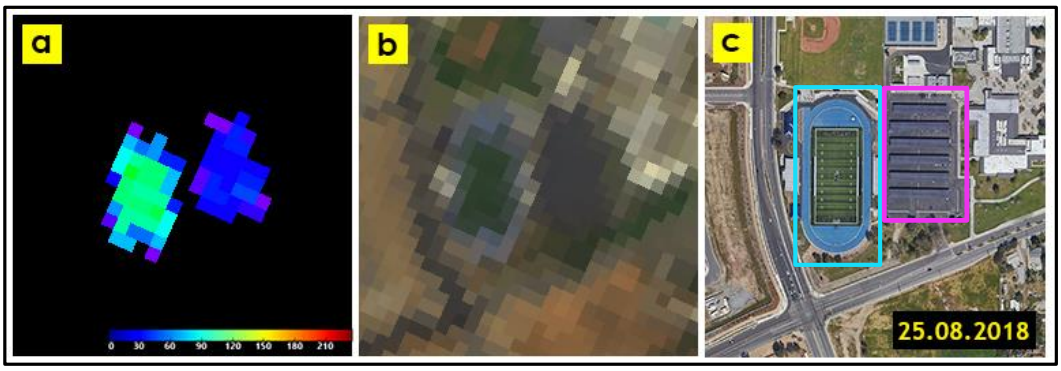

Figure 4.9. PEI Algorithm results and comparative images of SF8

Figure 4.10 presents the comparative images of the SF9. An artificial football pitch has been successfully detected by the algorithm. PIPV is between 4.66 and 77.66.

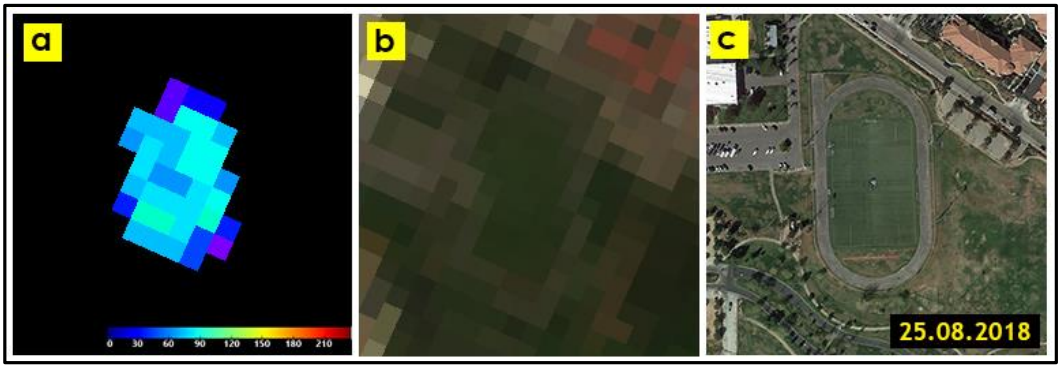

Figure 4.10. PEI Algorithm results and comparative images of SF9

Figure 4.11 presents the comparative images of the SF10. A greenhouse cluster has been successfully detected by the algorithm. PIPV is between 2.66 and 90.00.

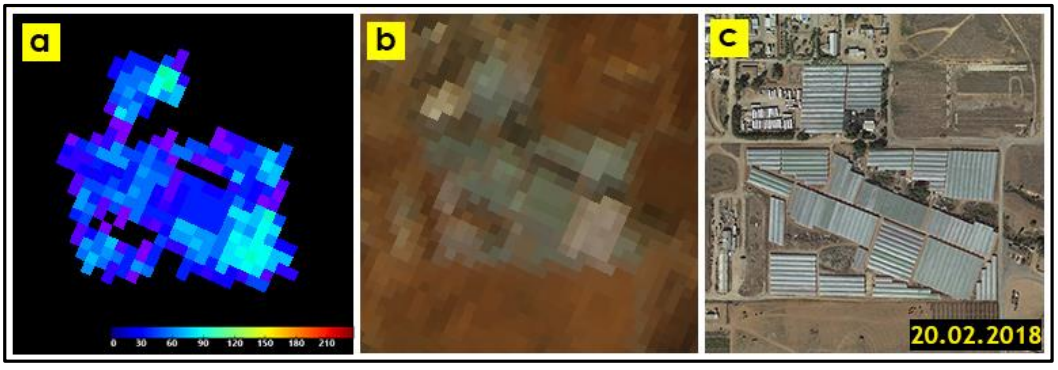

Figure 4.11. PEI Algorithm results and comparative images of SF10

Figure 4.12 presents the comparative images of the SF11. Two discrete greenhouses have been successfully detected by the algorithm. PIPV is between 0.66 and 125.00.

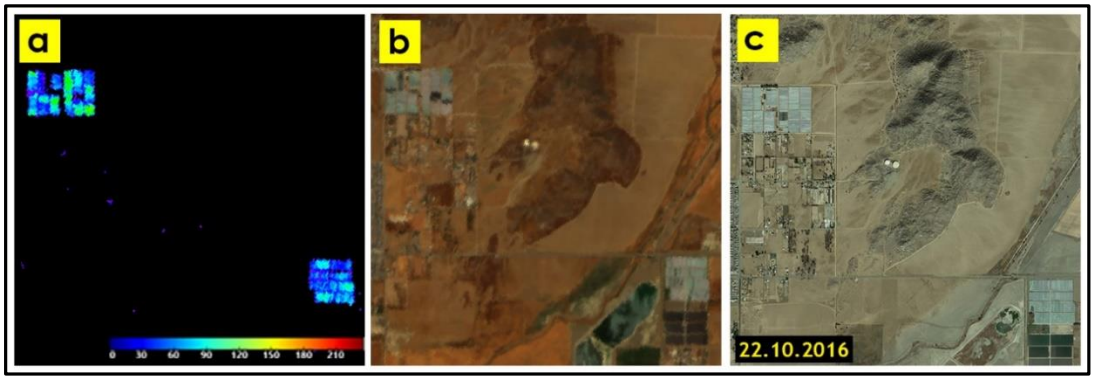

Figure 4.12. PEI Algorithm results and comparative images of SF11

Figure 4.13 presents the comparative images of the SF12. A tent-like structure has been successfully detected by the algorithm. PIPV is between 0.66 and 85.66.

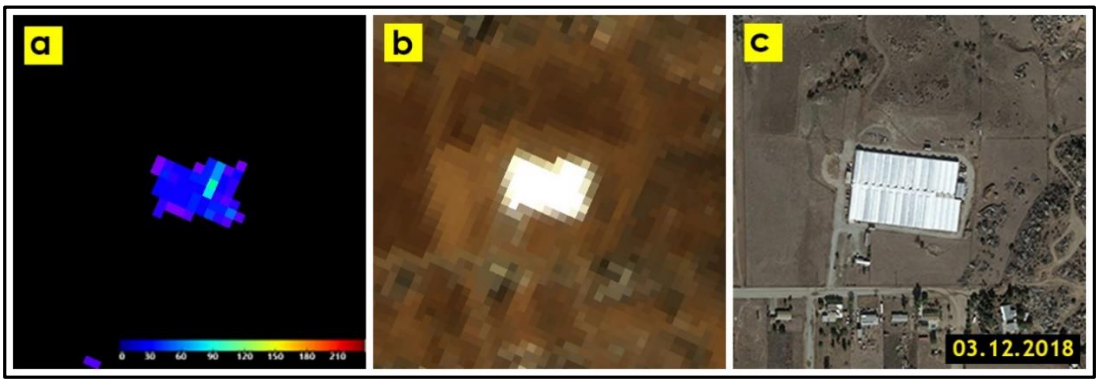

Figure 4.13. PEI Algorithm results and comparative images of SF12

Figure 4.14 presents the comparative images of the SF13. Solar panel cluster has been successfully detected by the algorithm. The PIPV of the gaps between the panels are relatively below zero. PIPV is between 3.00 and 201.66.

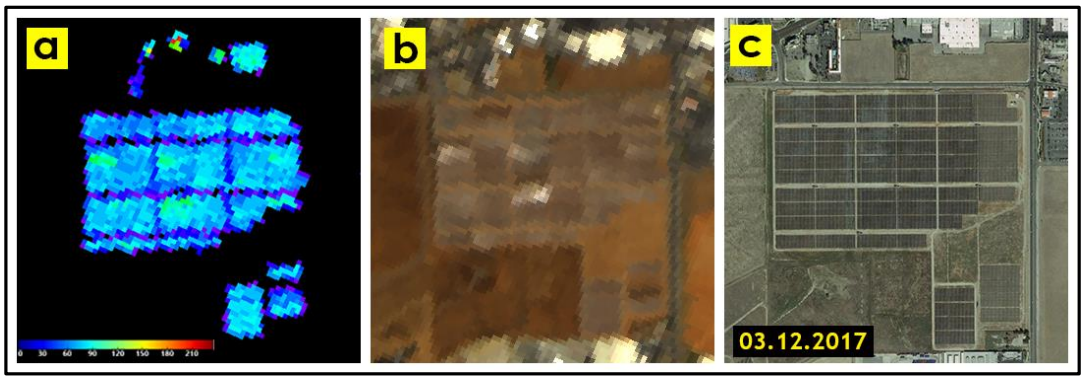

Figure 4.14. PEI Algorithm results and comparative images of SF13

Figure 4.15 presents the comparative images of the SF14. The greenhouse has been successfully detected by the algorithm. Since greenhouses may vary depending on the time, there may be differences between the two adjacent dated recent images, as seen in 4.15.C and 4.15.D. PIPV is between 2.00 and 81.00.

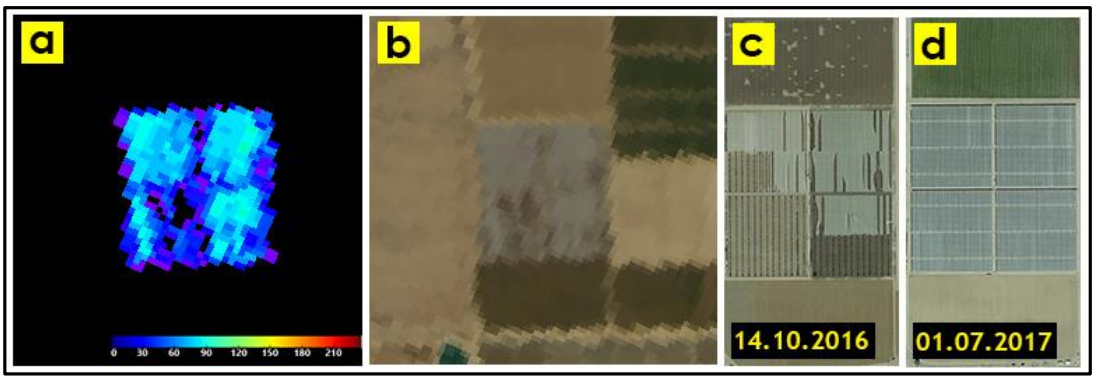

Figure 4.15. PEI Algorithm results and comparative images of SF14

Figure 4.16 presents the PEI algorithm output of SF15. Figure 4.17 presents 12.06.2017 dated true color composite (R:647.97 nm, G:550.30 nm, B:453.07 nm) AVIRIS image and Figure 4.18 presents 01.07.2017 dated high-resolution satellite image corresponding to SF15.

Greenhouses, tent-like structure and, solar panels have been successfully detected by the algorithm. Solar panels are marked with a magenta rectangle and a tent-like structure is marked with a yellow rectangle in Figure 4.17.

PIPV in SF15 is between 1.33 and 228.33. In SF15, the constant change of greenhouses can be observed from spectral changes, as well as from high-resolution satellite images.

As can be seen in Figure 4.17, there is water in the northeast of SF15. Atmospheric water has an absorption feature around 1730 nm. (Lenz, Schilling, Gross, & Middelmann, 2015) Since this case is thought to may affect the PEI algorithm negatively, the water part of the image has been masked.

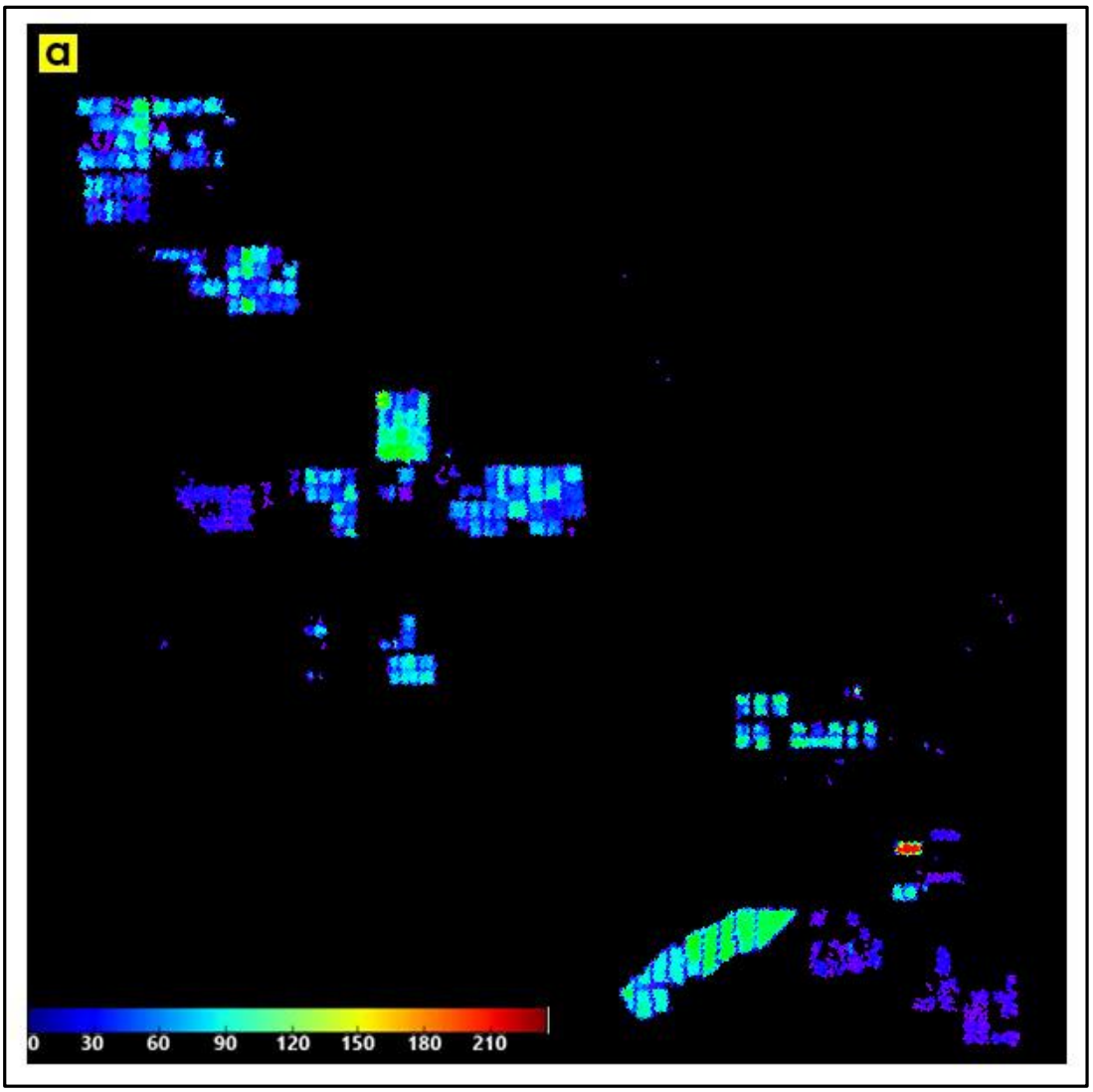

Figure 4.16. PEI Algorithm results of SF15

Figure 4.17. True color composite AVIRIS image corresponding to SF15

Figure 4.18. High-resolution satellite image corresponding to SF15

4.3. Spectral Math Function Outputs

Spectral Math Function (SMF) implements the PEI Algorithm and calculate the PIPV results. In addition, the function compares the ground truth and algorithm output, generate the confusion matrix, and correspondingly produce accuracy rates. The function can be found in Appendix A. Below is brief information about the images presented in figures.

Result of PEI Algorithm is shown as the first image of the figure plates. To obtain this image, the bands have been first selected and then the PEI algorithm was coded in the MATLAB environment by applying the formula given in Equation 4.2. In this image, both positive and negative values are displayed.

PIPV is shown as the second image of the figure plates. This image, which derived from the first image, shows only positive values of the PEI Algorithm result. In calculation and operation performed with MATLAB, generally, char and double data types are used. Therefore, the resulting values are converted to double data type. Gray values in the first and second images are directly related to the magnitude of values acquired from the algorithm results that can be interpreted as the strength of spectral radiance and degree of plastic object existence.

Mask of PIPV is shown as the third image of the figure plates. Masking the PIPV is a process that each pixel in the image is identified to be a member of a class without using any training data, it is actually an unsupervised classification. This image shows two discrete class clustered using the values generated by the PEI algorithm. The first class contains all values that are greater than zero, and the second class contains all values that are smaller than zero. The classification is based only on whether they are positive or negative, regardless of the magnitude of the values.

Ground truth is presented as the fourth image of the figure plates. Ground truth, which has been manually produced using the true color composite of AVIRIS image, has been generated to make comparison with the PIPV masked image shown in the third image and thus to perform accuracy assessments.

The figures below named from Figure 4.19 to Figure 4.33, show how the SMF Algorithm works in different study fields and the results of the algorithm from SF1 to SF15, respectively. Same concept is in every figure for ease of examination.

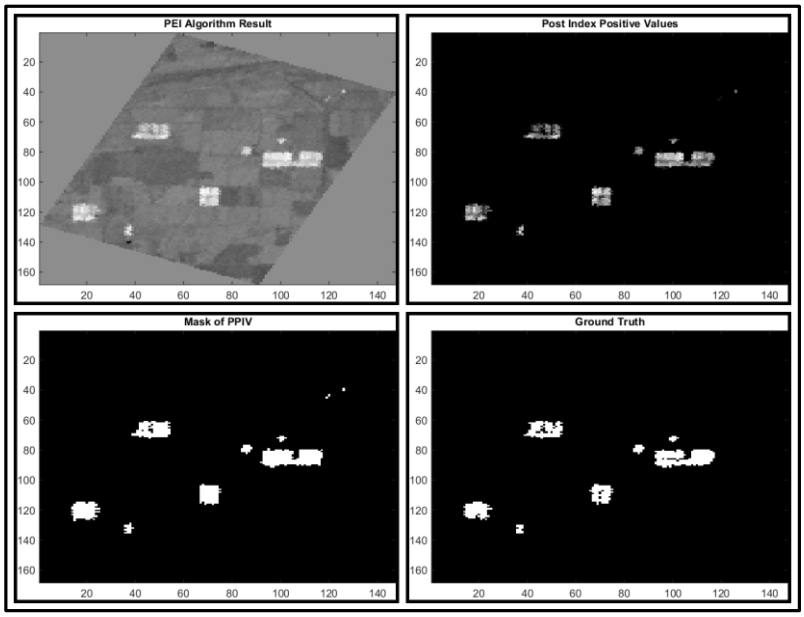

Figure 4.19. SMF output of SF1

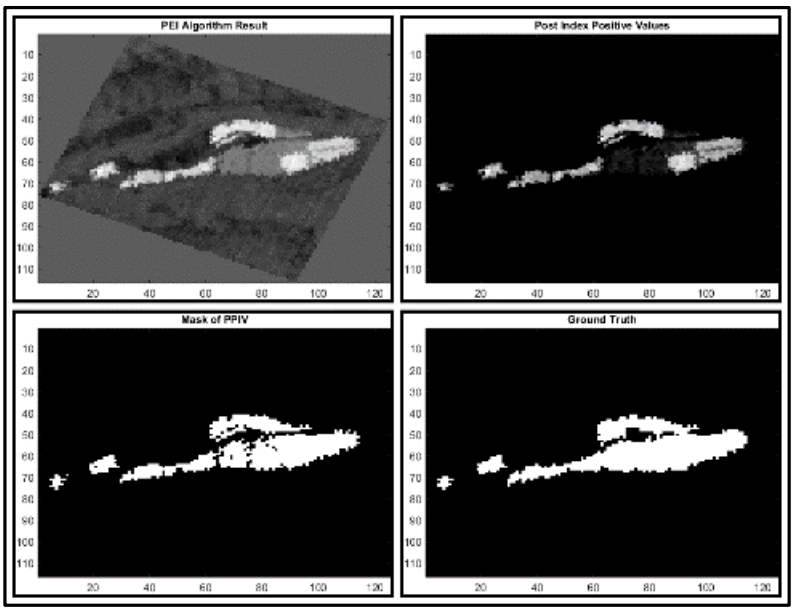

Figure 4.20. SMF output of SF2

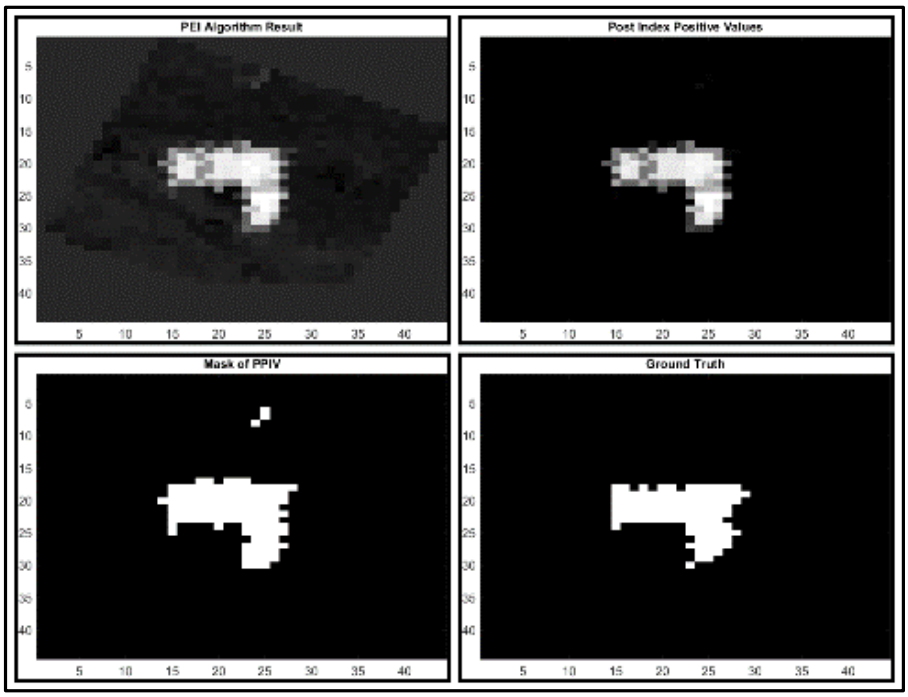

Figure 4.21. SMF output of SF3

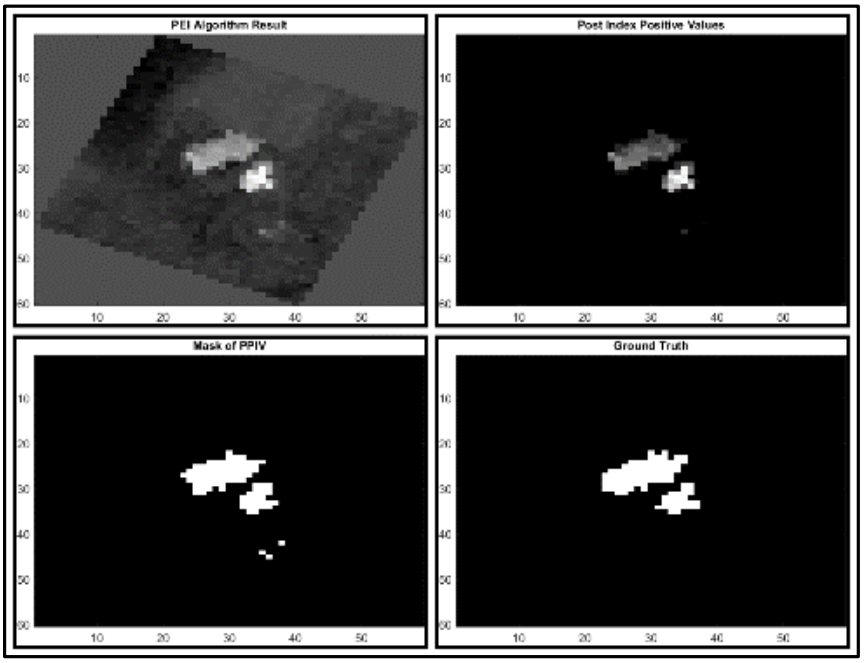

Figure 4.22. SMF output of SF4

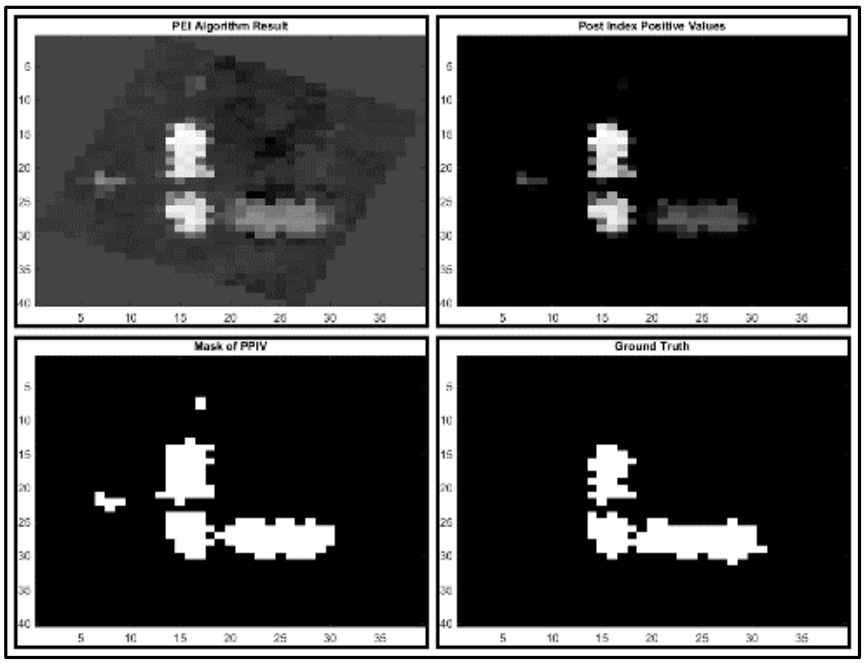

Figure 4.23. SMF output of SF5

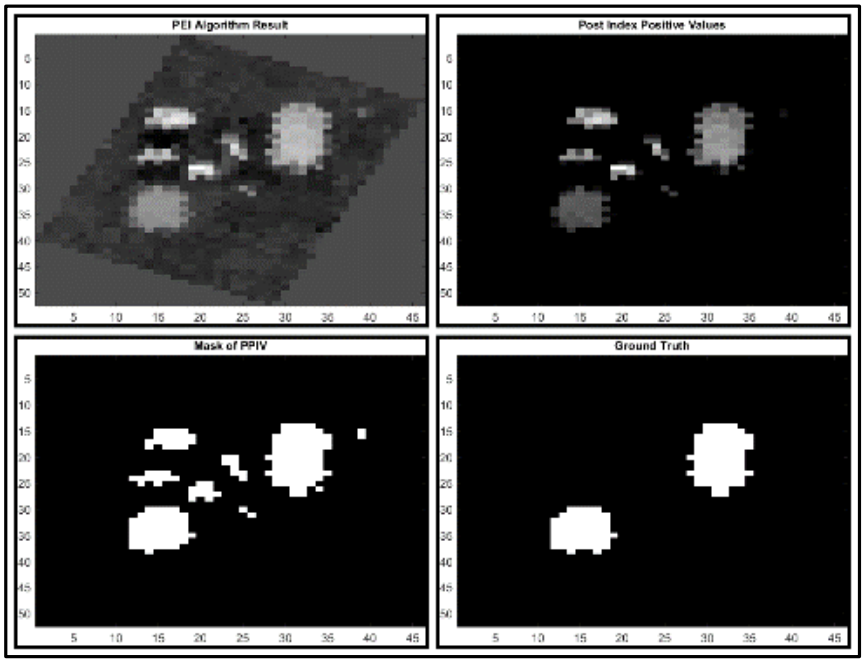

Figure 4.24. SMF output of SF6

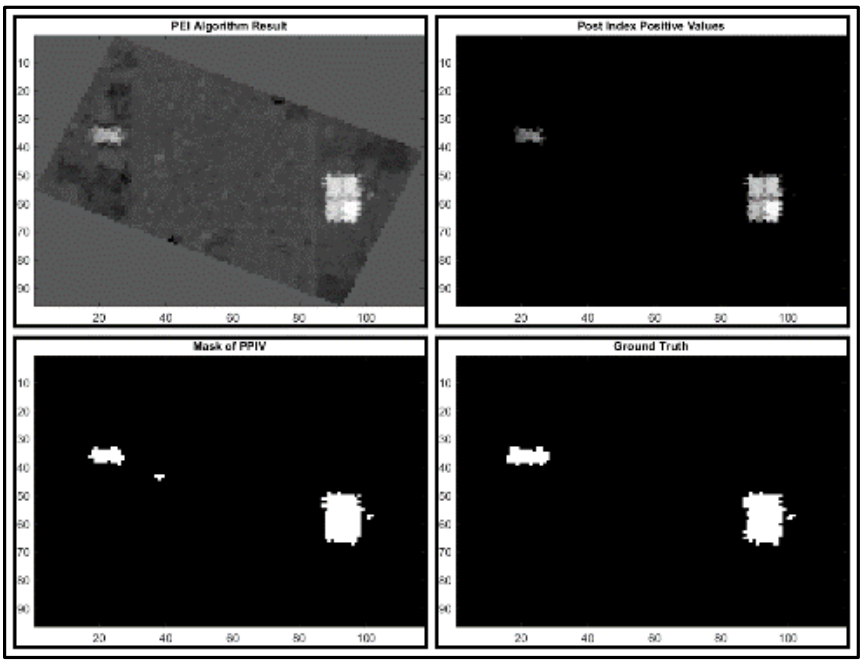

Figure 4.25. SMF output of SF7

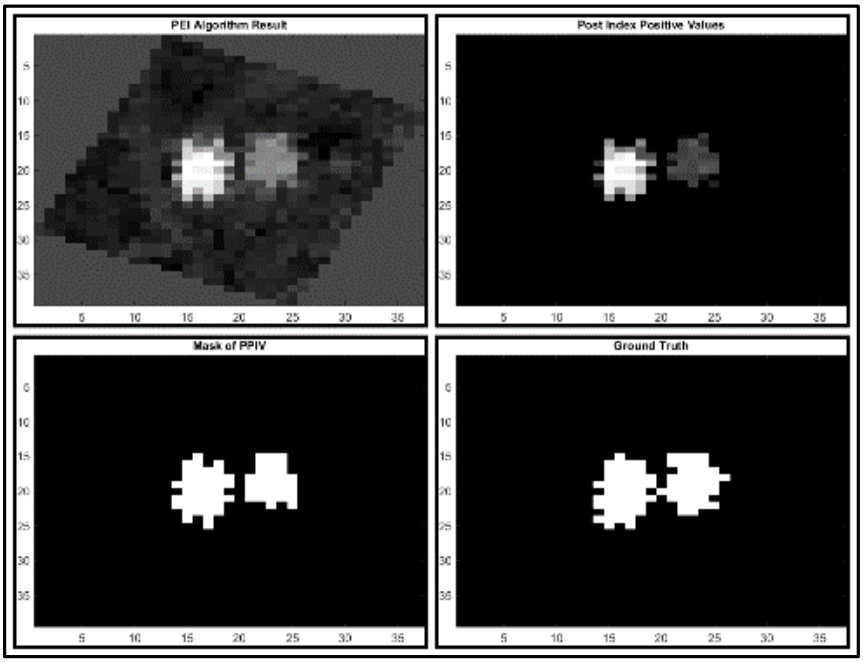

Figure 4.26. SMF output of SF8

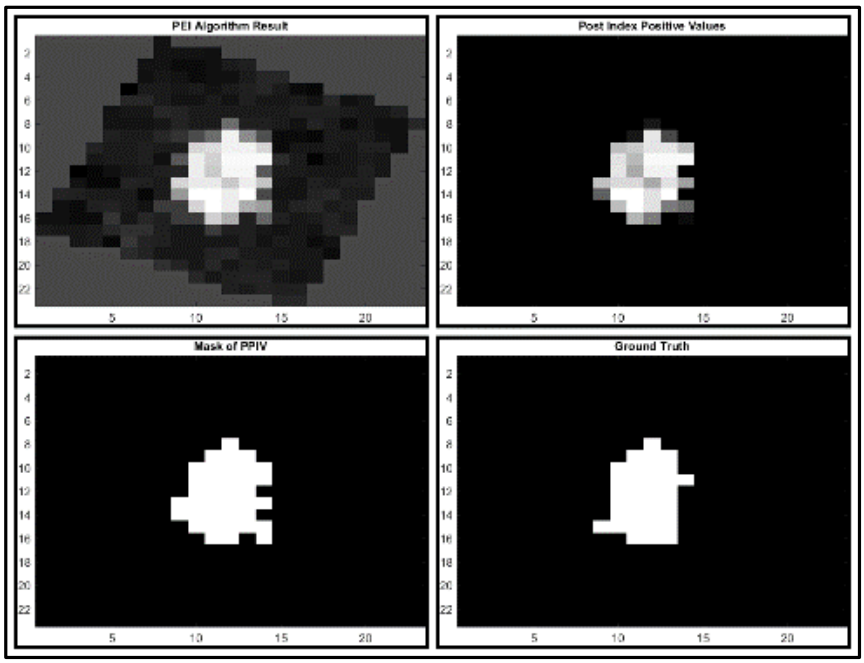

Figure 4.27. SMF output of SF9

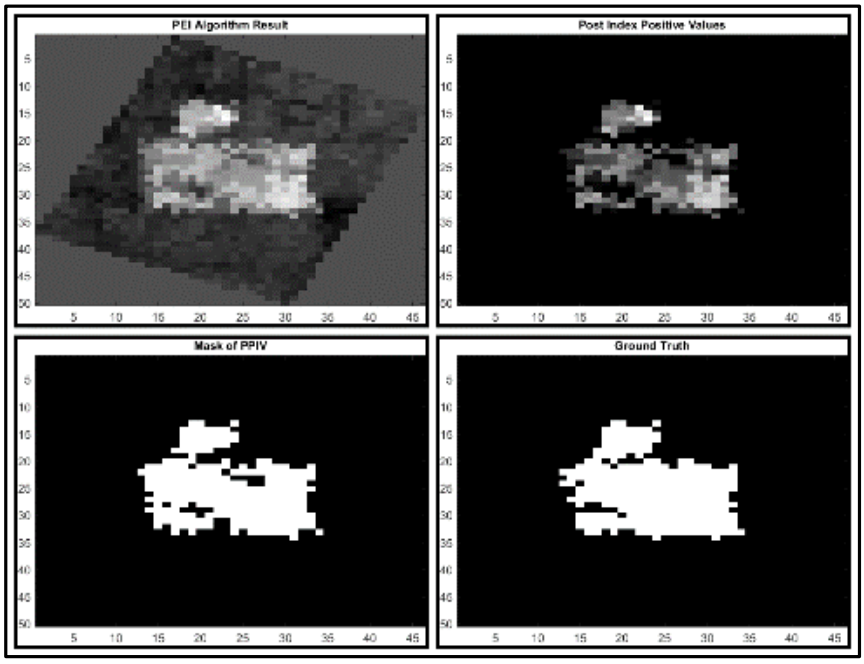

Figure 4.28. SMF output of SF10

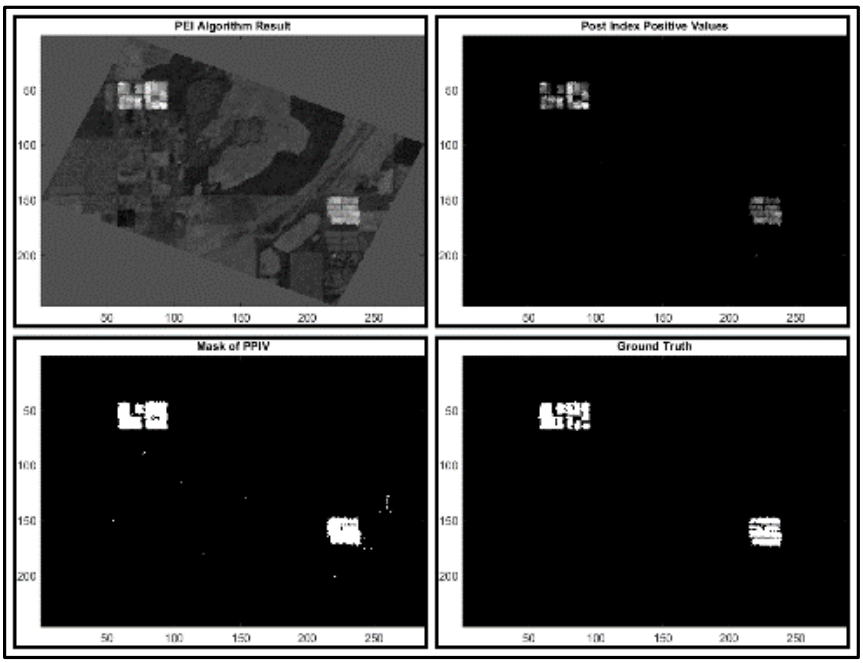

Figure 4.29. SMF output of SF11

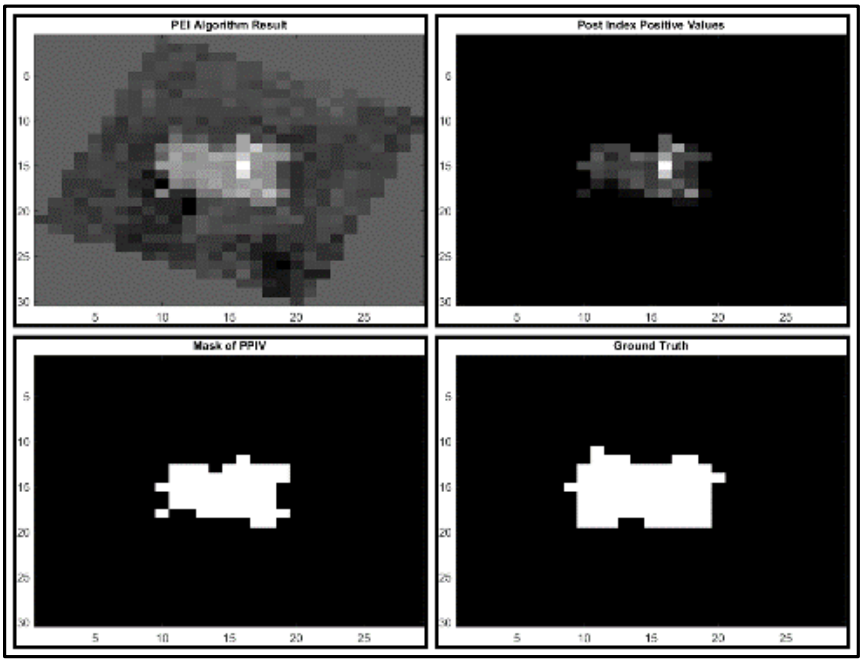

Figure 4.30. SMF output of SF12

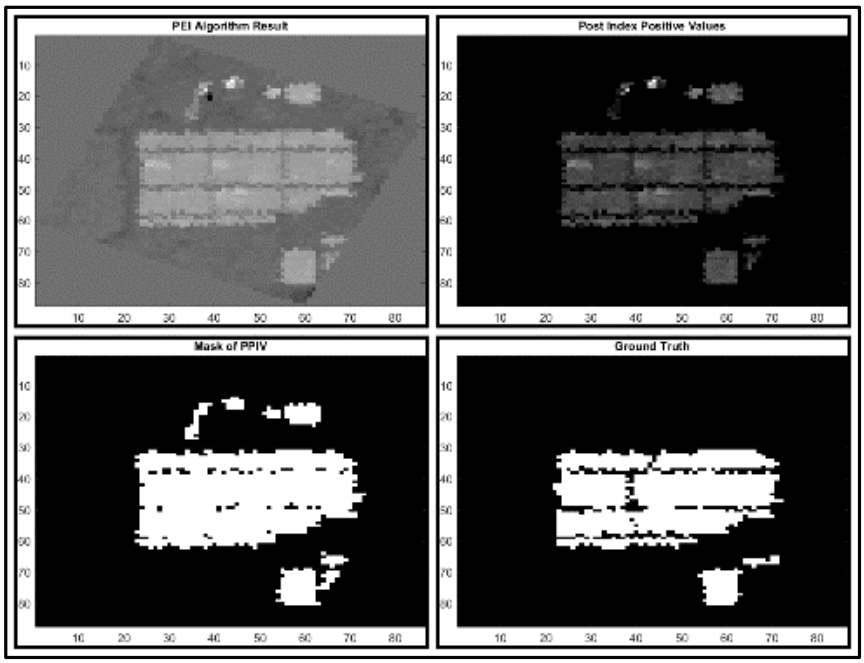

Figure 4.31. SMF output of SF13

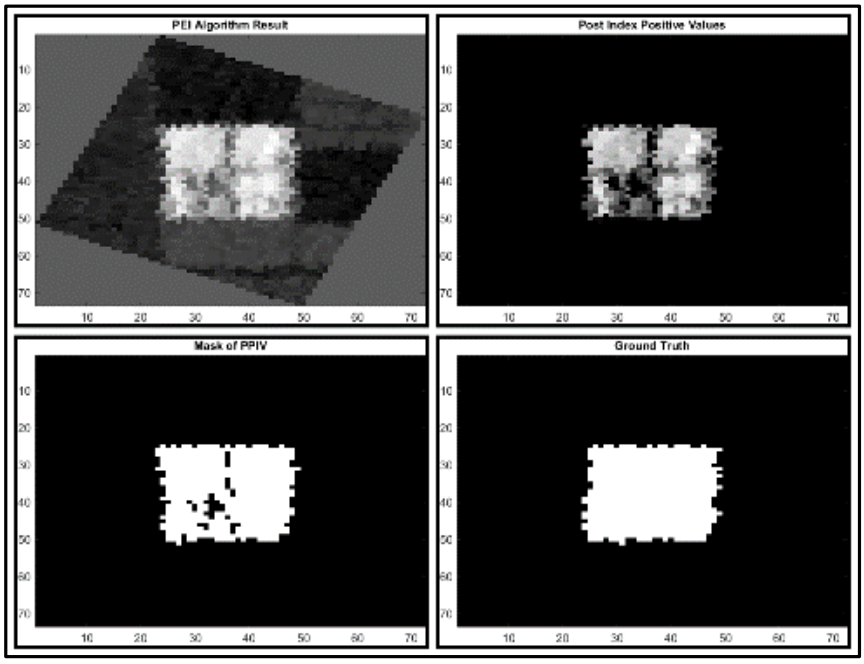

Figure 4.32. SMF output of SF14

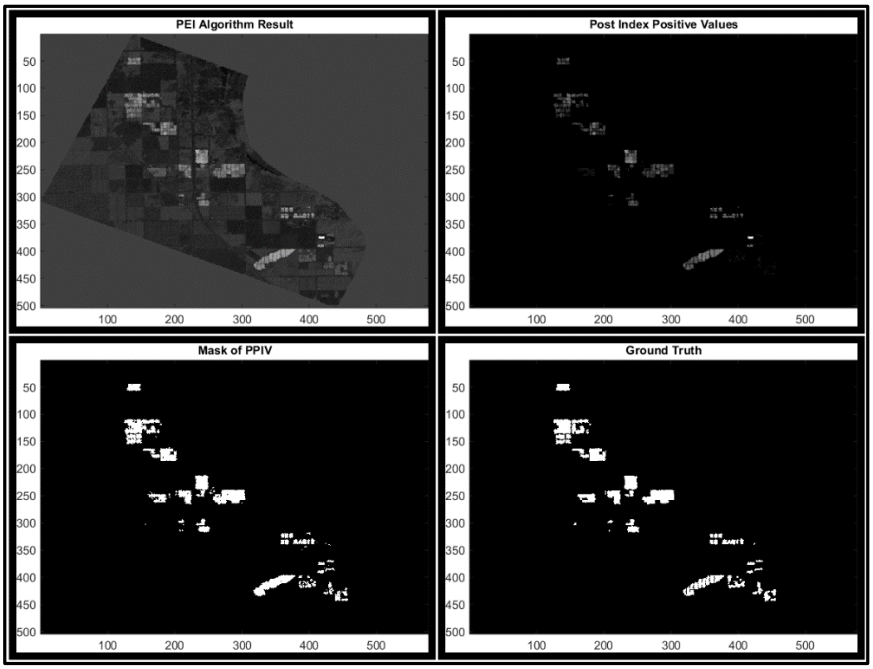

Figure 4.33. SMF output of SF15

CHAPTER 5

RESULTS AND DISCUSSIONS

5.1. Accuracy Assessment

The result of plastic detection is an unsupervised image classified as two separate classes as plastic and non-plastic. The detection and pixel based classification process is successful, but it is imperfective without the accuracy assessment, the last step for complete classification.

While conducting the accuracy assessment, it is aimed to determine the coherence between the data obtained as a result of classification and the ground truth representing the actual earth values. Thus, the degree of representation of the classes obtained as a result of the classification is determined. Ground truth can be generated from actual values obtained from field work at certain points or can be produced by aerial photographs or satellite images.

The ground truth used in this thesis has been produced manually by a visual interpretation with using a true color composite of 15.5-meter resolution AVIRIS data. This reference data, which is relatively inadequate for objects smaller than the spatial resolution, is quite sufficient for a plurality of plastic objects that have been successfully detected.

The most common method used to determine the classification accuracy is the error matrix called as confusion matrix. Confusion matrix; is a square order of numbers arranged in rows and columns in the number of pixels assigned as a specific type of terrain cover according to the actual terrain cover obtained from the ground truth (Jensen & Lulla, 1987). In other words, the confusion matrix compares the relationship between the known reference data, as known as ground truth, and their corresponding data acquired from the process of classification.

Many accuracy criteria can be acquired by using the confusion matrix. The most commonly used of these are user accuracy, producer accuracy, and overall accuracy. (Yan, 2003)

User Accuracy (UA) or precision represents the probability that the pixel assigned to any class actually belongs to that class. It is calculated by dividing the number of pixels or objects that are correctly classified for each class to the total number of pixels or objects classified in that category which is given in Equation 5.1.

Producer Accuracy (PA) or sensitivity refers to the possibility of classifying a pixel or object in its actual value. It is calculated by dividing the number of pixels or objects that are correctly classified for each class to the sum of the actual cover type sampling number selected for that class which is given in Equation 5.2.

If these UA and PA values are close to 100 and close to each other, the accuracy of classification can be considered as good. Otherwise, if one of these two values is close to 100 and the other one is too low, or the two values are too low, the selected training areas or the algorithm used may need to be re-evaluated.

Overall Accuracy (OA) is calculated for each class by dividing the total number of classified pixels to the total number of reference pixels which given in Equation 5.3. OA presents a general assessment of the accuracy of classes.

The accuracy criteria can be calculated in a simple way according to the formulas given below.

$$UA = \frac{\mathrm{a}}{(\mathrm{a} + \mathrm{b})} \tag{5.1}$$

$$PA = \frac{\mathrm{a}}{(\mathrm{a} + \mathrm{c})} \tag{5.2}$$

$$OA = \frac{(\mathrm{a} + \mathrm{d})}{(\mathrm{a} + \mathrm{b} + \mathrm{c} + \mathrm{d})} \tag{5.3}$$

where:

a = number of pixels classified as X when observed as X in reference

b = number of pixels classified as X when observed as not X in reference

c = number of pixels not classified as X when observed as X in reference

d = number of pixels classified as not X when observed as not X in reference

Confusion matrixes of plastic classes in study fields, which produced in accordance with the rules determined in these definitions, is given in tables between 5.1 and 5.15.

Histograms, which are an integrant part of accuracy assessment components, give in figures between 5.1 and 5.15. Histograms values have consisted of correctly classified pixels.

Table 5.1. Confusion Matrix of Plastic Class in SF1

		Observed Pixels	
		Plastic	*Non-Plastic*
Classified Pixels	*Plastic*	558	75
	Non-Plastic	15	13210

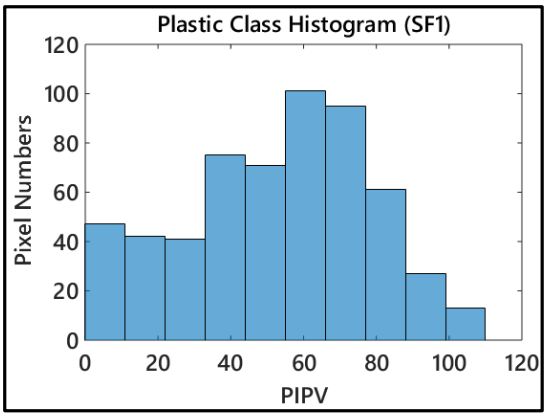

Figure 5.1. Correctly classified as plastic pixels' histogram (SF1)

Table 5.2. Confusion Matrix of Plastic Class in SF2

		Observed Pixels	
		Plastic	*Non-Plastic*
Classified Pixels	*Plastic*	970	162
	Non-Plastic	39	7028

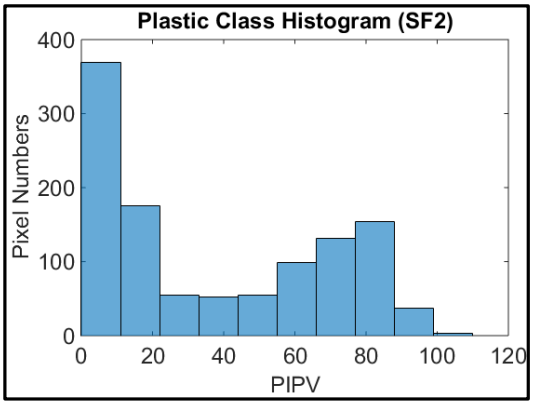

Figure 5.2. Correctly classified as plastic pixels' histogram (SF2)

Table 5.3. Confusion Matrix of Plastic Class in SF3

		Observed Pixels	
		Plastic	*Non-Plastic*
Classified Pixels	*Plastic*	99	6
	Non-Plastic	19	998

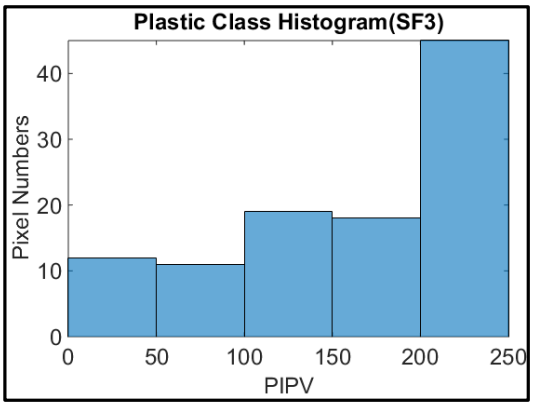

Figure 5.3. Correctly classified as plastic pixels' histogram (SF3)

Table 5.4. Confusion Matrix of Plastic Class in SF4

		Observed Pixels	
		Plastic	*Non-Plastic*
Classified Pixels	*Plastic*	89	11
	Non-Plastic	6	1920

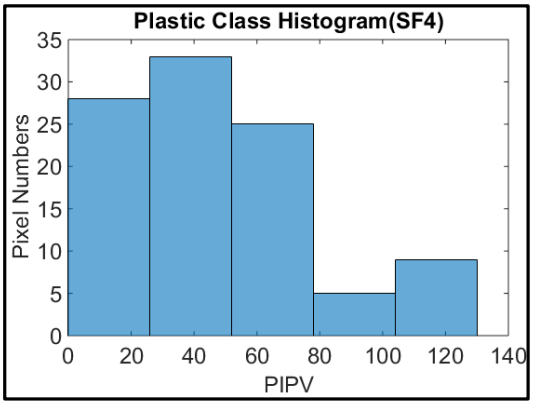

Figure 5.4. Correctly classified as plastic pixels' histogram (SF4)

Table 5.5. Confusion Matrix of Plastic Class in SF5

		Observed Pixels	
		Plastic	*Non-Plastic*
Classified Pixels	*Plastic*	102	8
	Non-Plastic	24	766

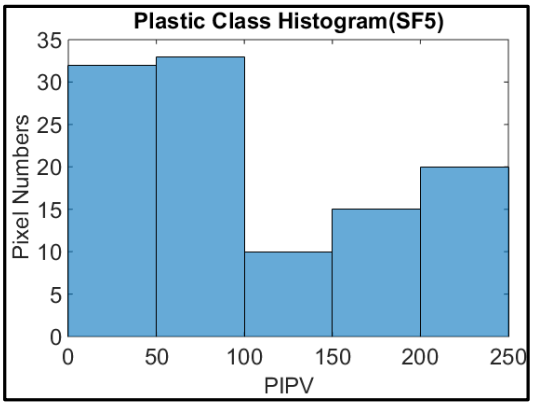

Figure 5.5. Correctly classified as plastic pixels' histogram (SF5)

Table 5.6. Confusion Matrix of Plastic Class in SF6

		Observed Pixels	
		Plastic	*Non-Plastic*
Classified Pixels	*Plastic*	131	3
	Non-Plastic	54	1150

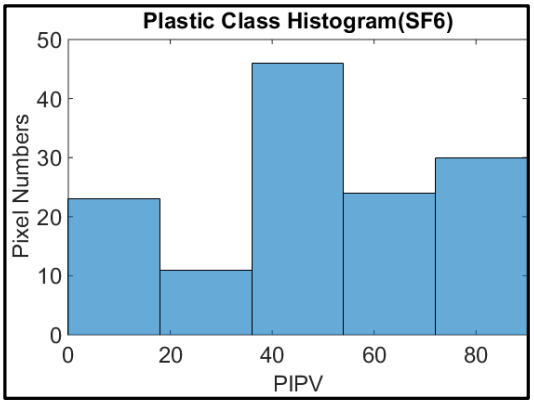

Figure 5.6. Correctly classified as plastic pixels' histogram (SF6)

Table 5.7. Confusion Matrix of Plastic Class in SF7

		Observed Pixels	
		Plastic	*Non-Plastic*
Classified Pixels	*Plastic*	232	28
	Non-Plastic	8	5791

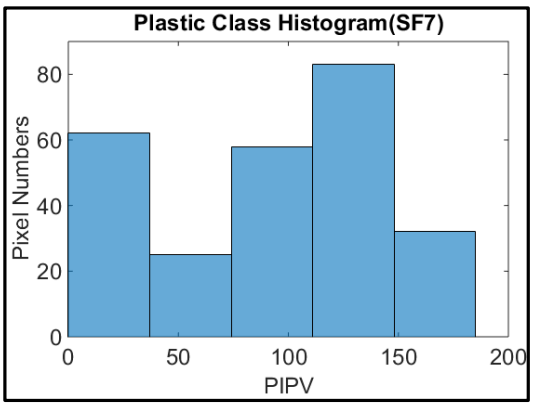

Figure 5.7. Correctly classified as plastic pixels' histogram (SF7)

Table 5.8. Confusion Matrix of Plastic Class in SF8

		Observed Pixels	
		Plastic	*Non-Plastic*
Classified Pixels	*Plastic*	71	13
	Non-Plastic	1	752

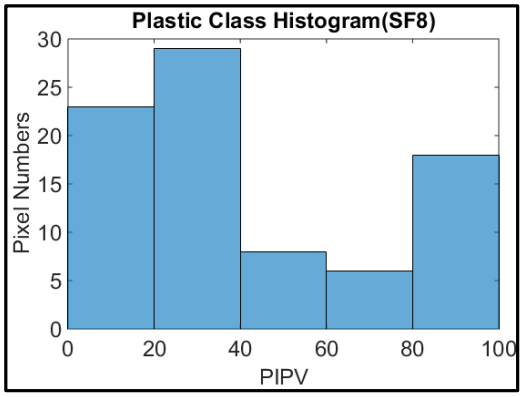

Figure 5.8. Correctly classified as plastic pixels' histogram (SF8)

Table 5.9. Confusion Matrix of Plastic Class in SF9

		Observed Pixels	
		Plastic	*Non-Plastic*
Classified Pixels	*Plastic*	31	2
	Non-Plastic	6	267

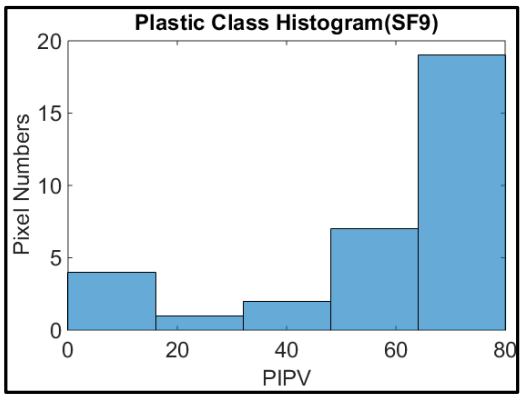

Figure 5.9. Correctly classified as plastic pixels' histogram (SF9)

Table 5.10. Confusion Matrix of Plastic Class in SF10

		Observed Pixels	
		Plastic	*Non-Plastic*
Classified Pixels	*Plastic*	251	33
	Non-Plastic	9	1027

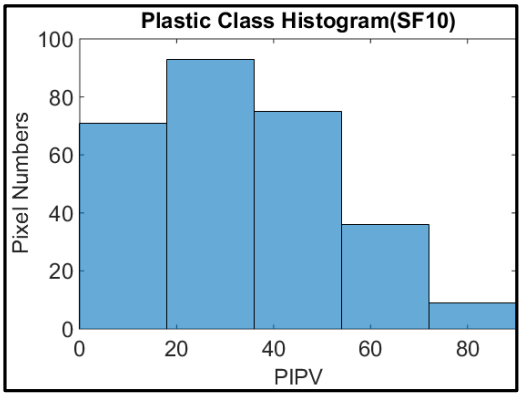

Figure 5.10. Correctly classified as plastic pixels' histogram (SF10)

Table 5.11. Confusion Matrix of Plastic Class in SF11

		Observed Pixels	
		Plastic	*Non-Plastic*
Classified Pixels	*Plastic*	1135	64
	Non-Plastic	233	37767

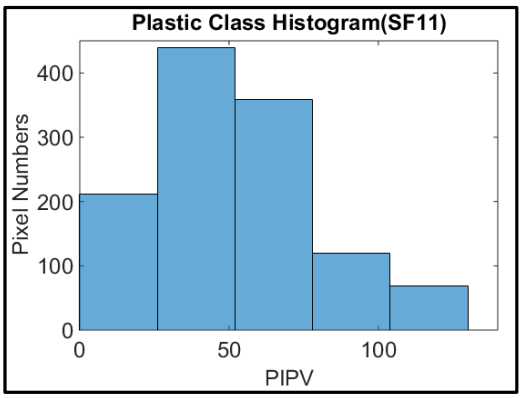

Figure 5.11. Correctly classified as plastic pixels' histogram (SF11)

Table 5.12. Confusion Matrix of Plastic Class in SF12

		Observed Pixels	
		Plastic	*Non-Plastic*
Classified Pixels	*Plastic*	52	24
	Non-Plastic	1	428

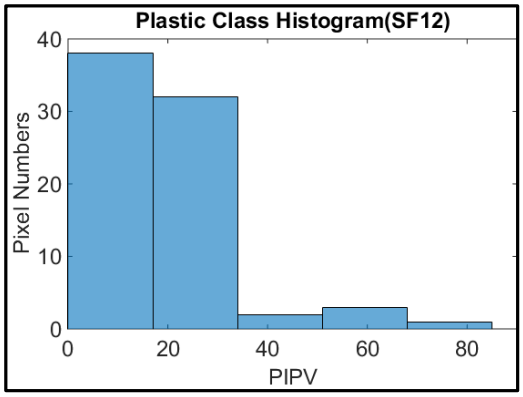

Figure 5.12. Correctly classified as plastic pixels' histogram (SF12)

Table 5.13. Confusion Matrix of Plastic Class in SF13

		Observed Pixels	
		Plastic	*Non-Plastic*
Classified Pixels	*Plastic*	1202	35
	Non-Plastic	300	2754

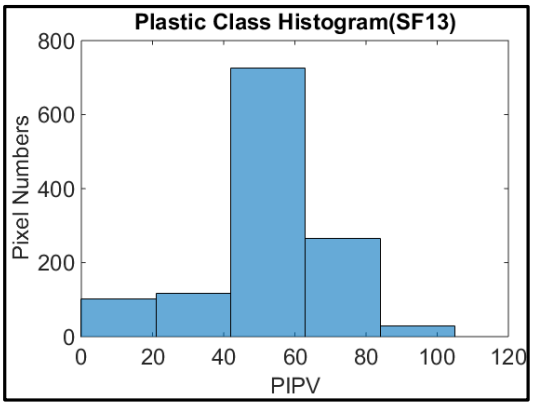

Figure 5.13. Correctly classified as plastic pixels' histogram (SF13)

Table 5.14. Confusion Matrix of Plastic Class in SF14

		Observed Pixels	
		Plastic	*Non-Plastic*
Classified Pixels	*Plastic*	552	52
	Non-Plastic	19	2402

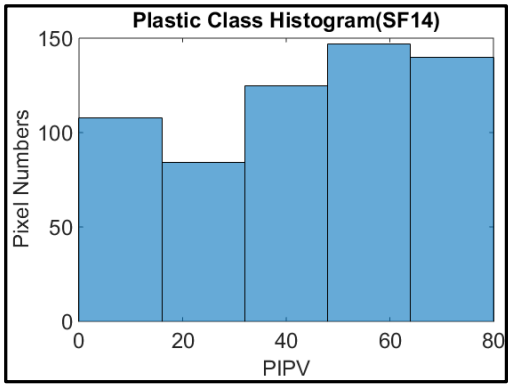

Figure 5.14. Correctly classified as plastic pixels' histogram (SF14)

Table 5.15. Confusion Matrix of Plastic Class in SF15

		Observed Pixels	
		Plastic	*Non-Plastic*
Classified Pixels	*Plastic*	6069	516
	Non-Plastic	710	113461

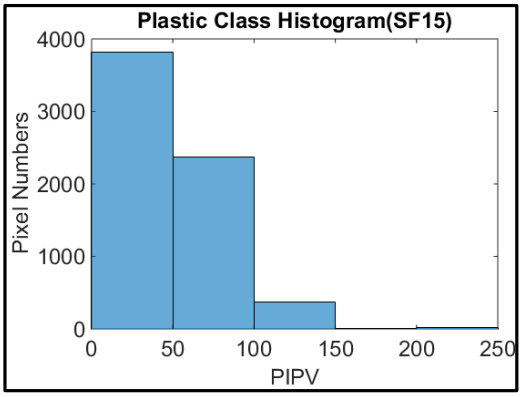

Figure 5.15. Correctly classified as plastic pixels' histogram (SF15)

Number of pixels and accuracy criteria regarding study fields are given in Table 5.16. The table also presents the types of detected objects in study fields.

Table 5.16. Object Types, Number of Pixels and Accuracy Criteria Regarding Study Fields

Study Fields	*Object Types*	*Number of Pixel*	*UA*	*PA*	*OA*
SF1	Greenhouse	13858	97.4 %	88.1 %	99.3 %
SF2	Greenhouse	8199	85.7 %	96.1 %	97.5 %
SF3	Football Pitch	1122	94.3 %	83.9 %	97.7 %
SF4	Football Pitch, Solar Panel	2026	89.0 %	93.7 %	99.1 %
SF5	Football Pitch, Solar Panel	900	92.7 %	80.1 %	96.4 %
SF6	Football Pitch, Solar Panel	1338	98.8 %	70.8 %	95.7 %
SF7	Football Pitch, Tent	6059	89.2 %	96.7 %	99.4 %
SF8	Football Pitch, Solar Panel	837	84.5 %	98.6 %	98.3 %
SF9	Football Pitch	306	93.9 %	83.8 %	97.4 %
SF10	Greenhouse	1320	88.4 %	96.5 %	96.8 %
SF11	Greenhouse	39199	94.7 %	83.0 %	99.2 %
SF12	Tent	505	68.4 %	98.1 %	95.0 %
SF13	Solar Panel	4291	97.2 %	80.0 %	92.2 %
SF14	Greenhouse	3025	91.4 %	96.7 %	97.6 %
SF15	Greenhouse, Football Pitch and Solar Panel	120756	92.1 %	89.5 %	98.9 %

Accuracy criteria have resulted in a highly satisfactory degree which mean value of UA is 90.51%, PA is 89.04% and OA is 97.37. It is useful to examine the results of UA, PA, and OA, which are correlated with each other but have different meanings.

UA values are quite high except for the error in SF12 class. When the confusion matrix of SF12 is analyzed, it can be seen that 52 of the 72 pixels are classified as plastic as should be but 24 pixels are misclassified. This error has reduced the UA accuracy criterion to 68%. The source of the error may be related to the reliability of the ground truth or the performance of the algorithm.

PA values are also high except for the error in SF6 class. When the confusion matrix of SF6 is analyzed, it can be seen that 131 of 185 pixels which should be in the plastic class can be detected but 54 pixels cannot be detected. In PIPV image of SF6, it is clearly seen that there are four more buildings detected as plastic. This unexpected situation has been discussed in section 5.2.

OA values are excessively high with values up to 99%. The reason for these extreme results is that negative PIPVs in the images are overwhelmingly more than positive PIPV.

5.2. Discussions of the Results

Different types of plastic objects have been successfully detected with the implementation of PEI Algorithm and SMF. However, it is crucial to evaluate the results of the implementations, objectively.

When the histograms of correctly classified plastic pixels are examined, a number of inferences can be made as follows.

The highest spectral reflectance has been seen in football pitches. Football pitches have a slightly better spectral reflection than other plastic objects. It is thought that the reason for this better reflection is related with that artificial turf is more homogenous than other objects and additionally, pitches, due to the fact they are clean and well-maintained, reflect their chemical properties better. As can be seen in Figure 3.13, the absorption of the pitches around 1.72 μm is significantly higher than other objects.

The lowest spectral reflectance has been seen in greenhouses. Since the greenhouses can be changed easily and quickly depending on the season and needs, it is possible to see them which composed of a different material or installed in different time even if they are side by side in the same field. This variability, which affects spectral reflectance, has also been seen in greenhouses in many study fields. In addition, greenhouses are pervious due to their use and are not made of a very solid material and can easily lose their form. The weak and pervious structure of the material negatively affects the spectral reflection. According to the observation made from the high-resolution satellite image, greenhouses which in the same color and the same type and are physically similar have nearly same spectral reflectance.

The spectral reflection of the solar panels is variable as seen in Figure 3.9 and 3.10. It is thought that the colors of the solar panels with different spectral reflections are different, they can be produced in different materials, and the types of materials cause different the spectral reflections. The difference can be seen in Figure 4.6 and 4.7.

Since it is known that the newer material reflects its spectral characteristics better than of degraded one, it is thought that football pitches in SF3 are relatively new can be seen in Figure 4.4. This assumption has been confirmed that, by the observation made from high-resolution satellite images, the pitches were built after 24.03.2015. The opposite of this situation has been observed in the football pitches in SF4 can be seen in Figure 4.5. It has been seen that the football pitch in SF4, which has a lower spectral reflection than the football pitches in SF3, was built before 1994 as a result of observation made from high-resolution satellite images. This shows that the aging material gradually lost its spectral properties. The relation between the newness of the material and the spectral character of it has been also observed in solar panels in SF5 with more than 230 PIPV and a tent-like in SF15 with more than 225 PIPV can be seen in Figure 4.6 and Figure 4.16.

In PIPV image of SF6, it is clearly seen that there are four more objects detected as plastic in addition to the two objects which exists in the ground truth and detected successfully. When the high-resolution satellite image of this region is examined, it has been observed that these four objects are four buildings of similar type and similar color marked with a red rectangle in Figure 5.16.

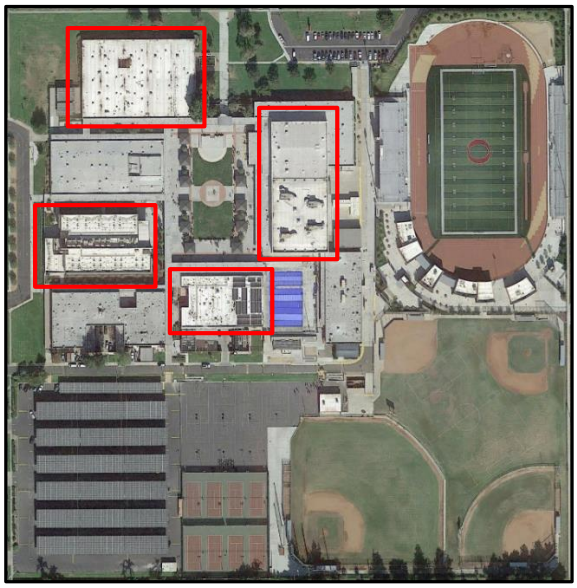

Figure 5.16 High-resolution satellite image corresponding to SF6

It is thought that the roofing materials of these buildings are probably plastic materials, and if so, this case which perceived as an error, actually shows that the algorithm performs quite well. Unfortunately, there is no data that can confirm this prediction.

Some plastic objects, which detection is impossible in visual inspection in the true color composite image because of the low resolution, has been clearly seen in PIPV masked image while they are not seen in ground truth image. This case has been seen many outputs. Difference between the images, which can be interpreted as an error, also naturally reduces the degree of accuracy. However, it is thought that this error is not related to the performance of the algorithm but rather to the reliability of the ground truth. It is considered that when a higher resolution image is used, a better ground truth with higher accuracy can be produced and the algorithm will perform better.

CHAPTER 6

CONCLUSIONS AND RECOMMENDATIONS

6.1. Conclusions

In this thesis, which written with the motivation of contributing to the fight against plastic pollution and to be useful developing effective and sustainable policies, plastic pollution and pollutant types have been investigated; plastic objects have been examined in terms of physical, chemical and spectral aspects; and have been detected on land with an unsupervised manner through shortwave infrared hyperspectral image and significant plus successful results have been obtained.

The data used to detect the presence of plastic on the land is 15.5-meter resolution 224 band hyperspectral image, which is calibrated, orthocorrected and atmospherically uncorrected radiance data, that acquired by AVIRIS. 15 different study field, each of which is divergent from each other and consisting of significant plastic object samples like a greenhouse, an artificial turf football pitch, a solar panel, and a tent has been selected in this image that covering an area of 10704 km^2.

As a result of a set of research, it is observed that plastic objects have a significant absorption around 1.72 μm. The positive value of this absorption has been associated with the presence of plastic and the feature of absorption has been mathematically expressed using two neighboring shoulders adjacent to the absorption. As a consequence of examining many different plastic spectra, the right shoulder was chosen as 1.74 μm and the left shoulder as 1.68 μm, which is a relatively remote point. It is seen that data values of plastic objects are generally between 50 and 150 and can reach up to 250. In order to get rid of the undesirable noisy-like pixels, of which the majority are thought to be non-plastic, the 10, which is noise killer constant, has been subtracted from the results. This algorithm, which has the capability of detecting plastic objects on land quickly and precisely without needing any reference data and

using only 3 shortwave-infrared bands, has been named as Plastic Existence Algorithm and the positive values generated as a result of the algorithm has been called Post Index Positive Value.

In Study Field-7, except for large objects such as the football pitch and solar panels, a small tent has been also successfully detected. The tent, which is 18 meters wide and 38 meters long, has been identified as 3 pixels in a 15.5-meter resolution image. This detection, of which comparative image is given in Figure 6.1, indicates that the algorithm is successful at a pixel level.

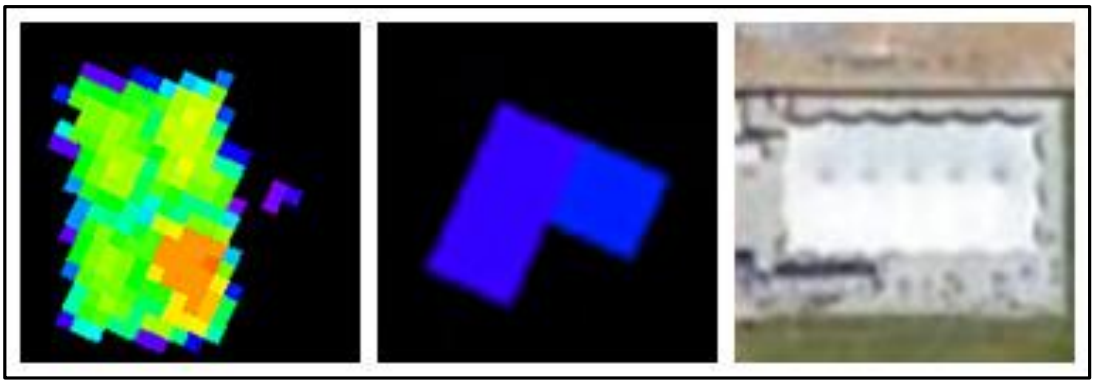

Figure 6.1. Comparative images of pixel level detection of tent in SF7

Since it is not possible to collect any data from the ground, the reference data or in other name ground truth has been produced manually by visual inspection method on the true color composite AVIRIS image, where red band: 647.97 nm, green band: 550.30 nm and blue band: 453.07 nm.

Implementation results have been compared with ground truth and pixels correctly classified as plastic are determined. It is seen that highly-satisfactory outcomes have been obtained as a result of this comparison.

6.2. Recommendations

In this thesis, the presence of plastic is associated with 1721 nm, since many types of plastics show the same character around that point. On the other hand, when the spectrum of plastic objects has been analyzed as a single graph, which can be seen in Figure 6.2, it has been observed that there are also other points that could be used as absorption feature. These points can be listed as 946 nm, 1129 nm, 1472 nm, 2006 nm and 2056 nm respectively. As mentioned before, the presence of water and moisture can be problematic in terms of the applied algorithm. An absorption feature to be selected from this list by considering the absorption of water can eliminate the problems caused by water and moisture.

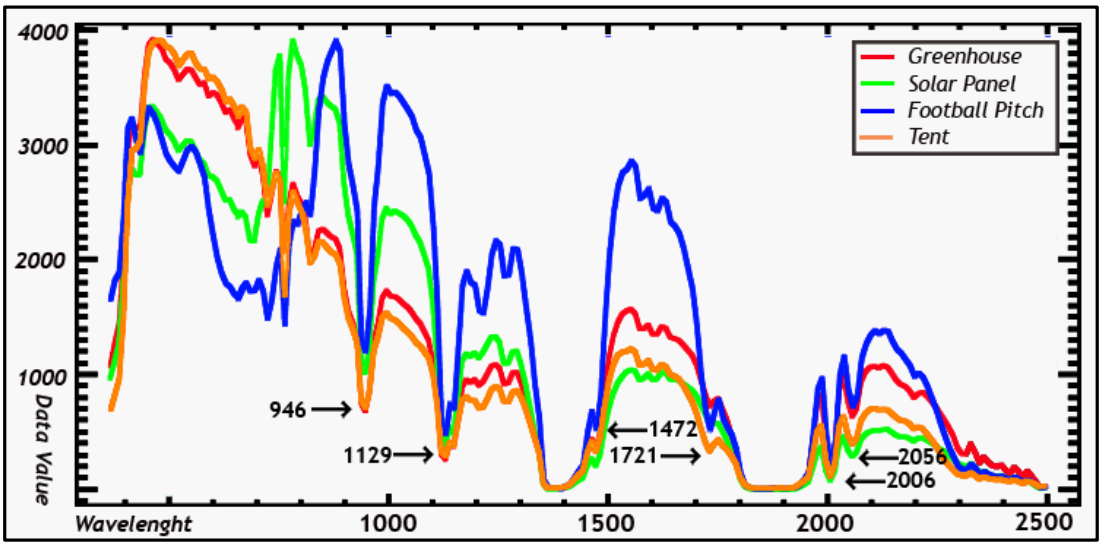

Figure 6.2. Combined spectra of four target

The low resolution of the image used in the thesis study, which is 15.5 meters, caused some problems in the production of the reference data as well as the performance of the algorithm. If a high-resolution image is used, the algorithm most probably performs better and more reliable reference data can have been generated. The high-resolution image also allows for the detection of smaller plastic objects. Thus, problems such as mixed pixel not be encountered, and the algorithm will not be required a constant called noise killer.

The SWIR, which makes the invisible visible, is extremely valuable. In this thesis, three SWIR bands have been used with the purpose of fast and precise plastic detection. However, it is also possible to detect and identify other materials using different regions of the SWIR. In terms of environmental pollution, the detection of heavy metals contaminating water with SWIR should be researched.

REFERENCES

Agüera, F., Fernando, J., & Manuel, A. (2008). Using texture analysis to improve per-pixel classification of very high resolution images for mapping plastic greenhouses. *ISPRS Journal of Photogrammetry and Remote Sensing*, 635-646.

Albregtsen, U. (2008). Reflection, refraction, diffraction, and scattering. Retrieved April 14, 2019, from https://www.uio.no/studier/emner/matnat/ifi/

Andrady, L. A. (2017). The plastic in microplastics: A review. *Marine Pollution Bulletin, 119*(1), 12-22.

Antonio, N., & Tarantino, E. (2015). "Combining ad hoc spectral indices based on LANDSAT-8 OLI/TIRS sensor data for the detection of plastic cover vineyard. *Remote sensing letters*, 933-941.

Asadzadeh, S., & De Souza Filho, C. (2016). Investigating the capability of WorldView-3 superspectral data for direct hydrocarbon detection. *Remote sensing of environment*, 162-173.

AVIRIS - Airborne Visible InfraRed Imaging Spectrometer. (2019). Retrieved from NASA Jet Propulsion Laboratory: https://aviris.jpl.nasa.gov/aviris/index.html

AVIRIS Data Portal. (2019). Retrieved from NASA Jet Propulsion Laboratory: https://aviris.jpl.nasa.gov/alt_locator/

AVIRIS Flight: f170612t01. (2019). Retrieved from NASA Jet Propulsion Laboratory: https://aviris.jpl.nasa.gov/cgi/flights_17.cgi?step=view_flightlog&flight_id=f170612t01

Barnes, D. K., Galgani, F., Thompson, C. R., & Barlaz, M. (2009). Accumulation and fragmentation of plastic debris in global environments. *Philosophical transactions of the Royal Society of London*.

Carraher, C. E. (2008). *Polymer Chemistry.*

Chen, Z., & Li, F. (2017). Mapping Plastic-Mulched Farmland with C-Band Full. *Remote Sensing*.

Chen, Z., Wang, L., Wu, W., Jiang, Z., & Li, H. (2016). Monitoring plastic-mulched farmland by Landsat-8 OLI imagery using spectral and textural features. *Remote Sensing*, 353.

Derraik, J. (2002). The pollution of the marine environment by plastic debris: a review. *Marine pollution bulletin*, 842-852.

Ecostress Spectral Library. (n.d.). Retrieved from Jet Propolsion Laboratory: https://speclib.jpl.nasa.gov/library

El-Magd, I., El-Kafrawy, S., & Farag, I. (2014). Detecting Oil Spill Contamination Using Airborne Hyperspectral Data in the River Nile, Egypt. *Open Journal of Marine Science*, 140.

Fernandez, E., Chatenoud, L., La Vecchia, C., Negri, E., & Franceschi, S. (1999). Fish consumption and cancer risk. *he American journal of clinical nutrition*, 85-90.

Geyer, R., Jambeck, J. R., & Law, K. L. (2017). Production, use, and fate of all plastics ever made. *Science Advances*.

Grantham Insitute. (2017, September 17). *Earth System Policy*. Retrieved April 22, 2019, from Grantham Insitute, Climate Change and Environment: https://granthaminstitute.com/2017/09/19/when-it-rains-it-pours-how-can-cities-save-the-ocean-from-plastic-pollution-during-heavy-rainfall/

Gundlach, J. (2012). *Designing Unmanned Aircraft Systems - A Comprehensive Approach.* American Institute of Aeronautics and Astronautics. Retrieved May 1, 2019, from https://app.knovel.com/hotlink/toc/id:kpDUASACA1/designing-unmanned-aircraft/designing-unmanned-aircraft

Hammer, J., Kraak, M. H., & Parsons, J. R. (2012). Plastics in the Marine Environment: The Dark Side of a Modern Gift. *Reviews of Environmental Contamination and Toxicology*.

Harding Jr, L., Miller, W., Swift, R., & Wright, C. (2001). Aircraft Remote Sensing. *Encyclopedia of Ocean Sciences (Second Edition)*, 138-146.

Hong, A., & Pine, D. (2005). Scattering properties of core–shell particles. *Journal of Polymer Science Part B: Polymer Physics*, *43*, 3534-3548.

Hydrocarbons. (2012). Retrieved March 7, 2019, from BC Open Textbooks: https://opentextbc.ca/chemistry/chapter/20-1-hydrocarbons/#CNX_Chem_20_01_alkanes

Infrared Radiation. (2019). Retrieved April 17, 2019, from Infratec: https://www.infratec.eu/sensor-division/service-support/glossary/infrared-radiation/

Jambeck, J., Geyer, R., Wilcox, C., Siegler, T., Perryman, M., Andrady, A., . . . Law, K. L. (2015). Plastic waste inputs from land into the ocean. *Science*, 768-771.

Jastifer, J., McNitt, A., Mack, C., Kent, R., McCullough, K., Anderson, R., & Coughlin, M. (2019). Synthetic turf: history, design, maintenance, and athlete safety. *Sports health*, 84-90.

Jensen, J., & Lulla, K. (1987). *Introductory digital image processing: a remote sensing perspective.*

Jordan, C. (2009). *Albatross chick at Midway Atoll Refuge.*

Karaca, A., Ertürk, A., Güllü, M., Elmas, M., & Ertürk, S. (2013). Automatic waste sorting using shortwave infrared hyperspectral imaging system. *2013 5th Workshop on Hyperspectral Image and Signal Processing: Evolution in Remote Sensing (WHISPERS)* (pp. 1-4). IEEE.

Koç San, D. (2013). Evaluation of different classification techniques for the detection of glass and plastic greenhouses from WorldView-2 satellite imagery. *Journal of Applied Remote Sensing*.

Kokaly, R., R.N., C., Swayze, G., Livo, K., Hoefen, T., Pearson, N., . . . Klein, A. (2017). *Spectral Library Version 7.* Retrieved from USGS: https://crustal.usgs.gov/speclab/QueryAll07a.php?page=1

Kutz, M. (2011). *Applied Plastics Engineering Handbook: Processing and Materials.* William Andrews.

Kühn, F., Konstanze, O., & Bernhard, H. (2004). Hydrocarbon Index–an algorithm for hyperspectral detection of hydrocarbons. *International Journal of Remote Sensing*, 2467-2473.

Law, K., Morèt-Ferguson, S., Godwin, D., Zettler, E., DeForcee, E., Kukulka, T., & Proskurowski, G. (2014). Distribution of surface plastic debris in the. *Environmental Science &*, 4732–4738.

Lehner, R. (2015). *Macro-, Meso-, Micro-, but What About Nanoplastic?* Retrieved March 19, 2019, from Planer Experts: http://www.planetexperts.com/macro-meso-micro-but-what-about-nanoplastic/

Lenz, A., Schilling, H., Gross, W., & Middelmann, W. (2015). Evaluation and performance analysis of hydrocarbon detection methods using hyperspectral data. *2015 IEEE International Geoscience and Remote Sensing Symposium (IGARSS)* (s. 2680-2683). Milan: Institute of Electrical and Electronics Engineers.

Liddell, H., & Scott, R. (1897). *Greek-English Lexicon.* New York: American Book Company.

Lloyd, A., Farooq, M., Diclaro, J., Kline, D., & Estep, A. (2013). Field evaluation of commercial off-the-shelf spatial repellents against the Asian tiger mosquito,

Aedes Albopictus (Skuse), and the potential for use during deployment. *S Army Medical Department Journal*.

Mason, S., Welch, V., & Neratko, J. (2018). Synthetic Polymer Contamination in Bottled Water. *Frontiers in chemistry*, 407.

Masoumi, Hamed, Safavi, S., & Khani, Z. (2012). Identification and classification of plastic resins using near infrared reflectance. *Int. J. Mech. Ind. Eng*, 213-220.

Mathieu, M., Roy, R., Launeau, P., Cathelineau, M., & Quirt, D. (2017). Alteration mapping on drill cores using a HySpex SWIR-320m hyperspectral camera: Application to the exploration of an unconformity-related uranium deposit. *Journal of Geochemical Exploration*, 71-88.

Merrington, A. (2017). *Applied Plastics Engineering Handbook.* doi:https://www.sciencedirect.com/science/article/pii/B9780323390408000092?via%3Dihub

North, E., & Halden, R. (2013). Plastics and Environmental Health: The Road Ahead. *Reviews on environmental health*, 1-8.

Olah, G., & Molnár, Á. (2003). *Hydrocarbon Chemistry.*

Ouellette, R. J., & Rawn, D. J. (2015). *Organic Chemistry Study Guide.* Elsevier Inc. doi:https://www.sciencedirect.com/science/article/pii/B9780128018897000285?via%3Dihub

Romeo, T., Pietro, B., Pedà, C., Consoli, P., Andaloro, F., & Fossi, M. (2015). First evidence of presence of plastic debris in stomach of large pelagic fish in the Mediterranean Sea. *Marine pollution bulletin*, 358-361.

Scafutto, R., De Souza Filho, C., & De Oliveira, W. (2017). Hyperspectral remote sensing detection of petroleum hydrocarbons in mixtures with mineral substrates: Implications for onshore exploration and monitoring. *ISPRS Journal of Photogrammetry and Remote Sensing*, 146-157.

Smith, K., Phillips, J., McCafferty, A., & Clark, R. (2016). *Developing integrated methods to address complex resource and environmental issues.* Retrieved from USGS: https://pubs.usgs.gov/circ/1413/circ1413.pdf

Svarc, J. (2018). *Solar PV Cell Construction*. Retrieved May 13, 2019, from Clean Energy Reviews: https://www.cleanenergyreviews.info/blog/solar-pv-cell-construction

Thenkabail, P., & Lyon, J. (2016). *Hyperspectral Remote Sensing of Vegetation.* CRC Press.

Woodford, C. (2018). *Plastic*. Retrieved February 23, 2019, from Explainthatstuff!: https://www.explainthatstuff.com/plastics.html

WorldView-3 Satellite Sensor. (2017). Retrieved April 30, 2019, from Satellite Imaging Corporation: https://www.satimagingcorp.com/satellite-sensors/worldview-3/

Yan, G. (2003). Pixel based and object oriented image analysis for coal fire research.

APPENDICES

A. Spectral Math Function MATLAB Codes

```
% These lines are coded to detect the existence of plastic with
using shortwave infrared bands.

% Codes implement PEI Algorithm and calculate the PIPV results.
% In addition, the function compares the ground truth and algorithm
% output, generate the confusion matrix, and correspondingly produce
% accuracy rates.


clear all;close all;clc;

%Import of Hyperspectral Data
im = imread('STR15.tif');
im = double(im);

%Band Selection:
B1680 = im(:,:,140); %point A, 1681.383 nm
B1731 = im(:,:,144); %point B, 1721.231 nm
B1741 = im(:,:,146); %point C, 1741.153 nm

%PEI Algorithm Implementation
PEI=((0.67*((B1741-B1680))+B1680-B1731))-10;
figure;imagesc(PEI)
title('PEI Algorithm Result')
colormap(gray)

%Post Index Positive Value Determination
PIPV = double((PEI>0)).*PEI;
figure;imagesc(PIPV)
title('Post Index Positive Values')
colormap(gray)

%Post Index Positive Value Mask
MPIPV = double((PEI>0));
figure;imagesc(MPIPV)
title('Mask of PIPV')
colormap(gray)
```

```
%Import of Ground Truth Data
GTRU=imread('GTR15.tif');
GTRU = GTRU>0;
GTRU = imresize(GTRU,[size(im,1) size(im,2)],'nearest');
GTRU = double(GTRU);
figure;imagesc(GTRU);
title('Ground Truth')
colormap(gray)

%PEI Algorithm and Ground Truth Data Comparison
i1 = find(im(:,:,1)==0);
GTRU(i1)=NaN;
MPIPV(i1)=NaN;

%Accuracy Assessment

OA = length(find(GTRU==MPIPV))/(length(MPIPV(:))-length(i1))

Cf_Mat = confusionmat(MPIPV(:),GTRU(:))

UA = Cf_Mat(2,2)/(Cf_Mat(2,2)+Cf_Mat(1,2))

PA = Cf_Mat(2,2)/(Cf_Mat(2,2)+Cf_Mat(2,1))

%OA can be also calculated as:

OA=(Cf_Mat(1,1)+Cf_Mat(2,2))/(Cf_Mat(1,1)+Cf_Mat(1,2)+Cf_Mat(2
,1)+Cf_Mat(2,2))

%Histogram of PIPV/Pixel Numbers
i2 = find(GTRU>0);
figure;
histogram(PIPV(i2),5)
title('PIPV Histogram')
xlabel('PIPV');
ylabel('Pixel Numbers');

% Generated by MATLAB on 19-May-2019 03:09:15
```